

LOW TEMPERATURE
PHOTOLUMINESCENCE PROPERTIES
OF SILICON AND SILICON-GERMANIUM ALLOYS

Thesis by
Gordon Stuart Mitchard

In Partial Fulfillment of the Requirements
for the Degree of
Doctor of Philosophy

California Institute of Technology
Pasadena, California

1981

(Submitted May 21, 1981)

TO MY PARENTS

ACKNOWLEDGEMENTS

It gives me great pleasure to thank Dr. Thomas C. McGill for providing me with the opportunity to do this work. His constant guidance and support during the course of my graduate studies was indispensable.

As well, I would like to thank my friends, and my colleagues at CalTech, for cultivating a congenial, stimulating and supportive environment during my years at CalTech. I am particularly grateful to Dr. S. A. Lyon for getting me started on the right foot, to A. T. Hunter and R. M. Feenstra for many helpful discussions, and to Dr. Y. C. Chang for his assistance in the interpretation of alloy photoluminescence.

I am deeply indebted to Dr. J. P. Baukus and the Extrinsic Silicon group at Hughes Research Laboratories. Without their expertise in the growth and characterization of semiconductor samples, none of this work would have been possible.

Last, but certainly not least, I would like to thank Vere Snell for her incomparable secretarial help, and for typing this thesis quickly, accurately and cheerfully.

For financial support, I gratefully acknowledge the Natural Sciences and Engineering Research Council of Canada, the California Institute of Technology, the Office of Naval Research, and the Advanced Research Projects Agency.

ABSTRACT

In this thesis, three examples of the application of the photoluminescence technique to indirect semiconductors at low temperatures are presented.

Chapter 2 deals with the effect of increasing impurity concentrations on the photoluminescence spectrum. We present results for the Si:(B,In) system. As the In concentration is increased, we observe quenching of B luminescence. We propose a model based on exciton transfer from B to In impurities, which agrees well with the experimental results when the exchange mechanism is assumed for the transfer. This is the first observation of exciton transfer in Si.

Chapter 3 deals with the properties of three sharp and relatively intense features in the photoluminescence spectrum of Si:In. We observe these lines, which are labelled "P,Q,R", only in the luminescence of Si:In. We present measurements of the lifetimes of P,Q,R luminescence which show that these lines have extremely long lifetimes. These results suggest that the P,Q,R lines are associated with an isoelectronic complex in Si. We present measurements of the temperature dependence of P,Q,R luminescence and P,Q,R lifetimes which support this conclusion. This is the first observation of luminescence associated with an isoelectronic complex in Si. In addition, we present results which show that the P,Q,R luminescence intensities are very sensitive to the sample surface preparation. This is the first observation of surface

sensitive photoluminescence.

Chapter 4 deals with the photoluminescence properties of undoped and In doped Si-rich Si-Ge alloys. We identify the alloy luminescence features on the basis of the temperature dependence, time dependence and pump power dependence of the luminescence intensities. We present results for the band gap shift and free exciton binding energy for each sample examined. In addition, we present a model for the observed broadening of bound exciton luminescence. Finally, we present observations which suggest that excitons bind to local fluctuations in alloy composition at low temperatures. This is the first investigation of the photoluminescence properties of Si-rich Si-Ge alloy semiconductors.

Parts of this thesis have been or will be published under the following titles:

- Chapter 2: Determination of Relative Impurity Concentrations Using Photoluminescence - A Case Study of the Si:(B,In) System, G. S. Mitchard and T. C. McGill, Appl. Phys. Lett. 37, 959 (1980).
- Chapter 3: Observation of Long Lifetime Lines in Photoluminescence From Si:In, G. S. Mitchard, S. A. Lyon, K. R. Elliott and T. C. McGill, Solid State Commun. 29, 425 (1979).
- Photoluminescence Studies of Acceptors in Silicon, S. A. Lyon, K. R. Elliott, G. S. Mitchard, T. C. McGill, J. P. Baukus, R. Baron, M. H. Young and O. J. Marsh, Proceedings of the Joint Meeting of the IRIS Specialty Groups on Infrared Detectors and Imaging, 1978 (Infrared Information and Analysis Centre, Ann Arbor, 1978), volume 1, page 273.
- Chapter 4: Photoluminescence of Si-Rich Si-Ge Alloys, G. S. Mitchard and T. C. McGill (in preparation).
- Nearest-Neighbour Effects on the Energy Levels of Acceptors in Silicon-Rich Si-Ge Alloys, R. Baron, M. H. Young, H. Winston, H. Kimura, G. S. Mitchard and T. C. McGill, Proceedings of the Eleventh International Conference on Defects and Radiation Effects in Semiconductors, Japan, 1980.

CONTENTS

ACKNOWLEDGEMENTS	iii
ABSTRACT	iv
CHAPTER 1: Investigation of Indirect Semiconductors at Low Temperature Using the Photoluminescence Technique	1
1.1 Introduction	2
1.1.1 Outline of Thesis	2
1.2 The Photoluminescence Technique	4
1.2.1 Optical Excitation of Semiconductors	4
1.2.2 Return to Equilibrium in Indirect Semiconductors at Low Temperature	5
1.2.2.1 Formation of Free Excitons	5
1.2.2.2 Recombination of Free Excitons	8
1.2.2.3 Formation of Bound Excitons	10
1.2.2.4 Recombination of Bound Excitons	12
1.2.2.5 Formation and Recombination of Exciton Complexes	13
1.3 Previous Application to Doped Si	16
1.3.1 Investigation of the Free Exciton and Bound Exciton States	16
1.3.2 Investigation of Relaxation Kinetics	17
1.3.3 Measurement of Impurity Concentrations	17
1.4 Applications of Current Interest	18
1.4.1 Heavily Doped Semiconductors	19
1.4.2 Irradiated Semiconductors	20
1.4.3 Defect Clusters in Semiconductors	20
1.4.4 Alloy Semiconductors	21
1.5 General Experimental Considerations	22
1.5.1 Material Properties	22
1.5.2 Experimental Apparatus	29

1.5.3	Experimental Conditions	33
1.5.3.1	Excitation Intensity	33
1.5.3.2	Sample Temperature	34
1.5.3.3	Time Delay	34
1.5.3.4	Sample Characteristics	34
1.5.4	Typical Si Photoluminescence	35
1.6	Summary of Results	38
1.6.1	Chapter 2	38
1.6.2	Chapter 3	40
1.6.3	Chapter 4	42
	References	44
CHAPTER 2:	Effect of Impurity Concentration on the Photoluminescence Spectrum - A Case Study of the Si:(B,In) System	49
2.1	Introduction	50
2.2	Rate Model of Doped Si Photoluminescence	51
2.2.1	The Rate Equations	51
2.2.2	The Steady-State Solution	53
2.2.3	Application When Free Exciton Luminescence is Observed	54
2.2.4	Application When Free Exciton Luminescence is Not Observed	56
2.3	Experimental Results for the Si:(B,In) System	61
2.3.1	The Si:(B,In) System	61
2.3.2	The Si:(B,In) Samples and Typical Photoluminescence Spectra	62
2.3.3	The Measurement of Luminescence Intensity Ratios	65
2.3.4	The Dependence of R_{BIn} on In Concentration	70
2.4	Discussion of the Experimental Results	72
2.4.1	The Low Concentration Result	72
2.4.2	The Effect of Increasing In Concentration	74
2.4.3	Rate Model Including Exciton Transfer	76

2.4.4	The Exciton Transfer Rate	79
2.4.5	Comparison of Modified Rate Model with Experimental Results	81
2.5	Summary and Conclusion	84
	References	86
CHAPTER 3:	Isoelectronic Complexes in Si - The "P,Q,R" Lines in Si:In	88
3.1	Introduction	89
3.2	The Si:In Samples	91
3.3	Experimental Results and Discussion	91
3.3.1	Typical Si:In Photoluminescence Spectrum	91
3.3.2	General Systematics of P,Q,R Luminescence	94
3.3.3	Temperature Dependence of P,Q,R Luminescence	94
3.3.3.1	Temperature-resolved Spectra	97
3.3.3.2	Temperature Dependence of P,Q,R Luminescence Intensity Ratios	97
3.3.4	Time Dependence of P,Q,R Luminescence	100
3.3.4.1	Time-resolved Spectra	100
3.3.4.2	Lifetimes of P,Q,R Luminescence	100
3.3.5	Isoelectronic Impurities	103
3.3.6	Temperature Dependence of P,Q,R Lifetimes	104
3.4	Model For P,Q,R Luminescence	106
3.4.1	Qualitative Features of the Model	106
3.4.2	The Rate Equations	107
3.4.3	The Rate Estimates	111
3.4.4	The Approximations	114
3.4.5	The Approximate Solution	116
3.4.6	Comparison With The Experimental Results	116
3.4.6.1	Lifetime Temperature Dependence	117
3.4.6.2	Thermalization Behaviour	120
3.5	Enhancement of P,Q,R Luminescence	124
3.5.1	Origin of P,Q,R Luminescence	124

3.5.2	Determination of Origin by Systematic Sample Comparison	124
3.5.3	Reproducibility of P,Q,R Luminescence	125
3.5.4	Measurement of Sample Homogeneity	127
3.5.5	Measurement of Luminescence Saturation	129
3.5.6	Effect of Surface Preparation and the Enhancement of P,Q,R Luminescence	132
3.5.7	Characteristics of the Enhancement Procedure	133
3.5.8	Models for the Enhancement	135
3.6	Summary and Conclusion	137
	References	140
CHAPTER 4: Photoluminescence Properties of Si-Rich Si-Ge Alloys		142
4.1	Introduction	143
4.2	The Si-Ge Alloy Samples	144
4.3	Experimental Results and Discussion for Undoped $\text{Si}_{1-x}\text{Ge}_x$	144
4.3.1	Typical Photoluminescence Spectrum and Identification of Phonon Replicas	146
4.3.2	Identification of Free Exciton Luminescence	146
4.3.3	Identification of Bound Exciton Luminescence	150
4.3.4	Comparison of Photoluminescence Spectrum of Sample C077 and Sample C021-3	156
4.3.5	Models for Bound Exciton Luminescence	156
	4.3.5.1 Bulk Fluctuation Model	156
	4.3.5.2 Nearest-Neighbour Configuration Model	159
4.3.6	Experimental Results Which Support the Nearest-Neighbour Configuration Model	159
	4.3.6.1 Hopping Conduction and Hall Effect Experiments	160
	4.3.6.2 Temperature Dependence of Bound Exciton Luminescence Peak Position	161
	4.3.6.3 Bound Exciton Luminescence Lineshape	161
	4.3.6.4 Time-resolved Spectra	163

4.3.7	Comparison of Si and Undoped $\text{Si}_{1-x}\text{Ge}_x$ Luminescence Energies	168
4.3.7.1	Band Gap Decrease for Sample C077 ($x=0.11$)	170
4.3.7.2	Free Exciton Binding Energy for Sample C077 ($x=0.11$)	170
4.3.7.3	Band Gap Decrease for Sample C021-3 ($x=0.067$)	172
4.3.8	Excitons Bound to Composition Fluctuations	174
4.3.8.1	Low Temperature Free Exciton Luminescence	174
4.3.8.2	Fluctuation Bound Excitons	174
4.3.8.3	Low Temperature Time-resolved Spectra	176
4.4	Experimental Results and Discussion for In Doped $\text{Si}_{1-x}\text{Ge}_x$	185
4.4.1	Typical Photoluminescence Spectrum	185
4.4.2	Identification of Free Exciton Luminescence	187
4.4.3	Identification of Bound Exciton Luminescence	188
4.4.3.1	Time-resolved Spectra and Isolation of B Bound Exciton Component	189
4.4.3.2	Temperature-resolved Spectra and Isolation of In Bound Exciton Component	191
4.4.4	Comparison of Si and $\text{Si}_{1-x}\text{Ge}_x$:In Luminescence Energies	193
4.5	Summary and Conclusion	197
	References	201

CHAPTER 1

INVESTIGATION OF INDIRECT SEMICONDUCTORS AT LOW TEMPERATURE
USING THE PHOTOLUMINESCENCE TECHNIQUE

1.1 INTRODUCTION

One of the fundamental techniques employed to determine the properties of a system involves a study of its return to equilibrium after external excitation. In general, the mechanisms responsible for return to equilibrium may be varied and complex, and depend on the nature of the system as well as on the initial and final states. Indeed, a thorough study usually involves the systematic variation of the initial and final states, as well as some consideration of the effect of systematic alteration of the system being examined.

This technique has been applied with notable success to the study of semiconductor materials. In particular, the processes responsible for return to equilibrium from electronic excited states of the system have been examined in detail. For pure substances, these studies provide information regarding the composition and electronic structure of the bulk material. For materials in which there are impurities and/or defects, information can be obtained about the composition and concentration of the defects, as well as about the new electronic states they introduce.

1.1.1 Outline of Thesis

In this thesis, a specific application of the general investigative technique described above is considered. The systems investigated are indirect semiconductors at low temperature. Electronic excitation from equilibrium results from optical photon irradiation.

Then return to equilibrium is investigated by examining the luminescence spectrum resulting from the various radiative recombination processes that occur. We refer to this procedure as the photoluminescence technique, and consider three examples of its application.

In Chapter 2, an investigation of the effect of increasing impurity concentrations on the photoluminescence spectrum is presented. The particular system considered is Si doped with B and In impurities. At high In concentrations, quenching of B luminescence is observed. A model is proposed to explain this effect which considers exciton transfer from B to In impurities. Good agreement with the experimental results is obtained when the exchange mechanism is assumed to be responsible for the transfer. This is the first observation of exciton transfer effects in Si.

In Chapter 3, an investigation of three sharp and relatively intense features in the photoluminescence spectrum of moderately doped Si:In is presented. These lines have been labelled "P,Q,R", and are only observed in Si:In. Measurements of the time dependence of P,Q,R luminescence show that these lines have extremely long lifetimes. These results suggest that they result from recombination of excitons bound to an isoelectronic complex which involves In. Measurements of the temperature dependence of P,Q,R luminescence intensities and lifetimes are consistent with this conclusion. This is the first observation of luminescence from an isoelectronic complex in Si.

Furthermore, we observe that the P,Q,R luminescence intensity is very sensitive to the sample surface preparation. This is the first observation of surface sensitive photoluminescence.

In Chapter 4, an investigation of the photoluminescence properties of undoped and In doped Si-Rich Si-Ge alloys is presented. The luminescence features are identified on the basis of measurements of the temperature dependence, time dependence and pump power dependence of the luminescence intensities. As a result of this identification, band gap shifts and free exciton binding energies are determined for the alloy samples studied. In addition, a model for the observed broadening of bound exciton luminescence was proposed. At low temperatures, photoluminescence features are observed which suggest the presence of excitons bound to local fluctuations in alloy composition. This is the first investigation of the photoluminescence properties of Si-rich Si-Ge alloy semiconductors.

1.2 THE PHOTOLUMINESCENCE TECHNIQUE

In this section, we consider the general features of the photoluminescence technique, and the processes that occur as a result of its use.

1.2.1 Optical Excitation of Semiconductors

There are a number of procedures for inducing electronic excited states in semiconductor materials. One of the most widely studied

techniques and the one which is perhaps simplest to analyze is optical excitation. This process is schematically illustrated in Fig. 1.1. As shown in the figure, the material is irradiated with photons which have greater energy than the band gap of the semiconductor. Absorption of these photons results in excitation of electrons across the gap. The photon energies involved are on the order of 1 eV. A photon with this energy has a wavevector of about 10^{-3} \AA^{-1} . This is negligible with respect to a zone boundary wavevector of about 1 \AA^{-1} , and so the transition depicted in Fig. 1.1 is effectively vertical.

1.2.2 Return to Equilibrium in Indirect Semiconductors at Low Temperature

As previously mentioned, the processes responsible for return to equilibrium depend on the system involved and on the initial and final states. Pankove ⁽¹⁾ gives a general review of all the radiative and nonradiative recombination processes that can occur following an electronic excitation such as the one described in the previous section. For our purposes, however, it will be sufficient to discuss only those processes which are important in indirect semiconductors at low temperature.

1.2.2.1 Formation of Free Excitons

To begin with, the highly excited electrons and holes which result from the photon absorption process relax to the band edges in a few nanoseconds ⁽²⁾, via optical and acoustic phonon emission. At low temperatures, further relaxation can occur when these free electrons

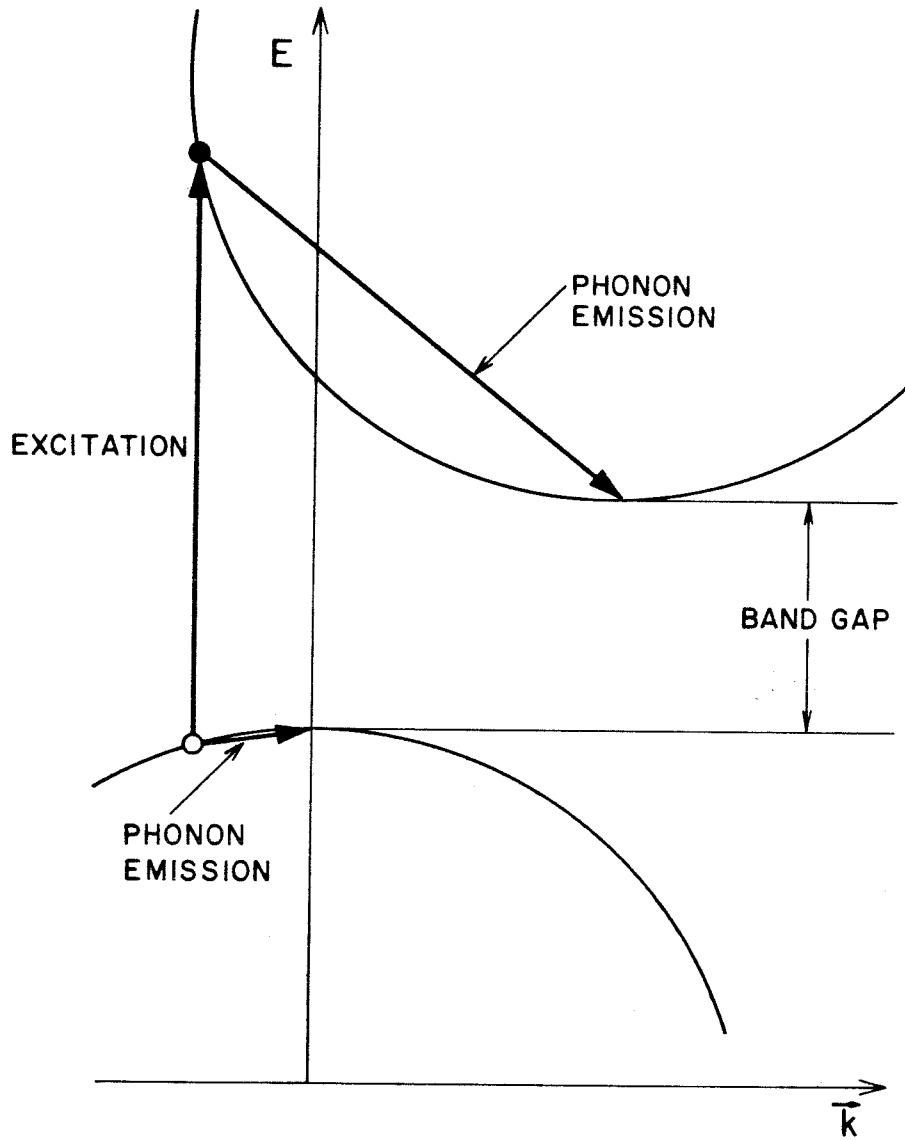


Figure 1.1. Schematic illustration of optical excitation of an indirect semiconductor, and the subsequent carrier relaxation via phonon emission.

and holes bind as a result of their mutual Coulomb attraction to form free excitons. If we assume spherical and isotropic band edges and a potential $-e^2/\epsilon r$, where ϵ is the dielectric constant of the material, the problem reduces to the hydrogen atom problem. Then the free exciton energy is given by

$$E_{FE}(n) = E_{gap} - \frac{m_r^* e^4}{2\hbar^2 \epsilon^2 n^2} + \frac{\hbar^2 K^2}{2 m_{ex}^*} \quad (1.1)$$

where

E_{gap} = the semiconductor band gap energy

$$m_r^* = \left[\frac{1}{m_e^*} + \frac{1}{m_h^*} \right]^{-1}$$

K = the wavevector associated with free exciton centre of mass motion

$$m_{ex}^* = m_e^* + m_h^*$$

and where

m_e^* = the electron effective mass

m_h^* = the hole effective mass.

From Eq. (1.1) we see that the free exciton behaves like a free particle with effective mass m_{ex}^* and centre of mass kinetic energy $\hbar^2 K^2 / 2 m_{ex}^*$. The internal states are hydrogenic, and are specified

by the principal quantum number n . The ground state binding energy is $E_D = E_{\text{gap}} - E_{\text{FE}}(1)$. At low temperatures, where $E_D \gg k_B T$, we expect that the majority of free electrons and holes produced by the optical excitation will bind to form free excitons. Also, at low temperatures $E_{\text{FE}}(2) - E_{\text{FE}}(1) \sim \frac{3}{4} E_D \gg k_B T$ and so we expect that the majority of free excitons will be in the ground state. Of course, as indicated in Eq. (1.1), the hydrogenic energy levels are broadened by the Boltzmann distribution of free exciton centre of mass kinetic energies. However, this broadening is on the order of $k_B T$, and is small compared to the hydrogenic energy level spacing at low temperatures.

On the basis of the hydrogenic free exciton model, we can also associate a Bohr radius with this free exciton state. In this case, the free exciton Bohr radius will be

$$a_{\text{FE}}^* = \frac{\epsilon \hbar^2}{m_r^* e^2} \quad (1.2)$$

1.2.2.2 Recombination of Free Excitons

In indirect semiconductors, the return to equilibrium is complicated by the fact that the conduction band minimum and valence band maximum do not occur at the same point in \vec{k} -space. As a result, free exciton recombination in indirect semiconductors requires the assistance of a bulk phonon to conserve momentum. The situation is illustrated schematically in Fig. 1.2. As shown in the figure, the recombination process results in the emission of a photon of energy

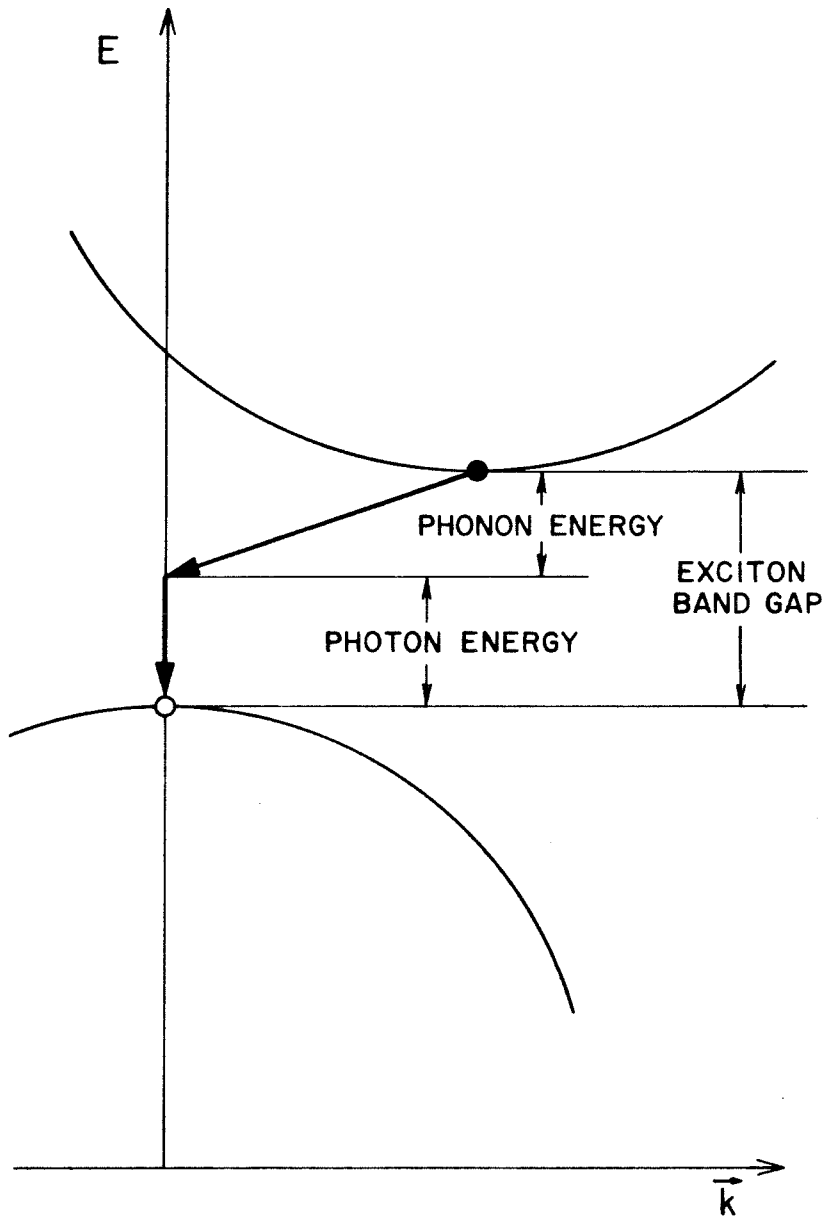


Figure 1.2. Free exciton recombination in an indirect semiconductor. The exciton band gap energy is the semiconductor band gap energy minus the free exciton binding energy. Note that the photon transition is effectively vertical, as discussed in the text.

$E = E_{FE}(1) - E_{\text{phonon}}$. Of course, at low temperatures only phonon emission is important and so the photon energy is reduced by the energy of the emitted phonon.

The effect of the Boltzmann distribution of free exciton centre of mass kinetic energies is included in $E_{FE}(1)$. This effect results in a predicted lineshape for free exciton luminescence which is ⁽³⁾

$$I(E) = \sqrt{E + E_{\text{phonon}} - E_0} \exp\left(-\frac{E + E_{\text{phonon}} - E_0}{k_B T}\right) \quad (1.3)$$

where E_0 is the value of $E_{FE}(1)$ for a free exciton with zero kinetic energy.

1.2.2.3 Formation of Bound Excitons

At this point we consider the introduction of substitutional donor or acceptor impurities into the semiconductor material. In the vicinity of an ionized donor impurity, an electron with effective mass m_e^* will move in a potential $-e^2/\epsilon r$. Once again, the solution of the hydrogen atom problem applies. The electron has states at energies given by

$$E_D(n) = -\frac{m_e^* e^4}{2\hbar^2 \epsilon^2 n^2} \quad (1.4)$$

measured with respect to the conduction band edge. Also, the donor Bohr radius will be

$$a_D^* = \frac{\epsilon \hbar^2}{m_e^* e^2} \quad (1.5)$$

Of course, analogous expressions can be obtained for acceptor impurities.

Free excitons can bind to neutral donor or acceptor impurities in semiconductors to form bound exciton complexes. There are primarily two contributions to the impurity potential which result in a bound state. The long range contribution to the potential is a result of the Van der Waals interaction between the neutral impurity and the exciton. In addition, there is a short range contribution which is a result of local lattice distortion around the impurity. This short range contribution is impurity dependent, and so we expect to observe exciton binding energies which are impurity dependent also. The binding energies have been experimentally determined to be approximately $E_i(1)/10$ ⁽⁴⁾, where $i = D$ or A for donor or acceptor impurities.

Other impurities have also been observed to bind excitons ^(5,6). In particular, we consider isoelectronic impurities in semiconductors. An isoelectronic impurity is usually the result of the substitutional replacement of one of the semiconductor atoms with another atom of the same valence. However, more complex isoelectronic complexes have been observed. ⁽⁶⁾ Binding of excitons to isoelectronic impurities results from the short range part of the impurity potential. In particular, it is thought that one carrier is tightly bound by the short range potential, while the other carrier is bound by the resulting long range Coulomb potential. ⁽⁷⁾

1.2.2.4 Recombination of Bound Excitons

There are a number of qualitative differences between free exciton and bound exciton radiative recombination in indirect semiconductors. These differences result from the carrier localization which occurs when free excitons are bound. First, the bound exciton has no centre of mass motion and so thermal broadening of the luminescence line is not observed as it is for free excitons. Second, spatial localization of the carriers results in \vec{k} -space spreading of the carrier wavefunctions. As a result, there is some probability that recombination can occur without the assistance of a momentum conserving phonon. The strength of this no-phonon recombination process depends on the amount of \vec{k} -space spreading of the carrier wavefunctions, which in turn depends on the degree of carrier localization. Since the carrier localization is sensitive to the short range part of the impurity potential, we expect that the strength of the no-phonon recombination process will be strongly impurity dependent ⁽⁸⁾.

Of course, phonon assisted radiative recombination processes will also occur for bound excitons in a manner analogous to free exciton phonon assisted radiative recombination. When phonon assistance is present, however, the recombination process does not depend on \vec{k} -space spreading of the carrier wavefunctions. As a result, the strength of the phonon assisted processes is nearly independent of impurity type ⁽⁸⁾.

In addition to these radiative recombination processes, excitons bound to neutral donor or acceptor impurities can recombine non-

radiatively in a process which is not available to excitons bound to isoelectronic impurities. This is the Auger recombination process, which is schematically illustrated in Fig. 1.3. In this case, the recombination energy is transferred to the third carrier in the complex, which is ejected from the impurity deep into the appropriate band. Momentum conservation must also be satisfied by the ejected carrier, which must have a wavevector on the constant energy surface required for energy conservation. As a result, the strength of the Auger process depends on the \vec{k} -space spreading of the carrier wavefunctions. The dependence, in fact, is similar to that of the no-phonon radiative recombination process for bound excitons. Consequently, we expect that the strength of the Auger process will also depend sensitively on impurity type ⁽⁸⁾.

In indirect gap semiconductors, the Auger recombination process can dominate radiative recombination processes by orders of magnitude. Of course, the Auger transition is not possible without the presence of a third Auger carrier in the complex. For this reason, Auger recombination is not possible for excitons bound to isoelectronic impurities, and as a result, the recombination is primarily radiative. For this reason, excitons bound to isoelectronic impurities can exhibit lifetimes which are orders of magnitude longer than those observed for donor or acceptor bound excitons.

1.2.2.5 Formation and Recombination of Exciton Complexes

The relaxation processes described in the previous sections

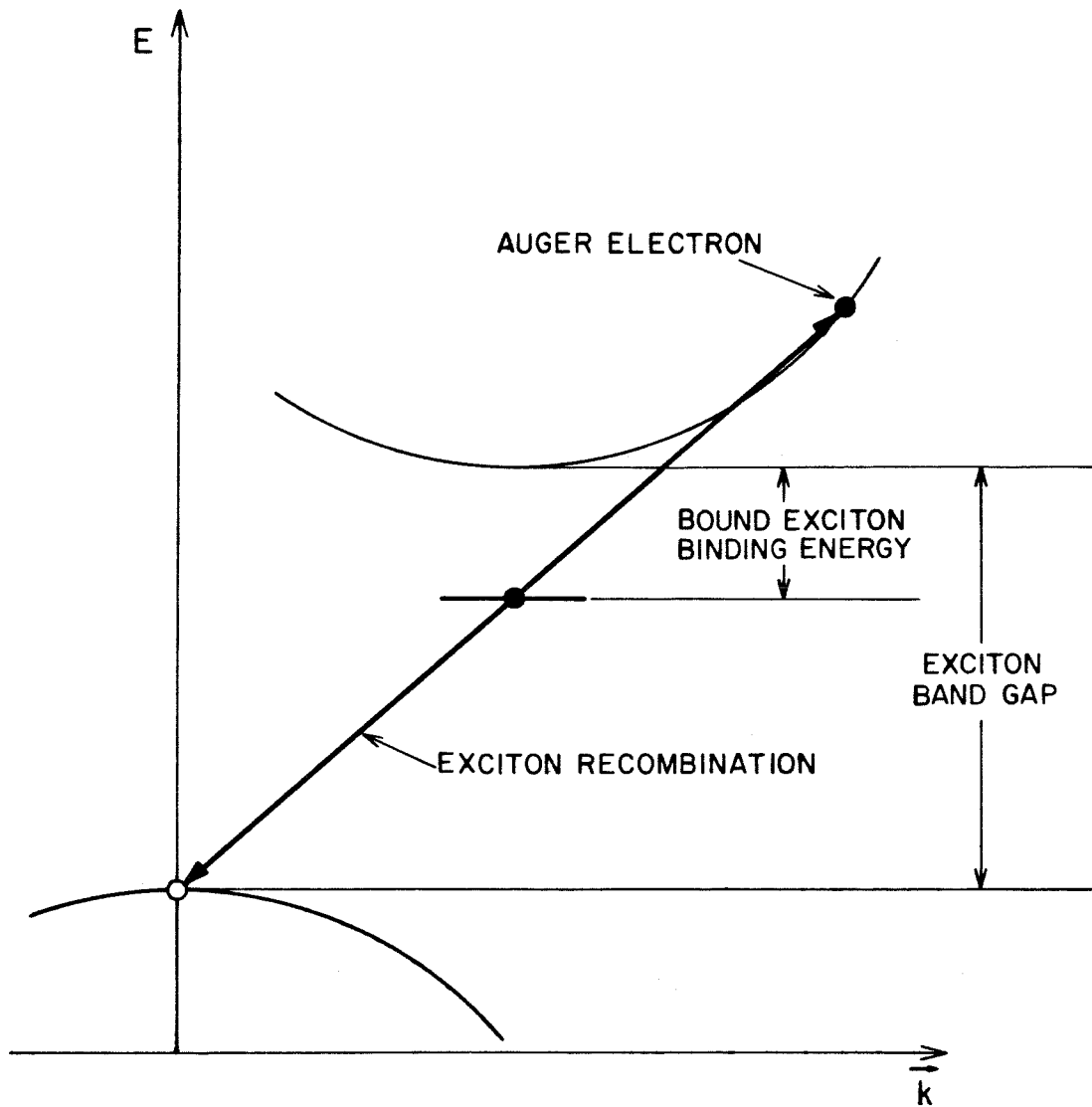


Figure 1.3. Schematic illustration of Auger recombination for excitons bound to a neutral donor impurity. The exciton band gap energy is the semiconductor band gap energy minus the free exciton binding energy. The level shown is a schematic representation of the donor bound exciton state. Note that the Auger electron conserves both energy and wavevector.

are the dominant mechanisms by which the optically excited indirect semiconductor returns to equilibrium at low temperatures. At high optical excitation intensities, however, further relaxation to other excitonic states may occur. We mention two examples here.

As the free exciton density increases, it becomes possible for two free excitons to bind together, forming a free excitonic molecule or biexciton. In this case, two free electrons and two free holes are bound by their mutual Coulomb interaction. Two radiative recombination processes have been observed for this free exciton complex. In the first, one electron-hole pair recombines radiatively (with phonon assistance), leaving behind a free exciton ⁽⁹⁾. This process is analogous to the recombination of a simple free exciton, which was discussed in Section 1.2.2.2. In the second, total radiative annihilation of the biexciton occurs ⁽¹⁰⁾. It is interesting to note that this process does not require phonon assistance. The two electrons in the complex can recombine from opposite conduction band minima in \vec{k} -space, thereby satisfying the momentum conservation requirement.

At high free exciton densities, it is also possible for more than one free exciton to bind to a neutral donor or acceptor impurity, forming bound multiexciton complexes. These bound multiexciton complexes can decay in a manner analogous to the recombination of a simple bound exciton, which was considered in Section 1.1.2.4. In this case, radiative or Auger recombination of one electron-hole pair can occur, leaving behind a complex with one less bound exciton. In addition, what appears to be the simultaneous radiative recombination of two

electrons with two holes has also been observed for bound multiexciton complexes ⁽¹⁰⁾. This recombination process is obviously not possible for simple bound excitons.

1.3 PREVIOUS APPLICATION TO DOPED Si

The photoluminescence technique described in the previous section has been applied with considerable success to intrinsic and lightly doped extrinsic Si. In general, the technique has been applied to identify the various relaxation paths described in the previous sections, and to examine the different excitonic states that occur during this relaxation. In addition, the relaxation kinetics have been examined in an effort to determine which processes dominate the return to equilibrium. Finally, in some cases quantitative analysis of the photoluminescence spectrum has resulted in detailed information about the equilibrium properties of the system. In this section we briefly consider these previous applications of the photoluminescence technique.

1.3.1 Investigation of the Free Exciton and Bound Exciton States

In early experiments on undoped Si, the free exciton recombination processes described in Section 1.2.2.2 were observed, and as a general rule were correctly interpreted ⁽¹¹⁾. The first observation of the bound exciton recombination processes described in Section 1.2.2.4 occurred in 1960 ⁽⁴⁾. Since that time, photoluminescence from Si lightly doped with various donor and acceptor impurities has been studied experimentally in some detail. The luminescence associated with

the different Group III acceptors and Group V donors has been identified (12,13). High resolution experiments have revealed fine structure in the luminescence features associated with transitions from excited bound exciton states (14-19). Transitions to excited states of the neutral impurity atoms have also been observed (12,18,20,21). At higher excitation intensities, luminescence from free biexcitons has been observed (9,10). Bound multiexciton complexes have also been observed, and studied in great detail (15,17-20,21-26). At this point, then, the various excitonic states and recombination processes which exist for donor and acceptor doped Si have been identified.

1.3.2 Investigation of Relaxation Kinetics

In conjunction with the investigations described above, observations of the time dependence of luminescence have indicated which relaxation processes dominate as the optically excited system returns to equilibrium. Time dependent measurements of bound exciton recombination luminescence (27,28) has established the strong domination of the Auger recombination mechanism in Si (8,29). In addition, acceptor free exciton capture cross sections have been measured. Finally, certain properties of the electronic structure of bound multiexciton complexes have been established on the basis of exacting measurements of bound exciton luminescence decay. (26,32)

1.3.3 Measurement of Impurity Concentrations

In the studies described above, the details of the relaxation

processes which return the optically excited semiconductor to equilibrium have been examined. However, the photoluminescence technique has also been applied to investigate equilibrium properties of the system itself. For instance, the photoluminescence technique provides a measure of the semiconductor band gap energy. Also, qualitative examination of the photoluminescence spectrum provides information concerning the presence of impurities in the material, and usually some indication of their identity.

In addition, in some cases it has been possible to quantitatively analyze the photoluminescence spectrum in terms of impurity concentrations. This analysis has been possible only in particularly simple systems in which the photoluminescence spectrum is very well understood. In particular, Si lightly doped with B and P impurities has been considered ^(33,34). In the initial investigations of this type, misleading results were obtained because the effect of saturation of impurity centres with bound excitons was not properly accounted for ⁽³³⁾. However, subsequent work has taken this effect into account ⁽³⁴⁾. It now appears that the photoluminescence spectrum of lightly doped Si:(B,P) system is quantitatively as well as qualitatively well understood.

1.4 APPLICATIONS OF CURRENT INTEREST

As the discussion in the previous section has indicated, the photoluminescence technique has been applied very successfully to the study of the properties of Si doped with relatively low concentrations of simple substitutional donor and acceptor impurities. Currently,

however, there is considerable interest in extending this application to more complex systems which are frequently of very definite technological interest. In this section we will consider briefly a few of these areas of current interest.

1.4.1 Heavily Doped Semiconductors

In technological applications, impurity doping levels are generally much higher than they are in the relatively lightly doped material we have considered so far. As a result, there is interest in using the photoluminescence technique to examine the effects which result from increasing impurity concentrations. As indicated in the previous sections, our understanding of the photoluminescence spectrum of Si lightly doped with donor and acceptor impurities is relatively complete. As a natural extension of this work, the examination of the photoluminescence from heavily doped Si:P has received recent attention (35-43). As the doping level increases, the bound exciton luminescence is observed to broaden and shift to lower energies (40,42). These lower energy features are thought to correlate with the formation of nearest-neighbour impurity clusters (42,43). Eventually, the effect of impurity band formation is observed (37,39). However, detailed understanding of these high concentration effects will be obtained only after further investigation of Si:P and other systems.

1.4.2 Irradiated Semiconductors

In the fabrication of Si based integrated circuits, various irradiation processes are commonly employed. Doping as a result of ion implantation or neutron transmutation and electron beam lithography are examples of this type of treatment. Generally, these processes produce a wide variety of defects and defect clusters in the irradiated material, which can have complicated electronic characteristics and anneal behaviour. As a result, there is considerable interest in the use of the photoluminescence technique to examine irradiated semiconductors. Since the luminescence from lightly doped Si is so well characterized, Si is a logical material on which to base such investigations. Some work in this general area has been done ⁽⁴⁴⁻⁴⁷⁾, but there is room for considerable further investigation.

1.4.3 Defect Clusters in Semiconductors

The interest in heavily doped and irradiated semiconductors discussed in the previous sections has directed attention toward the general question of defect and defect/impurity complexes in semiconductors. Once again, Si is a material which is well understood and well characterized, and so forms a logical base from which to proceed with such investigations. At the present time, it is thought

that In-C complexes (a shallow acceptor called the "X-level" in Si:In)^(48,49), isoelectronic complexes (C clusters in Si:C)⁽⁵⁰⁾ and the "P,Q,R" lines in Si:In⁽⁵¹⁾, O donor complexes⁽⁵²⁻⁵⁶⁾ and O-C complexes⁽⁵⁶⁾ all exist in relatively "routine" Si samples.

The photoluminescence spectrum is usually sensitive to the presence of these complexes. As a result, use of the photoluminescence technique appears particularly promising in this application.

1.4.4 Alloy Semiconductors

The compositional disorder inherent in alloy semiconductors has been the subject of experimental and theoretical interest for some time. In addition, the fact that the band gap can be varied with alloy composition has resulted in considerable technological interest. These properties of alloy semiconductors are reflected in their photoluminescence spectra, which in general provide useful and relatively easily interpreted information. Current interest exists in applying the photoluminescence technique to the III-V and II-VI ternary alloys⁽⁵⁷⁻⁶⁰⁾. A notable example is $\text{Hg}_{1-x}\text{Cd}_x\text{Te}$ ⁽⁶⁰⁾, in which band-to-band, band-to-acceptor, donor-to-acceptor and bound exciton luminescence has been observed and identified. A second example is Si-rich $\text{Si}_{1-x}\text{Ge}_x$. In this case, the extensive understanding of Si luminescence properties which was described in the previous sections can be employed to permit a detailed interpretation of luminescence from the alloy. A more thorough discussion of this application of the photoluminescence technique can be found in Chapter 4,

1.5 GENERAL EXPERIMENTAL CONSIDERATIONS

There are certain general features associated with the application of the photoluminescence technique to the systems considered in this thesis. In this section, some of these general considerations are discussed.

1.5.1 Material Properties

In Chapters 2 and 3, the photoluminescence technique is applied to Si doped with various donor and acceptor impurities. As we have previously discussed, Si has been the subject of considerable investigation. The bulk material properties have been extensively examined and are well documented. Some of the more relevant properties are listed in Table 1.1.

The electronic excitation and relaxation characteristics of Si are very dependent on its band structure. A calculation of the Si band structure is shown in Fig. 1.4. As this figure illustrates, Si has an indirect band gap of approximately 1.166 eV at 0 K. The valence band maximum occurs at $\vec{k} = 0$, while the conduction band minimum occurs at $\vec{k} \sim (0.85, 0, 0) \frac{2\pi}{a}$, where a is the Si lattice constant. As we have discussed, this implies that free exciton recombination in Si must be phonon assisted. The phonon dispersion curves for Si are shown in Fig. 1.5. We see that phonons with the appropriate wavevector are the 19 meV transverse acoustic (TA) phonon, the 41 meV longitudinal acoustic (LA) phonon, the 56 meV

Table 1.1. Properties of Si and Ge.

	ENERGY GAP, E_g (eV)		LOWEST CONDUCTION BAND MINIMUM (Indirect)	$\left(\frac{dE_g}{dt}\right)_{300\text{K}}$ (ev/K)	$\left(\frac{dE_g}{dP_g}\right)_T$ (eV/bar)	EFFECTIVE MASS			REFRACTIVE INDEX, n	STATIC DIELECTRIC CONSTANT, ϵ	LATTICE CONSTANT, a (Å)	MOBILITY ($\text{cm}^2/\text{V}\cdot\text{sec}$)	
	0 K	300 K				m_e^*	m_t	m_h^*				μ_e	μ_h
Si	1.166	1.11	100	-2.3×10^{-4}	-1.5×10^{-6}	0.98	0.19	0.52	3.44	11.7	5.43	1350	480
Ge	0.74	0.67	111	-3.7×10^{-4}	5.0×10^{-6}	1.58	0.08	0.3	4.00	16.3	5.66	3900	1900

(J. I. Pankove, Optical Processes in Semiconductors (Dover Publications, Inc., New York, 1971))

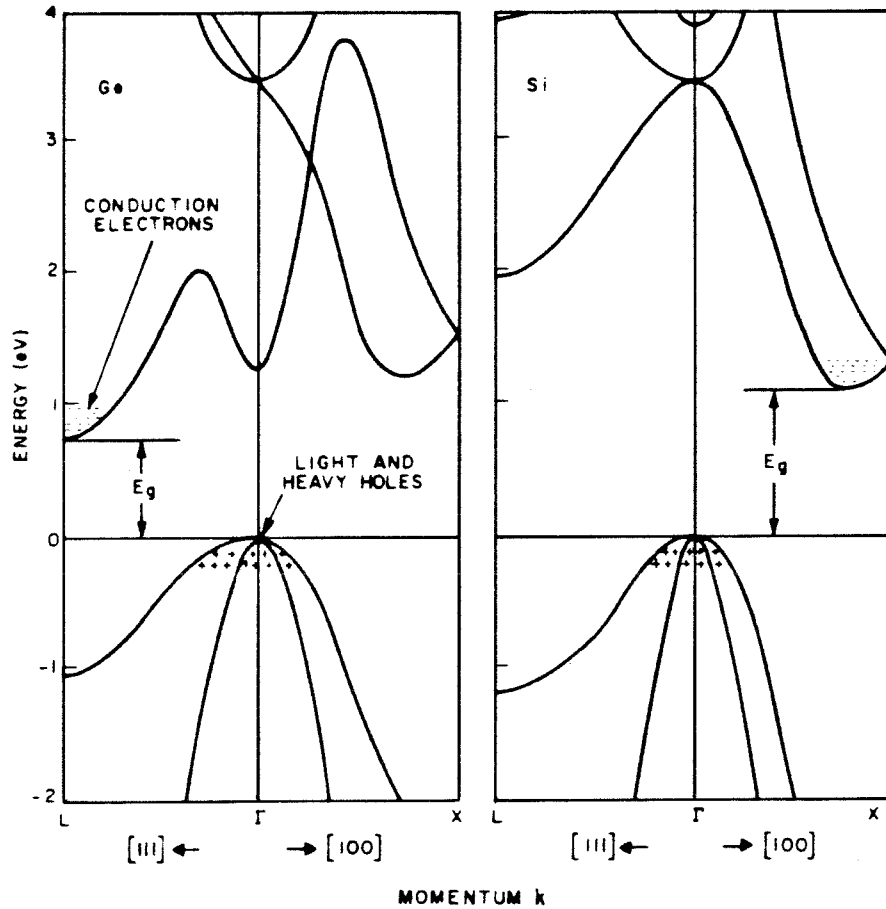


Figure 1.4. Si and Ge band structures. The energy gap is indicated by E_g . "+" signs indicate holes in the valence band and "-" signs indicate electrons in the conduction band. In both band structures, the valence band maximum is at $\vec{k} = 0$. For Ge, the conduction band minimum occurs at $\vec{k} = (1,1,1) \frac{2\pi}{a}$. For Si, the conduction band minimum occurs at $\vec{k} = (0.85,0,0) \frac{2\pi}{a}$.

(S. M. Sze, Physics of Semiconductor Devices (Wiley-Interscience, New York, N.Y., 1969) p. 22)

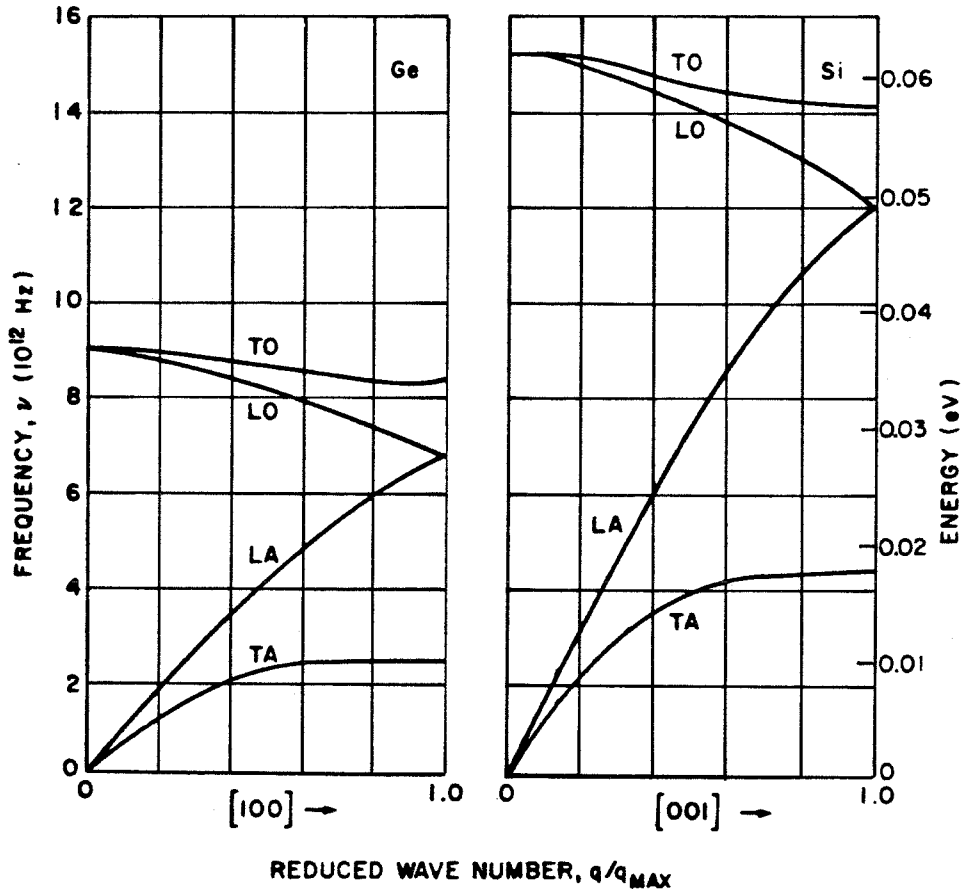


Figure 1.5. Si and Ge phonon dispersion curves. The transverse acoustic (TA), longitudinal acoustic (LA), longitudinal optical (LO) and transverse optical (TO) branches are shown. Radiative recombination in Si involves the assistance of $q = (0.85, 0, 0) \frac{2\pi}{a}$ TA, LO or TO phonons. The energies of these phonons are approximately 19 meV, 56 meV and 58 meV, respectively.

(S. M. Sze, Physics of Semiconductor Devices (Wiley-Interscience, New York, N.Y., 1969), p.51)

longitudinal optical (LO) phonon and the 58 meV transverse optical (TO) phonon.

The introduction of donor and acceptor impurities into the bulk Si introduces new levels in the band gap. These levels are shown in Fig. 1.6 for a wide variety of impurities. In the materials studied in Chapters 2 and 3, the primary impurities are P, B and In. These impurities have ionization energies of 45.5 meV, 44.5 meV and 155 meV, respectively, and are therefore relatively shallow.

Many of the properties of the Si-rich Si-Ge alloy semiconductors studied in Chapter 4 are qualitatively similar to those of Si. However, the presence of 10% Ge atoms mixes in some of the characteristics of Ge, and produces quantitative differences.

One of the major differences between Si and Ge lies in the band structure. In Fig. 1.4, we show the band structure of Ge as well as the band structure of Si. While both materials have indirect band gaps, Ge has a smaller gap energy. It is about 0.74 eV at 0 K. In addition, the conduction band minimum lies at $\vec{k} = (1,1,1) \frac{2\pi}{a}$. As a result of these differences, the Si-Ge alloy band gap energy shows a variation with alloy composition, which is shown in Fig. 1.7. At low Ge concentrations, we see a variation with composition which is characteristic of the $\langle 100 \rangle$ conduction band minimum in Si. At high Ge concentrations, we see a variation with composition which is characteristic of the $\langle 111 \rangle$ conduction band minimum in Ge. The two minima are at the same energy for a Ge concentration of approximately 15%.

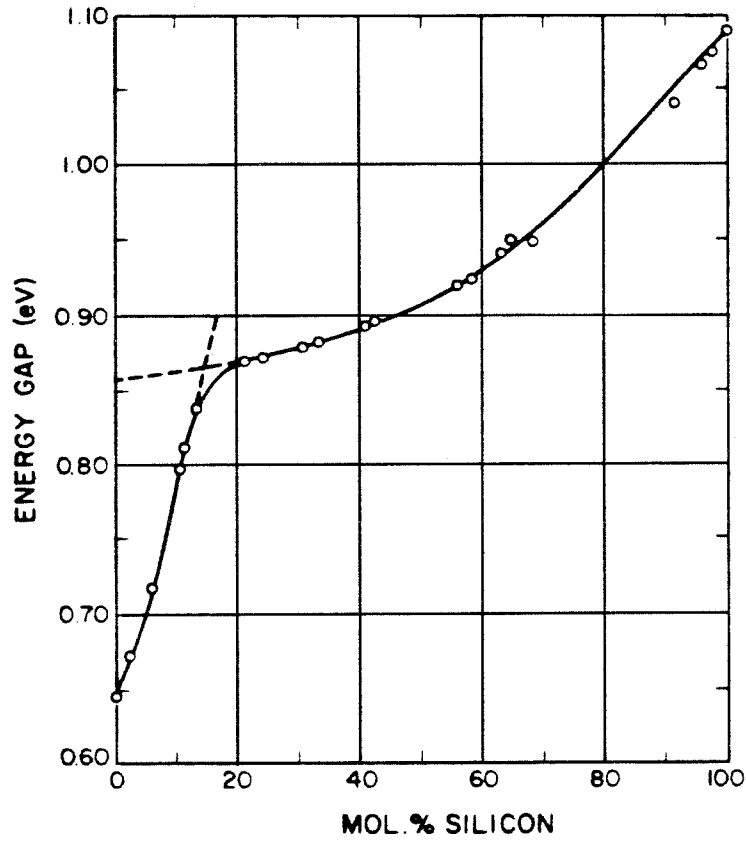


Figure 1.7. Composition dependence of the band gap in Si-Ge alloys at 296 K.
(R. Braunstein, A. R. Moore and F. Herman, Phys. Rev. 109, 695 (1958))

There are other differences between Si and Ge which also have an effect on the alloy. For example, the phonon dispersion curves for Ge are shown in Fig. 1.5 along with those for Si. We see that the phonon energies in Ge are typically lower. As a result, we expect that the phonon energies in the alloy will be somewhat lower than those in Si. Similarly, we see in Fig. 1.6 that the impurity ionization energies for the shallow donors and acceptors are typically lower in Ge than they are in Si. We expect, therefore, that ionization energies in the alloy will be lower than those observed in Si. These effects can all be observed in the photoluminescence spectrum of the alloy.

1.5.2 Experimental Apparatus

The applications of the photoluminescence technique described in Chapters 2, 3 and 4 were accomplished with the experimental apparatus schematically depicted in Fig. 1.8. The samples being examined were lapped and chemically etched to ensure a smooth, damage-free surface. Then the samples were placed in a Janis Super Varitemp dewar, in which the measurement temperature could be varied between 1.4 K and room temperature. Sample temperatures were measured with a Lakeshore Cryotronics Ge resistor, mounted in the sample holder in close proximity to the sample. Temperature control was accomplished with a Lakeshore Cryotronics temperature controller, in conjunction with a Si diode temperature sensor and sample block heater.

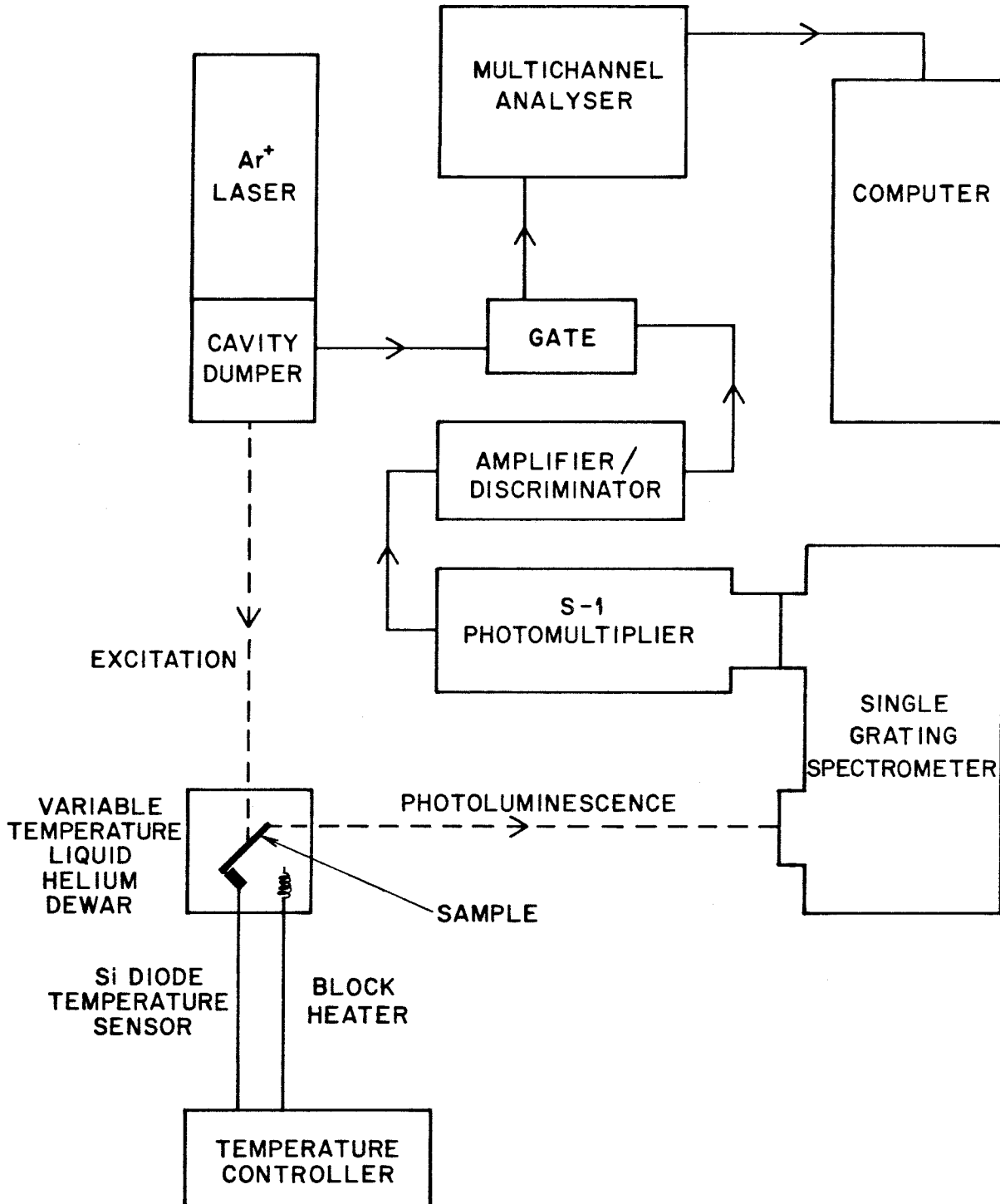


Figure 1.8. Schematic illustration of the photoluminescence experiment, as described in the text.

The primary source of optical excitation was a Spectra Physics Model 165 Ar⁺ laser operated in cw mode. The laser was equipped with a cavity dumper for pulsed mode operation, which enabled observation of the time dependence of the photoluminescence intensities. For the pump power and surface preparation experiments described in Chapter 3, a 5 mW HeNe laser was used. Also, for the time dependence measurements discussed in Chapter 3, a pulsed GaAs laser mounted directly on the sample holder was used.

We can examine the effect of these optical excitations by referring to Fig. 1.9. In this figure, the absorption coefficient as a function of photon energy is shown for Si and Ge. At energies which are less than the semiconductor band gap, the absorption coefficient is very small. However, for above-band-gap excitation the absorption coefficient is appreciable. For Ar⁺ laser photons (primarily 5145 Å) the absorption length in Si is approximately 2 μm. For HeNe laser photons (6328 Å) it is about 7 μm, and for GaAs laser photons (8500 Å) it is approximately 60 μm. These absorption lengths indicate that the lasers produce optical excitation of the bulk material.

The luminescence from the optically excited samples was wavelength analyzed with a Spex Model 1269 single-pass spectrometer, and detected with an S-1 photomultiplier (RCA 7102) cooled to liquid nitrogen temperature. The data was acquired in photon counting mode. Pulses from the photomultiplier were sent through a PAR amplifier/discriminator circuit, and accumulated in an ND 60 multichannel

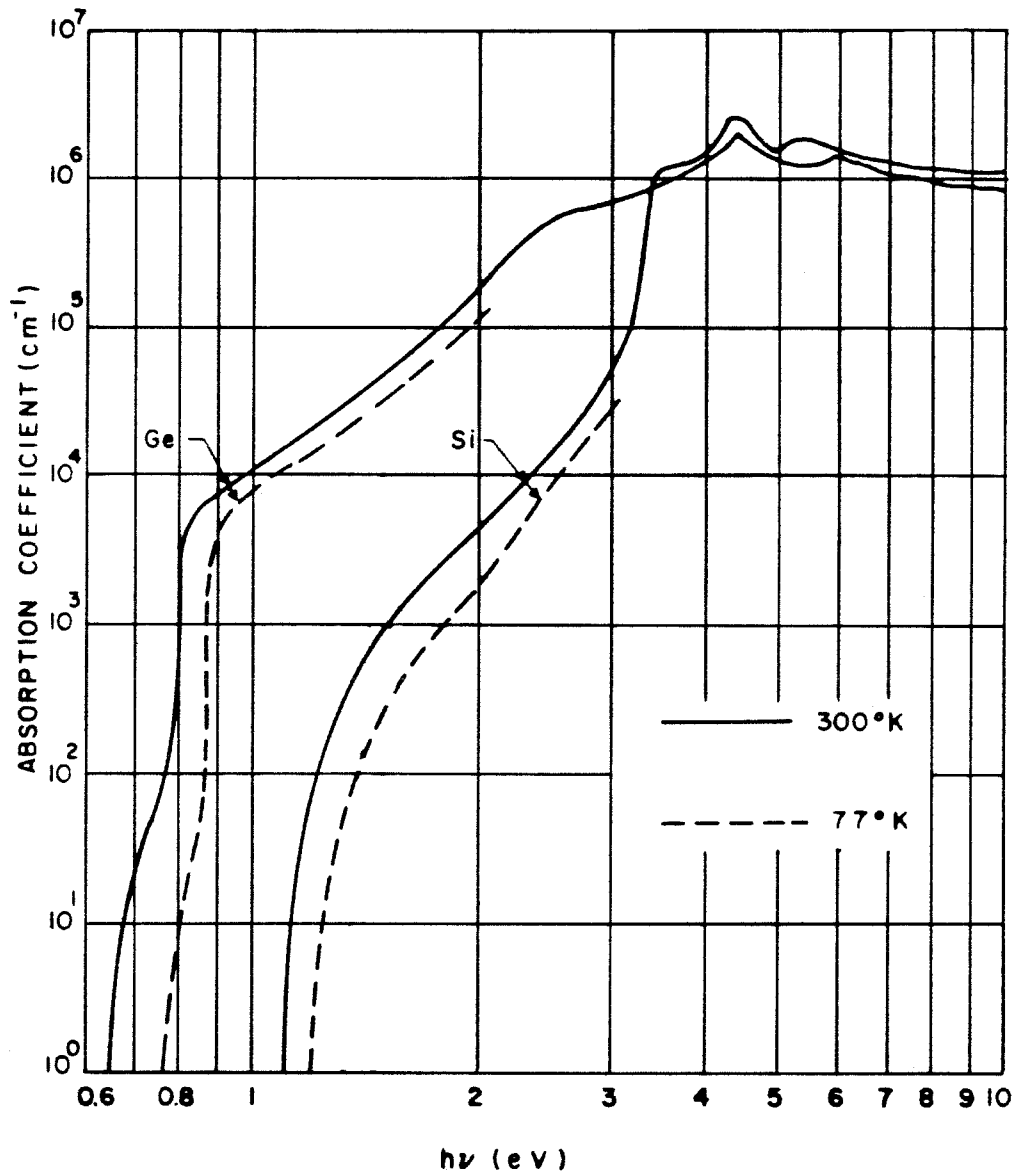


Figure 1.9. The absorption coefficient of Si and Ge as a function of photon energy, for energies near the band gap energy. Absorption coefficients at 77 K and 300 K are shown.

(S. M. Sze, Physics of Semiconductor Devices, (Wiley-Interscience, New York, N.Y. 1969), p. 54)

analyzer. From the multichannel analyzer, the data was sent to a PDP 11/34 computer for analysis and storage.

1.5.3 Experimental Conditions

The experimental apparatus described in the previous section allows us to apply the photoluminescence technique to the study of indirect semiconductors such as Si and Si-Ge at low temperatures. Fundamentally, of course, this apparatus allows us to obtain the photoluminescence spectrum of the optically excited material for a given set of experimental conditions. This spectrum can then be analyzed to determine luminescence lineshapes, integrated intensities, peak energies, and so on. Systematic variation of the experimental conditions enables us to obtain specific information about the equilibrium properties of the systems under study, as well as about their response to excitation and the mechanisms responsible for return to equilibrium. We consider the effect of variation of certain of these experimental parameters here.

1.5.3.1 Excitation Intensity

Measurement of the dependence of luminescence intensities on the optical excitation intensity can provide information about exciton complex formation, since luminescence from exciton complexes increases with excitation intensity relative to luminescence from solitary

excitons. The intensity of luminescence from solitary excitons is directly proportional to the excitation intensity, until high free exciton densities are obtained. Then saturation effects are observed. The observation of intensity saturation can provide information about impurity concentrations and the kinetics of the relaxation and recombination processes.

1.5.3.2 Sample Temperature

Measurement of the dependence of luminescence intensities on temperature can provide information about the presence of excited exciton states, which become populated as the temperature increases. As well, information can be obtained about the thermal binding energies of excitons bound to impurities.

1.5.3.3 Time Delay

Measurement of the dependence of luminescence intensities on time after optical excitation can provide information about the kinetics of the relaxation and recombination processes which return the system to equilibrium. The parameters which govern these processes, such as thermal binding energies and exciton capture cross sections, can be measured and their relative importance for a given set of experimental conditions can be determined.

1.5.3.4 Sample Characteristics

Measurement of the dependence of luminescence intensities on sample characteristics can provide important information about the

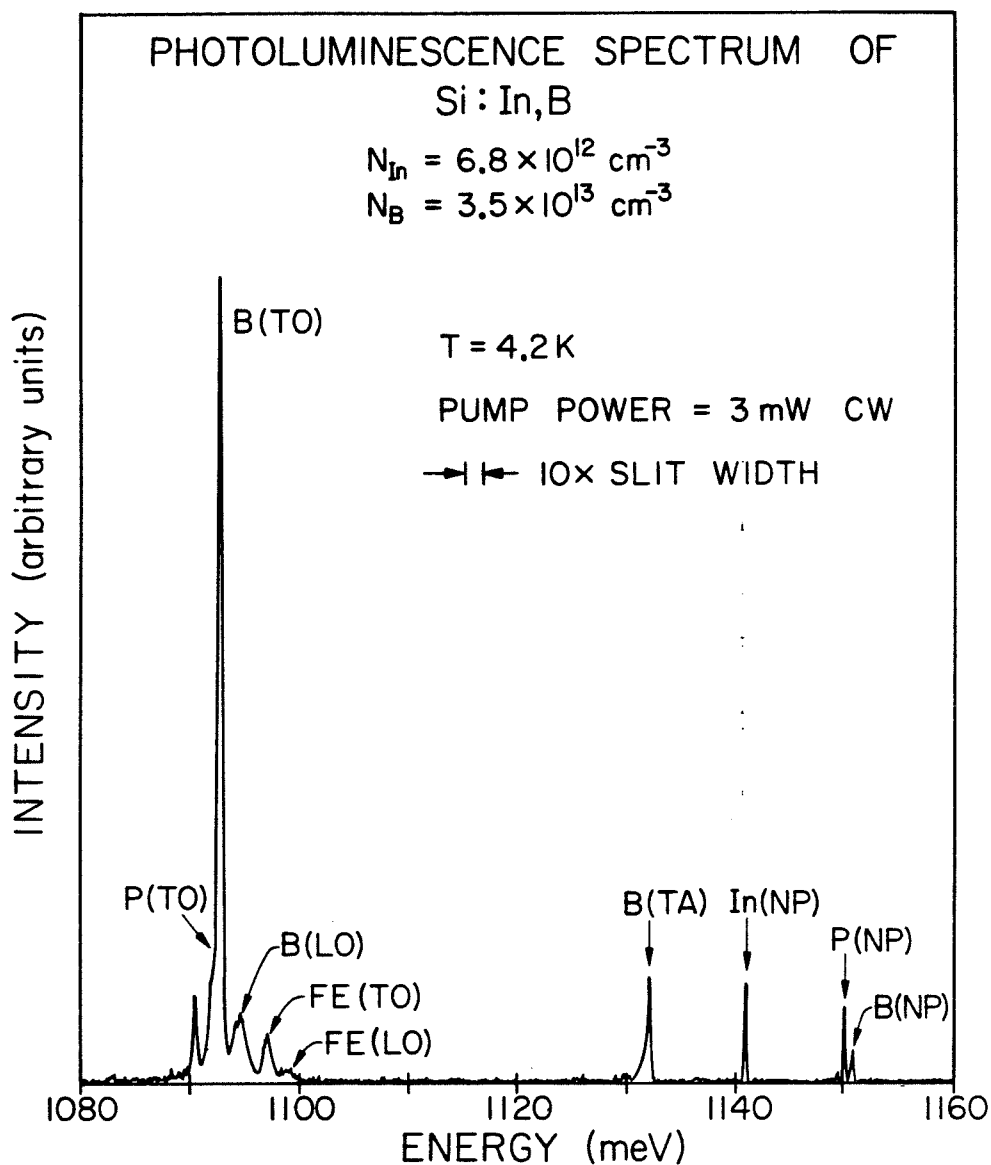


Figure 1.10. Typical photoluminescence spectrum of Si:(B,P,In). Transverse optical (TO) and longitudinal optical (LO) phonon assisted free exciton recombination luminescence is observed. These lines are labelled FE(TO) and FE(LO), respectively. In addition, no-phonon (NP) bound exciton recombination luminescence is observed for excitons bound to P, B and In impurities. These lines are labelled P(NP), B(NP) and In(NP), respectively. Various replicas of these lines are also observed. Transverse acoustic (TA), and TO and LO phonon assisted B bound exciton recombination luminescence is observed. These lines are labelled B(TA), B(TO) and B(LO), respectively. Finally, TO phonon assisted P recombination luminescence is observed. This line is labelled P(TO).

Table 1.2. Properties of free excitons in Si and Ge.

	BOHR RADIUS, (a) a_0^* (Å)	DISSOCIATION ENERGY, E_D (meV)	EFFECTIVE MASS, (d) m_{ex}^*	LIFETIME, (d) τ_{FE} (µsec)
Si	43	14.7 (b)	0.6 m_0	~ 2
Ge	114	4.15 (c)	0.335 m_0	~ 7

(a) Obtained using $E_D = \frac{e^2}{2\epsilon_0 a_0^*}$

(b) K. L. Shaklee and B. Nahory, Phys. Rev. Lett. 24, 942 (1970).

(c) G. A. Thomas, A. Frova, J. C. Hensel, R. E. Miller and P. A. Lee, Phys. Rev. B13, 1692 (1976).

(d) S. A. Lyon, Ph. D. Thesis, California Institute of Technology 1979.

be seen on this intensity scale.

In an optically excited semiconductor doped with donor and acceptor impurities, formation of bound excitons also occurs. Some of the properties of excitons bound to the Group III acceptor and Group V donor impurities in Si are listed in Table 1.3. The photoluminescence spectrum shown in Fig. 1.10 reflects the formation of these bound excitons. No-phonon (NP) bound exciton recombination luminescence is observed for excitons bound to P, B and In impurities. These lines are labelled P(NP), B(NP) and In(NP), respectively. In addition, replicas of the NP B bound exciton luminescence are observed which result from TA, TO and LO phonon assisted recombination. In principle, replicas resulting from TA, LA, TO and LO phonon assisted recombination should be observed for all the NP bound exciton lines. The absence of particular TA, LO or TO replicas is just the result of the measurement sensitivity and the intensity scale. However, LA phonon assisted recombination is never observed in Si. The absence of this phonon replica is not understood.

1.6 SUMMARY OF RESULTS

As a result of our application of the photoluminescence technique to the Si and Si-Ge alloy systems, we obtain the following results:

1.6.1 Chapter 2

(i) A model for the photoluminescence spectrum of lightly doped semiconductors is developed. At low excitation intensities, where saturation effects can be neglected, quantitative analysis of the

Table 1.3. Properties of bound excitons in Si.

	IMPURITY	IMPURITY IONIZATION ENERGY (meV)	BOUND EXCITON DISSOCIATION ENERGY (meV)	BOUND EXCITON LIFETIME (nsec)	NO-PHONON BOUND EXCITON LINE POSITION (meV)
DONORS	Li	33 (a)	3.4 (c)	1150 (h)	1151.2 (g)
	Sb	42.7 (b)	4.64 (d)		1150.0 (g)
	P	45.5 (b)	4.7 (g)	272 (h)	1149.9 (f)
	As	53.7 (b)	5.51 (d)	80 (h)	1149.1 (g)
	Bi	69 (a)	7.71 (d)		1146.9 (g)
ACCEPTORS	B	44.5 (b)	3.9 (g)	1006 (i)	1150.7 (f)
	Al	68.5 (b)	5.1 (g)	104 (j)	1149.5 (f)
	Ga	72 (b)	5.7 (g)	58 (j)	1148.9 (f)
	In	155 (b)	13.7 (g)	2.7 (h)	1140.9 (f)
	Tl	260 (a)	44.2 (g)		1110.4 (e)

- (a) S. M. Sze, *Physics of Semiconductor Devices*, (Wiley-Interscience, New York, 1969) p. 30.
 (b) F. Bassani, G. Iadonisi and B. Preziosi, *Rep. Prog. Phys.* 37, 1099 (1974).
 (c) K. Kosai and M. Gershenzon, *Phys. Rev. B9*, 723 (1974).
 (d) E. C. Lightowers, M. O. Henry and M. A. Vouk, *J. Phys.* C10, L713 (1977).
 (e) K. R. Elliott, D. L. Smith and T. C. McGill, *Solid State Commun.* 27, 317 (1978).
 (f) S. A. Lyon, Ph. D. Thesis, California Institute of Technology, 1979.
 (g) Obtained using a FE (NP) threshold energy of 1154.6 meV.
 (h) W. Schmid, *Phys. Stat. Sol. (b)* 84, 529 (1977).
 (i) R. Sauer, *Proceedings of the Twelfth International Conference on the Physics of Semiconductors*, edited by H. M. Pilkun, (Teubner, Stuttgart, 1974) p. 42.
 (j) S. A. Lyon, G. C. Osbourn, D. L. Smith and T. C. McGill, *Solid State Commun.* 23, 425 (1977).

photoluminescence spectrum in terms of impurity concentrations is possible for these semiconductors.

(ii) The predictions of the model are tested by examining the Si:(B,In) system. In particular, the effect of increasing the In concentration is considered. Care is taken to ensure that saturation effects are not present during the measurements. For In concentrations above 10^{15}cm^{-3} , we observe that quenching of B luminescence occurs, and the predictions of the simple model become invalid. For In concentrations above $2 \times 10^{16} \text{cm}^{-3}$, B luminescence is not observed in any sample studied.

(iii) A modification to the photoluminescence model is proposed, which includes the effect of exciton transfer from B to In impurities. When the exchange mechanism is assumed for exciton transfer in Si, agreement with the experimental results is quite good. We propose, therefore, that exciton transfer begins to occur above In concentrations of 10^{15}cm^{-3} . This is the first observation of exciton transfer in Si.

1.6.2 Chapter 3

(i) Detailed measurements of the photoluminescence spectrum of moderately doped Si:In are made. A large number of previously unobserved features are observed and tabulated. Three of these features are labelled "P,Q,R" and studied in detail.

(ii) The P,Q,R lines are only observed in Si doped with In.

This result suggests that the P,Q,R lines are the result of recombination of excitons bound to a complex which involves In.

(iii) Measurements of the dependence of P,Q,R luminescence intensity on time after excitation are made. These measurements revealed that the "P,Q,R" lines have extremely long lifetimes, orders of magnitude longer than the lifetimes observed for bound excitons in Si. This suggests that lines P,Q,R are due to recombination of excitons bound to an isoelectronic complex in Si. This is the first observation of luminescence from an isoelectronic centre in Si.

(iv) Measurements of the temperature dependence of P,Q,R luminescence intensity are made. These measurements reveal that the P/R luminescence intensity ratio is independent of temperature, which suggests that lines P and R are due to transitions from the same initial state of the complex. The width of line R suggests that line R is a local phonon mode replica of line P. Line Q appears only at high temperatures, which suggests that line Q is due to a transition from an excited state of the bound exciton complex.

(v) The pump power dependence of P,Q,R line luminescence intensities is measured. The P/R luminescence intensity ratio is independent of pump power. This result supports the suggestion that line R is a local mode replica of line P.

(vi) Detailed temperature dependent lifetime measurements are made. The same general temperature dependence is observed for the three lines, which is qualitatively explained on the basis of the

presence of a somewhat longer lifetime for the excited state of the bound exciton complex. A quantitative model was proposed for the observed behaviour. In the high temperature regime, where thermalization dominates, application of the model produces values for the exciton thermal binding energies. These results support the suggestion that lines P,Q,R result from recombination of excitons bound to an isoelectronic complex. They also support the suggestion that line R is a local phonon mode replica of line P.

(vii) The P,Q,R luminescence intensities are observed to be extremely dependent on the details of the surface preparation of the sample. This is the first observation of surface sensitive photoluminescence.

1.6.3 Chapter 4

(i) The photoluminescence spectra of undoped $\text{Si}_{1-x}\text{Ge}_x$ for $x = 0.11$ and $x = 0.067$ were examined in detail for the first time. No-phonon free exciton recombination luminescence is identified, and the no-phonon free exciton luminescence threshold is obtained.

(ii) Bound exciton luminescence associated with residual B impurities in the material is identified. A model was proposed to explain the observed broadening of the bound exciton line, based on the nearest-neighbour configuration of Ge atoms.

(iii) On the basis of this model, comparison with the Si luminescence spectrum is made. A determination of the band gap shift and the shift in free exciton binding energy for the $x = 0.11$ and $x = 0.067$ alloys is made.

(iv) At very low temperatures, a shifting and broadening of the free exciton line is observed. This feature is attributed to the filling of tail states which are formed in the free exciton density of states as a result of the alloy compositional disorder.

(v) The photoluminescence spectrum of $\text{Si}_{1-x}\text{Ge}_x\text{In}$ for $x = 0.10$ is also examined for the first time. Free exciton recombination luminescence is observed and a free exciton threshold energy is obtained.

(vi) Bound exciton luminescence associated with In and residual P impurities in the material is observed. Combinations of time and temperature resolution are employed to systematically isolate and identify these components.

(vii) Measurement of the free exciton threshold results in a determination of the band gap shift for the $x = 0.10$ alloy.

REFERENCES

1. J. I. Pankove, Optical Processes in Semiconductors, (Dover Publications, Inc., New York, N.Y., 1971).
2. J. C. Hensel and K. Suzuki, Phys. Rev. B9, 4219 (1974).
3. R. B. Hammond, D. L. Smith, and T. C. McGill, Phys. Rev. Lett. 35, 1535 (1975).
4. J. R. Haynes, Phys. Rev. Lett. 4, 361 (1960).
5. D. G. Thomas, J. J. Hopfield, and C. J. Frosch, 15, 857 (1965).
6. P. J. Dean, J. Lumin. 7, 51 (1973).
7. J. J. Hopfield, D. G. Thomas, and R. T. Lynch, Phys. Rev. Lett. 17, 312 (1966).
8. G. C. Osbourn, S. A. Lyon, K. R. Elliott, D. L. Smith, and T. C. McGill, Solid-State Electron, 21, 1339 (1978).
9. M. L. W. Thewalt and J. A. Rostworowski, Solid State Commun. 25, 991 (1978).
10. W. Schmid, Phys. Rev. Lett. 45, 1726 (1980).
11. See, for example, J. R. Haynes, M. Lax and W. F. Flood, J. Phys. Chem. Solids 8, 392 (1959).
12. P. J. Dean, J. R. Haynes, and W. F. Flood, Phys. Rev. 161, 711 (1967).
13. M. A. Vouk and E. C. Lightowers, J. Lumin. 15, 357 (1977).
14. M. A. Vouk and E. C. Lightowers, Proceedings of the Thirteenth

International Conference on the Physics of Semiconductors,

Rome, 1976, edited by F. G. Fumi, (Tipografia Marves, Rome, 1977),
p. 1098.

15. E. C. Lightowers and M. O. Henry, J. Phys. C, 10, L247 (1977).
16. E. C. Lightowers, M. O. Henry, and M. A. Vouk, J. Phys. C, 10,
L713 (1977).
17. M. L. W. Thewalt, Phys. Rev. Lett. 38, 521 (1977); Solid State
Commun. 21, 937 (1977).
18. M. L. W. Thewalt, Can. J. Phys. 55, 1463 (1977).
19. S. A. Lyon, D. L. Smith, and T. C. McGill, Phys. Rev. B 17,
2620 (1978).
20. R. Sauer, J. Lumin. 12/13, 495 (1976).
21. K. R. Elliott, S. A. Lyon, D. L. Smith, and T. C. McGill, Phys.
Lett. 70A, 52 (1979).
22. Ya. Pokrovskii, Phys. Status Solidi
23. R. Sauer, Phys. Rev. Lett. 31, 376 (1973).
24. K. Kosai and M. Gershenson, Phys. Rev. B 9, 723 (1974).
25. R. Sauer and J. Weber, Phys. Rev. Lett. 39, 770 (1977).
26. R. Sauer, W. Schmid and J. Weber, Solid State Commun. 24, 507
(1977).
27. S. A. Lyon, G. C. Osbourn, D. L. Smith, and T. C. McGill, Solid
State Commun. 23, 425 (1977).
28. W. Schmid, Phys. Status Solidi B 84, 529 (1977).

29. G. C. Osbourn and D. L. Smith, Phys. Rev. B 16, 5426 (1977).
30. K. R. Elliott, D. L. Smith and T. C. McGill, Solid State Commun. 24, 461 (1977).
31. R. M. Feenstra and T. C. McGill, Solid State Commun. 36, 1039 (1980).
32. A. T. Hunter, S. A. Lyon, D. L. Smith, and T. C. McGill, Phys. Rev. B 20, 2431 (1979).
33. M. Tajima, Jpn. J. Appl. Phys. 16, 2263 (1977); Jpn. J. Appl. Phys. 16, 2265 (1977); Appl. Phys. Lett. 32, 719 (1978).
34. H. Nakayama, T. Nishino, and Y. Hamakawa, Jpn. J. Appl. Phys. 19, 501 (1980).
35. R. E. Halliwell and R. R. Parsons, Can. J. Phys. 52, 1336 (1974).
36. R. W. Martin and R. Sauer, Phys. Status Solidi B 62, 443 (1974).
37. J. A. Rostworowski, M. L. W. Thewalt, and R. R. Parsons, Solid State Commun. 18, 93 (1976).
38. B. Bergersen, J. A. Rostworowski, M. Eswaran, R. R. Parsons, and P. Jena, Phys. Rev. B 14, 1633 (1976).
39. M. Eswaran, B. Bergersen, J. A. Rostworowski, and R. R. Parsons, Solid State Commun. 20, 811 (1976).
40. T. Nishino, H. Nakayama, and Y. Hamakawa, J. Phys. Soc. Japan 43, 1807 (1977).
41. R. R. Parsons, Can. J. Phys. 56, 814 (1978).
42. Y. Shiraki and H. Nakashima, Solid State Commun. 29, 295 (1979).

43. R. R. Parsons, *Solid State Commun.* 29, 1 (1979).
44. R. J. Spry and W. D. Compton, *Phys. Rev.* 175, 1010 (1968).
45. C. E. Jones, E. S. Johnson, W. D. Compton, J. R. Noonan, and B. G. Streetman, *J. Appl. Phys.* 44, 5402 (1973).
46. J. R. Noonan, C. G. Kirkpatrick, and B. G. Streetman, *Solid State Commun.* 15, 1055 (1974).
47. K. R. Elliott (to be published).
48. R. Baron, M. H. Young, J. K. Neeland, and O. J. Marsh, *Appl. Phys. Lett.* 30, 594 (1977).
49. R. Baron, J. P. Baukus, S. D. Allen, T. C. McGill, M. H. Young, H. Kimura, H. V. Winston, and O. J. Marsh, *Appl. Phys. Lett.* 34, 257 (1979).
50. J. Weber, W. Schmid and R. Sauer, *J. Lumin.* 18/19, 93 (1979); *Phys. Rev. B* 21, 2401 (1980).
51. G. S. Mitchard, S. A. Lyon, K. R. Elliott, and T. C. McGill, *Solid State Commun.* 29, 425 (1978); Chapter 3.
52. M. Tajima, A. Kanamori and T. Iizuka, *Jpn. J. Appl. Phys.* 18, 1401 (1979).
53. K. Yasutake, M. Umeno, H. Kawabe, H. Nakayama, T. Nishino, and Y. Hamakawa, *Jpn. J. Appl. Phys.* 19, L544 (1980).
54. H. Nakayama, J. Katsura, T. Nishino, and Y. Hamakawa, *Jpn. J. Appl. Phys.* 19, L547 (1980).

55. M. Tajima, S. Kishino, M. Kanamori, and T. Iizuka, J. Appl. Phys. 51, 2247 (1980).
56. T. Nishino, H. Nakayama, J. Katsura, and Y. Hamakawa, Appl. Phys. Lett. 38, 623 (1981).
57. A. Onton, J. Lumin. 7, 95 (1973) and references therein.
58. D. J. Wolford, R. E. Anderson, and B. G. Streetman, J. Appl. Phys. 48, 2442 (1977) and references therein.
59. Zh. I. Alferov, V. I. Amosov, D. Z. Garbuzov, Yu. V. Zhilyaev, S. G. Konnikov, P. S. Kop'ev and V. G. Trofim, Fiz. Tekh. Poluprov. 6, 1879 (1972) [Sov. Phys.-Semicond. 6, 1620 (1973)] and references therein.
60. A. T. Hunter, D. L. Smith, and T. C. McGill, Appl. Phys. Lett. 37, 200 (1980) and references therein.
61. R. Baron, M. H. Young, H. Winston, H. Kimura, G. S. Mitchard, and T. C. McGill, Proceedings of the Eleventh International Conference on Defects and Radiation Effects in Semiconductors, Japan, 1980.
62. B. L. Gel'mont, A. R. Gadzhiev, B. I. Shklovskii, I. S. Shlimak, and A. L. Efros, Fiz. Tekh. Poluprov. 8, 2377 (1974) [Sov. Phys.-Semicond. 8, 1549 (1975)].

CHAPTER 2

EFFECT OF IMPURITY CONCENTRATION
ON THE PHOTOLUMINESCENCE SPECTRUM-
A CASE STUDY OF THE Si:(B,In) SYSTEM

2.1 INTRODUCTION

The development of photoluminescence as a method for evaluating semiconductor materials has been of interest for some time, mainly as a result of the convenience of the technique and its sensitivity to small impurity concentrations. Since the first observation of impurity-related photoluminescence in Si by Haynes ⁽¹⁾ in 1960, much work has been directed towards the understanding and characterization of the luminescence spectra of various semiconductors ⁽²⁾. Only recently, however, have attempts been made to use photoluminescence as a quantitative tool for measuring impurity concentrations. At this point, only the Si:B, Si:P, and Si:(B,P) systems have been investigated, and only the low concentration regime has been considered. Tajima ⁽³⁾ attempted an empirical calibration but failed to account for saturation effects, and as a result achieved only limited success. Nakayama et al. ⁽⁴⁾ considered low-level saturation effects (that is, creation of bound multiexciton complexes), and produced a set of rate equations which were successfully used to model these systems in the low concentration regime.

Often, however, it is necessary to determine concentrations of background impurities and defects at levels substantially below that of some majority dopant present at high concentration.

The Si:(B,In) system considered in this chapter is an example of this situation. For IR detector applications, it is necessary to measure small concentrations of shallow impurities such as B in the presence of large In concentrations.

Our work reveals that while the low impurity concentration case is well understood, effects resulting from the presence of multiple impurities at high concentrations lead to luminescence spectra which are much more difficult to interpret quantitatively in terms of impurity concentrations. At impurity concentrations well below those that are of technological interest, we observe quenching of the shallow impurity luminescence. A model is proposed which includes the effect of exciton transfer from the shallow impurities to the deep impurity. Finally, by comparing the model prediction to the experimental results, a mechanism for the exciton transfer is established.

2.2 RATE MODEL OF DOPED Si PHOTOLUMINESCENCE

2.2.1 The Rate Equations

To examine the effect of increasing impurity concentrations on the Si photoluminescence spectrum, we first develop a model for the system in the low impurity concentration limit. We assume that an above-band-gap optical pump produces free excitons (FE) at a generation rate g . These FE can then decay or be captured

by impurity atoms to form bound excitons (BE). The BE can subsequently decay or be thermally released. Application of detailed balance leads to the following set of rate equations:

$$\frac{dn_{FE}}{dt} = g - (v_{FE} + \sum_i \gamma_i) n_{FE} + \sum_i \rho_i n_i \quad (2.1)$$

$$\frac{dn_i}{dt} = \gamma_i n_{FE} - (v_i + \rho_i) n_i \quad (2.2)$$

where

n_{FE} = the free exciton (FE) density

g = the FE generation rate

v_{FE} = the FE decay rate

n_i = the density of excitons bound to impurity type i
(BE_i)

v_i = the BE_i decay rate

γ_i = the rate of FE capture by impurity type i

ρ_i = the rate of thermal release of BE_i ,

The number of FE captured per unit time, $\gamma_i n_{FE}$, is proportional to the FE flux, $v_{th} n_{FE}$, and the density of capturing centres, $(N_i - n_i)$; that is

$$\gamma_i n_{FE} = \sigma_i (N_i - n_i) v_{th} n_{FE} \quad (2.3)$$

where

- σ_i = the impurity type i capture cross section for FE
 v_{th} = the FE thermal velocity
 N_i = the density of impurity type i .

Application of detailed balance and mass action yields the following result for the rate of thermal release of BE_i :

$$\rho_i = \sigma_i v_{th} N_{FE} \exp\left(-\frac{E_i}{k_B T}\right) \quad (2.4)$$

where

$$N_{FE} = 2 \left(\frac{m_{ex} k_B T}{2\pi \hbar^2} \right)^{3/2}$$

= the thermally averaged FE density of states

E_i = the BE_i binding energy.

2.2.2 The Steady-State Solution

Eqs. (2.1) and (2.2) can be solved quite simply for a steady state solution if the pump power is low enough to justify the assumption $n_i \ll N_i$. This implies, of course, the absence of saturation effects, such as multiple bound exciton or electron hole droplet formation. In this limit we obtain the equations

$$n_{FE} = \frac{g}{v_{FE} + \sum_i v_i \xi_i} \quad (2.5)$$

$$n_i = \xi_i n_{FE} \quad (2.6)$$

where we have defined, for convenience,

$$\xi_i = \frac{\gamma_i}{\nu_i + \rho_i} \quad (2.7)$$

This dimensionless ratio ξ_i will appear frequently in the rate model. Physically, ξ_i is the ratio of the FE capture rate, γ_i , to the total BE_i loss rate, $(\nu_i + \rho_i)$. Note that the total loss rate is the sum of the rates for whatever recombination paths may exist for the BE_i , ν_i , plus the rate of thermal release of BE_i , ρ_i . Also, note that ξ_i depends linearly on N_i through its dependence on the capture rate. When the application of the steady state solution is discussed, we will frequently find it notationally more convenient to discuss variation in ξ_i rather than variation in N_i directly.

2.2.3 Application When Free Exciton Luminescence Is Observed

When the impurity concentrations are very low and the pump power is sufficiently high, FE luminescence can be observed in the photoluminescence spectrum. When this is the case, the impurity concentration N_i can be obtained from the ratio of BE_i to FE luminescence intensities. From Eq. (2.6) we see that

$$N_i = \frac{1}{R_i} \frac{I_i}{I_{FE}} \quad (2.8)$$

where

$$R_i = \frac{f_i}{f_{FE}} \frac{\xi_i}{N_i} \quad (2.9)$$

and

FE = the FE oscillator strength

f_i = the BE_i oscillator strength

I_{FE} = the FE luminescence intensity

I_i = the BE_i luminescence intensity.

This result demonstrates how it is possible to use photoluminescence to measure the concentration of impurities in the very low concentration regime. Since the ratio R_i is independent of pump power and concentration, a single calibration allows us to obtain the value of N_i from a knowledge of R_i and the ratio of BE_i to FE luminescence intensities. Of course, application of this method requires that the absence of saturation effects assumed in the solution of Eqs. (2.1) - (2.2) is maintained. Otherwise, the simple linear relationship Eq. (2.8) is not obtained, as reference to the work of Tajima⁽³⁾ will verify.

It is important to note that Eq. (2.8) simply gives the behaviour of the ratio I_i/I_{FE} as N_i is varied. To determine independently the behaviour of I_i and I_{FE} , we must return to Eqs. (2.5) and

(2.6). Consider the case of a single impurity, impurity i , and consider variation of the parameter ξ_i . The behaviour of the rate theory in this case is schematically illustrated in Fig. 2.1. Suppose that ξ_i (or N_i) is increased while the generation rate g (that is, the laser pump power) is held constant. Then Eq. (2.5) predicts a decrease in n_{FE} and therefore in I_{FE} . Of course, Eq. (2.6) predicts an increase in n_i and therefore in I_i , in such a way that Eq. (2.8) is maintained.

As a result of this dependence of I_{FE} on N_i , the rate theory predicts that it may be possible to quench completely the FE luminescence intensity simply by increasing N_i . Of course, increasing the laser pump power increases g and therefore n_{FE} , according to Eq. (2.5). So it may be possible to some extent to overcome this quenching effect by increasing the pump power. However, at higher pump powers, sample heating can become an important factor, and then R_i will no longer be independent of pump power. For routine analysis, it becomes exceedingly desirable to operate in a pump power region in which sample heating effects are negligible.

2.2.4 Application When Free Exciton Luminescence Is Not Observed

Practically speaking, in many cases of interest impurity concentrations are high enough that FE luminescence is not observed.

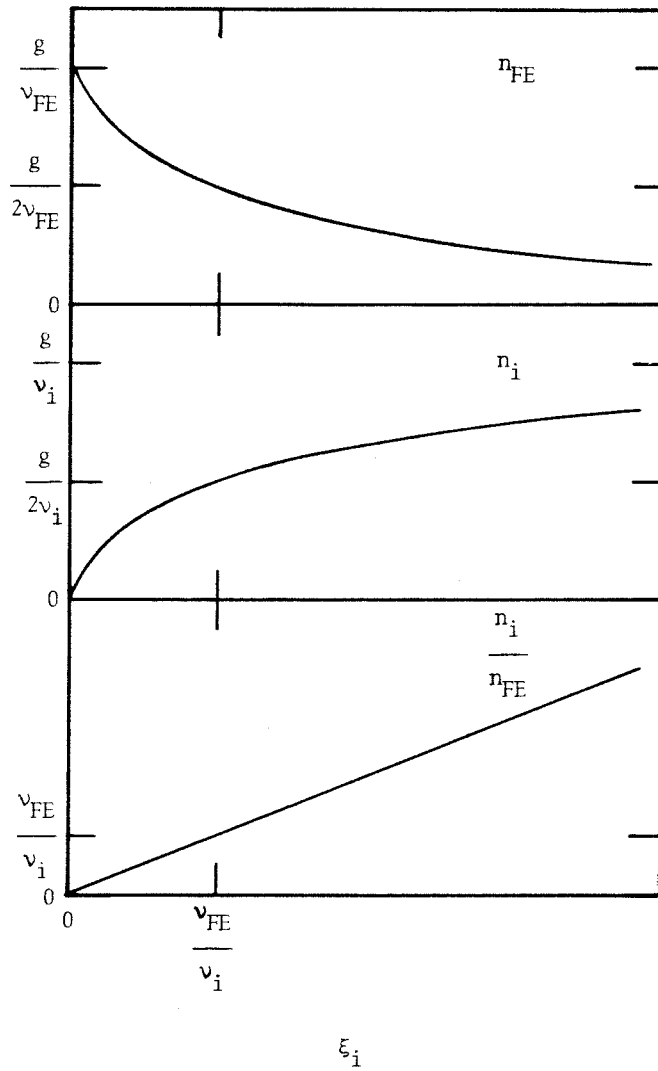


Figure 2.1. Schematic behaviour of the rate theory in the case of a single impurity. As the impurity concentration is increased at constant generation rate, g , the free exciton density, n_{FE} , decreases. However, the bound exciton density, n_i , increases in such a way that the ratio n_i/n_{FE} remains proportional to ξ_i .

In these situations, Eq. (2.6) can still be solved for relative impurity concentrations in terms of BE luminescence intensity ratios as follows:

$$\frac{N_i}{N_j} = \frac{1}{R_{ij}} \frac{I_i}{I_j} \quad (2.10)$$

where

$$R_{ij} = \frac{f_i}{f_j} \frac{N_j}{N_i} \frac{\xi_i}{\xi_j} \quad (2.11)$$

Application of this result is similar to that of Eq. (2.8), and similar considerations apply. Eq. (2.11) predicts that the ratio R_{ij} is independent of pump power and impurity concentration, and so the R_{ij} can be determined from measurements on one calibrated sample. Then, if one impurity concentration is known, for example that of the majority dopant, the concentration of other impurities in the material can be determined from the R_{ij} and the observed luminescence intensity ratios. Once again, care must be taken to ensure that saturation effects are not present in order to apply Eq. (2.10) successfully.

In this case as well it is important to note that Eq. (2.10) simply gives the behaviour of the ratio I_i/I_j as the impurity concentrations are varied. To determine independently the behaviour of I_i and I_j , we must once again return to Eqs. (2.5) and (2.6). Consider the case of two impurities, impurity i

and impurity j , and consider variation of the parameter ξ_i . The behaviour of the rate theory in this case is schematically illustrated in Fig. 2.2. Suppose that ξ_i (or N_j) is increased while g and N_i are held constant. As Eq. (2.5) indicates, this results in a decrease in n_{FE} . According to Eq. (2.6), a decrease in n_{FE} in turn results in a decrease in n_i . Since I_i is proportional to n_i , the final result is a decrease in I_i . Of course, Eq. (2.6) predicts an increase in I_j in such a way that Eq. (2.10) is preserved.

As a result of this coupling of N_j and I_i through the FE gas, the rate theory of the system predicts that it may be possible to quench completely the BE_i luminescence intensity simply by increasing N_j . Of course, as previously mentioned, increasing the laser pump power may overcome this effect to a certain extent, but sample heating effects must be avoided.

There is one important point to be made as a result of these considerations. We wish to determine at what point the simple rate theory presented in Eqs. (2.1) and (2.2) becomes inapplicable as the impurity concentrations are increased. Total quenching of shallow luminescence will be observed in many samples, but because of the coupling effect between I_i and N_j described above, this observation alone is not sufficient to conclude that the rate theory has become inapplicable. It is necessary, in fact, to show explicitly that Eq. (2.10) is no longer valid at high concentrations.

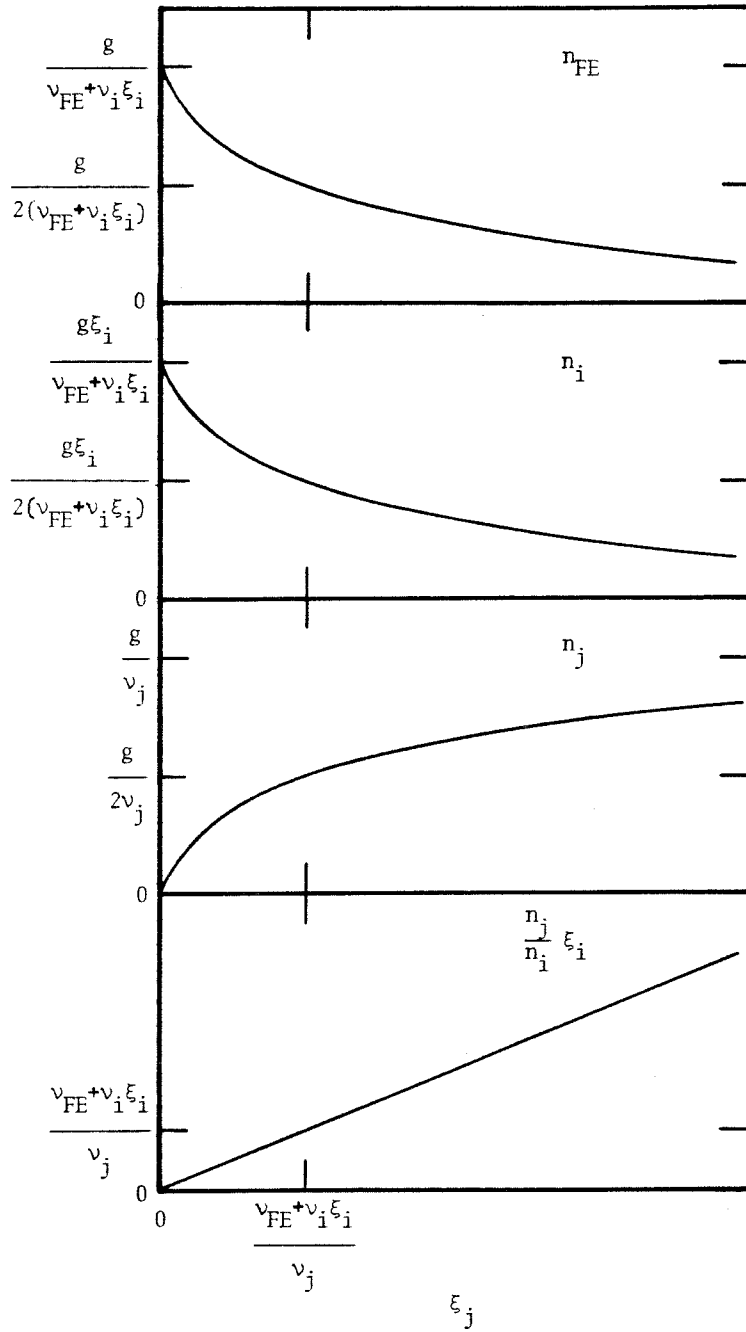


Figure 2.2. Schematic behaviour of the rate theory in the case of two impurities. As the impurity concentration, ξ_j , is increased at constant generation rate, g , the free exciton density, n_{FE} , decreases. This in turn results in a decrease in the impurity i bound exciton density, n_i . However, the impurity j bound exciton density, n_j , increases in such a way that the ratio $\frac{n_j}{n_i} \xi_i$ remains proportional to ξ_j .

2.3 EXPERIMENTAL RESULTS FOR THE Si:(B,In) SYSTEM

2.3.1 The Si:(B,In) System

To investigate systematically the effects of high impurity concentrations in a multiple impurity system, we undertook a careful study of one particularly interesting system: Si doped with B and In. Si:(B,In) was chosen as a model system for the study because heavily doped Si:In is a very important material for detector applications, and because the low concentration photoluminescence properties of the Si:B and Si:In subsystems are relatively well understood. First, both B and In bound exciton luminescence has been studied extensively and the spectra are well characterized ⁽⁵⁾. Also the decay mechanisms for excitons on B and In have been identified ⁽⁶⁾ and the decay rates have been measured ^(7,8). Finally, the capture cross sections for excitons on B ^(9,10) and In ^(10,11) have been determined as a function of temperature. In addition, the Si:In and Si:(P,B,In) systems are of current interest. Recently, very long-lived lines have been observed in the heavily doped Si:In spectrum ⁽¹²⁾, which are discussed in detail in Chapter 3. Also, a series of low energy lines have been observed in the heavily doped Si:(P,In) spectrum, which are not present in the Si(B,In) spectrum ^(13,14). These lines were attributed to donor-to-acceptor recombination luminescence involving P and In. In these investigations, the anomalous absence of B luminescence in the Si:(B,In) spectrum was also reported, and was attributed to interaction between dissimilar acceptor bound exciton states.

Technologically interesting material has high In concentrations, around 10^{17} cm^{-3} or higher. In these materials, the presence of unintentional shallow impurities such as B or P is undesirable. We were interested, therefore, in investigating the use of photoluminescence as a technique for measuring the concentration of residual B impurities in heavily doped Si:In, based on the rate theory developed in Section 2.2. In particular, we have systematically examined the B bound exciton luminescence intensity as a function of increasing In concentration. In this way we have been able to determine the range of In concentrations over which the theory, and hence the photoluminescence technique, is applicable. Also, we have been able to examine in detail the way in which the theory breaks down as the In concentration is increased.

2.3.2 The Si;(B,In) Samples and Typical Photoluminescence Spectra

The measurements discussed in this chapter were made on crystals grown by the Czochralski and float-zone techniques. Impurity concentrations were determined from Hall effect measurements performed at Hughes Research Laboratories, where the samples were grown. The samples studied and their impurity concentrations are given in Table 2.1.

Typical photoluminescence spectra are shown in Fig. 2.3.

Table 2.1. Samples of Si doped with In and B studied using photoluminescence. The numbers identifying the samples correspond to the ingot number at Hughes Research Laboratories. All the concentrations were measured using the Hall experiment at Hughes Research Laboratories. The estimated accuracy is $\pm 25\%$.

SAMPLE	N_B (cm^{-3})	N_{In} (cm^{-3})	N_B/N_{In}
Z20601	5.2×10^{12}	1.0×10^{17}	5.2×10^{-5}
C11204.T	1.4×10^{14}	1.3×10^{17}	1.1×10^{-3}
C11204.M	1.0×10^{14}	3.4×10^{16}	3.0×10^{-3}
Z20601R	9.8×10^{13}	4.3×10^{16}	2.3×10^{-3}
Z074	3.9×10^{13}	1.7×10^{16}	2.3×10^{-3}
C117	7.8×10^{13}	2.1×10^{16}	3.7×10^{-3}
C11204.S	6.3×10^{13}	1.3×10^{16}	4.8×10^{-3}
C112.M	4.2×10^{15}	2.4×10^{17}	1.8×10^{-2}
Z20601A	1.9×10^{14}	5.5×10^{15}	3.5×10^{-2}
Z104011	2.7×10^{13}	2.0×10^{14}	1.1×10^{-1}
Z163.T	3.9×10^{13}	2.2×10^{13}	1.8
C120A	8.2×10^{16}	2.0×10^{16}	4.1
Z163.S	3.5×10^{13}	6.8×10^{12}	5.1

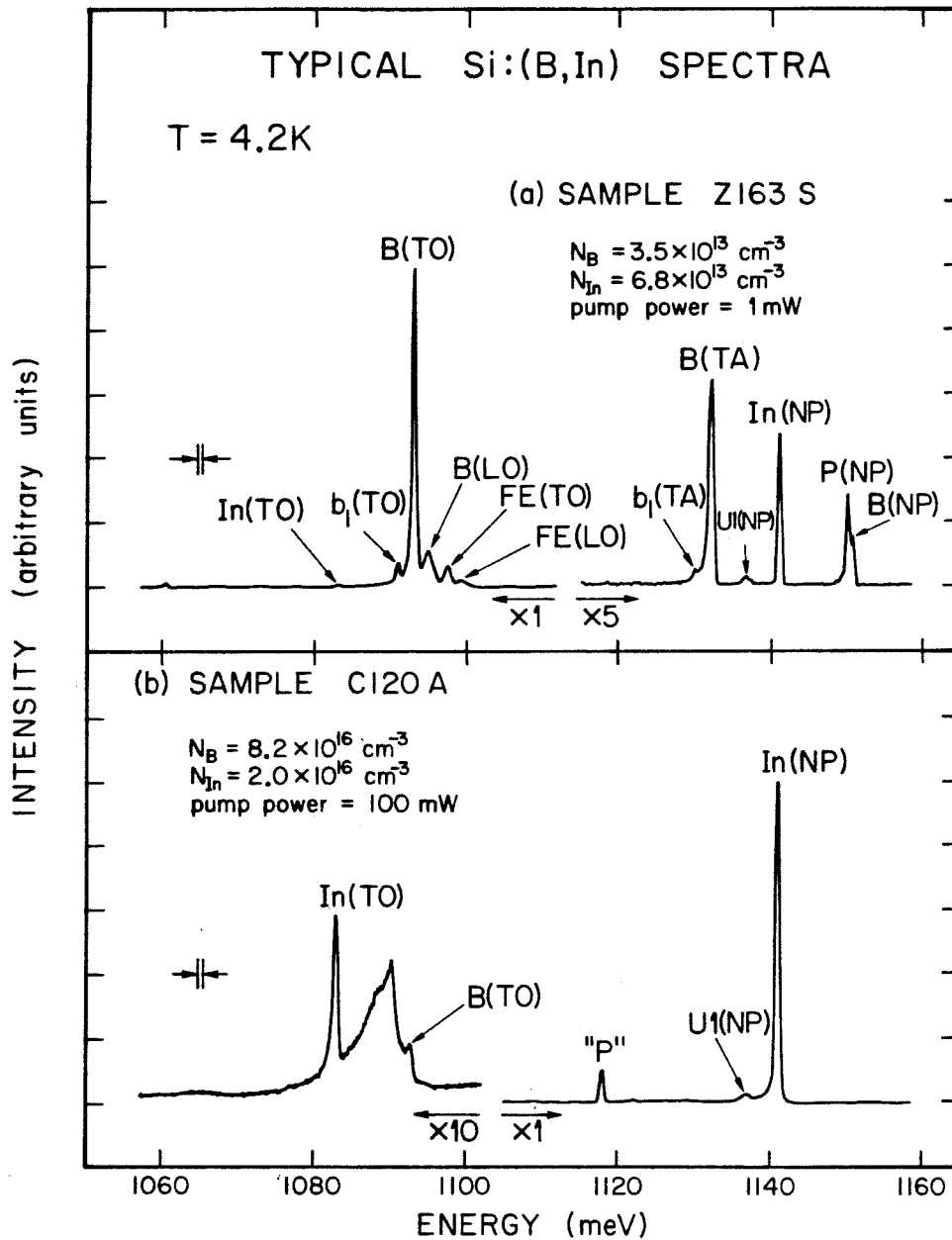


Figure 2.3. Spectra of two Si:(B,In) samples included in this study.

(a) Sample Z163.S, the most lightly doped sample.

(b) Sample c120A, the most heavily doped sample from which BE_B luminescence could still be observed.

Refer to the text for an explanation of the line assignments. The scale factors (e.g., "X5") give the relative intensity magnification.

Fig. 2.3(a) is a spectrum of sample Z163,S, the most lightly doped sample studied, and Fig. 2.3(b) is a spectrum of sample C120A, the most heavily doped sample from which B bound exciton luminescence could still be observed. Luminescence lines due to FE and BE_B , BE_P and BE_{In} recombination are visible in the no-phonon (NP), transverse acoustic phonon (TA), longitudinal optical phonon (LO) and/or transverse optical phonon (TO) replicas. In addition, the first B bound multiexciton complex (b_1) is visible in the TA and TO replicas. Finally, the previously reported (12,15) long-lived luminescence line "P" and the lower energy In luminescence line U1 can be seen in the NP region.

2.3.3 The Measurement of Luminescence Intensity Ratios

As previously mentioned, successful application of the rate theory presented in Section 2.2 requires that luminescence intensities be measured in a pump power region for which saturation effects are not important. In this study, luminescence intensity ratios were obtained using a technique that guarantees this condition. First, the intensity of NP BE_{In} and TO BE_B luminescence (I_{In}^{NP} and I_B^{TO} , respectively) was measured as a function of pump power for each sample studied. In the low pump power region where saturation does not occur, the luminescence intensity varied linearly with pump power; that is,

$$I_i = \alpha_i P \quad (2.12)$$

where

P = laser pump power,

This is the behaviour predicted by Eq. (2.6). Second, straight lines were least squares fit to the NP BE_{In} and TO BE_B pump power dependence data in the linear region, and the slopes, α_i , were obtained. Finally, the $I_{B TO} / I_{In NP}$ luminescence intensity ratio was calculated as the ratio of these slopes, since

$$\frac{I_i}{I_j} = \frac{\alpha_i}{\alpha_j} \quad (2.13)$$

Typical results of a measurement of this type at 4.2 K are shown in Figs. 2.4, 2.5 and 2.6 for sample Z104011. Fig. 2.4 shows the usual luminescence signal obtained at the low pump powers required to avoid saturation effects. Also shown on the figure are the Gaussian least squares fits used to determine the integrated line intensities. For the NP BE_{In} luminescence line, a single Gaussian was satisfactory for this purpose. However, for the TO BE_B it was necessary to fit two Gaussians, one representing the TO BE_B line and the second accounting for the TO BE_P line which is visible as a low energy shoulder on the TO BE_B line.

Measurements similar to these were carried out over a wide range of pump powers. The results are shown in Figs. 2.5 and 2.6.

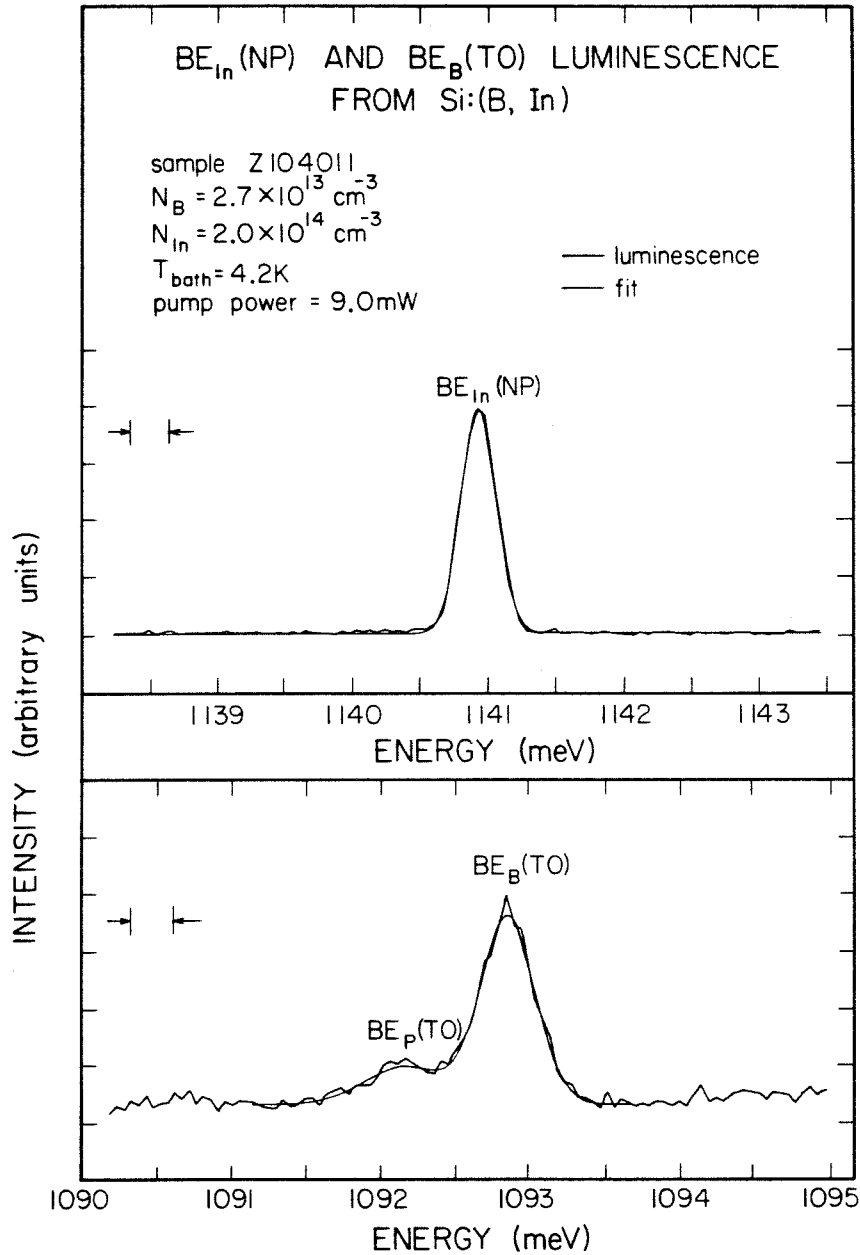


Figure 2.4. Typical photoluminescence measurement of I_{In}^{NP} and I_B^{TO} in the unsaturated pump power regime for sample Z104011. Gaussian least-squares fits to the observed luminescence are also shown.

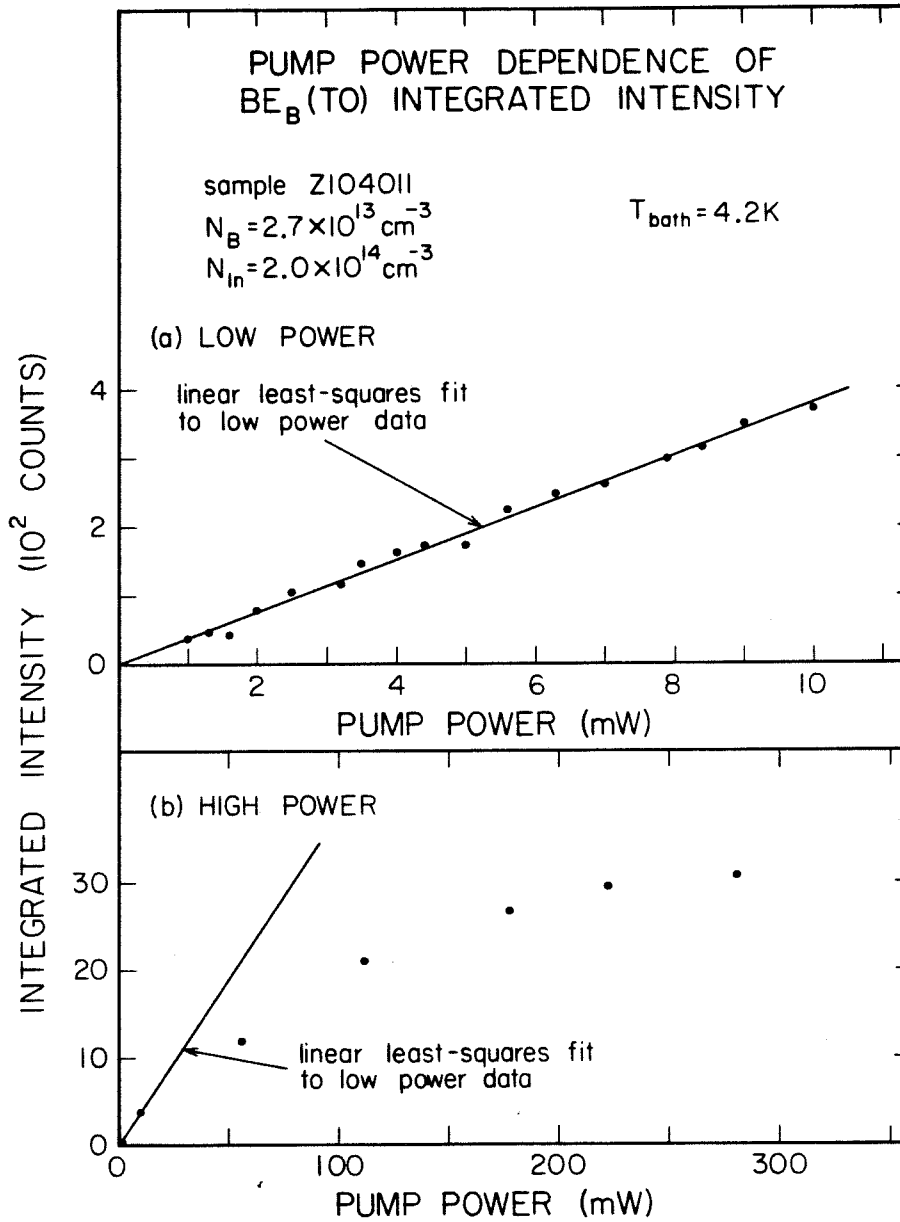


Figure 2.5. Pump power dependence of the TO BE_B luminescence intensity in sample Z104011.
 (a) The low pump power regime, where the luminescence intensity is proportional to pump power.
 (b) The high pump power regime, where saturation effects are observed.
 The same linear least-squares fit is shown in both cases.

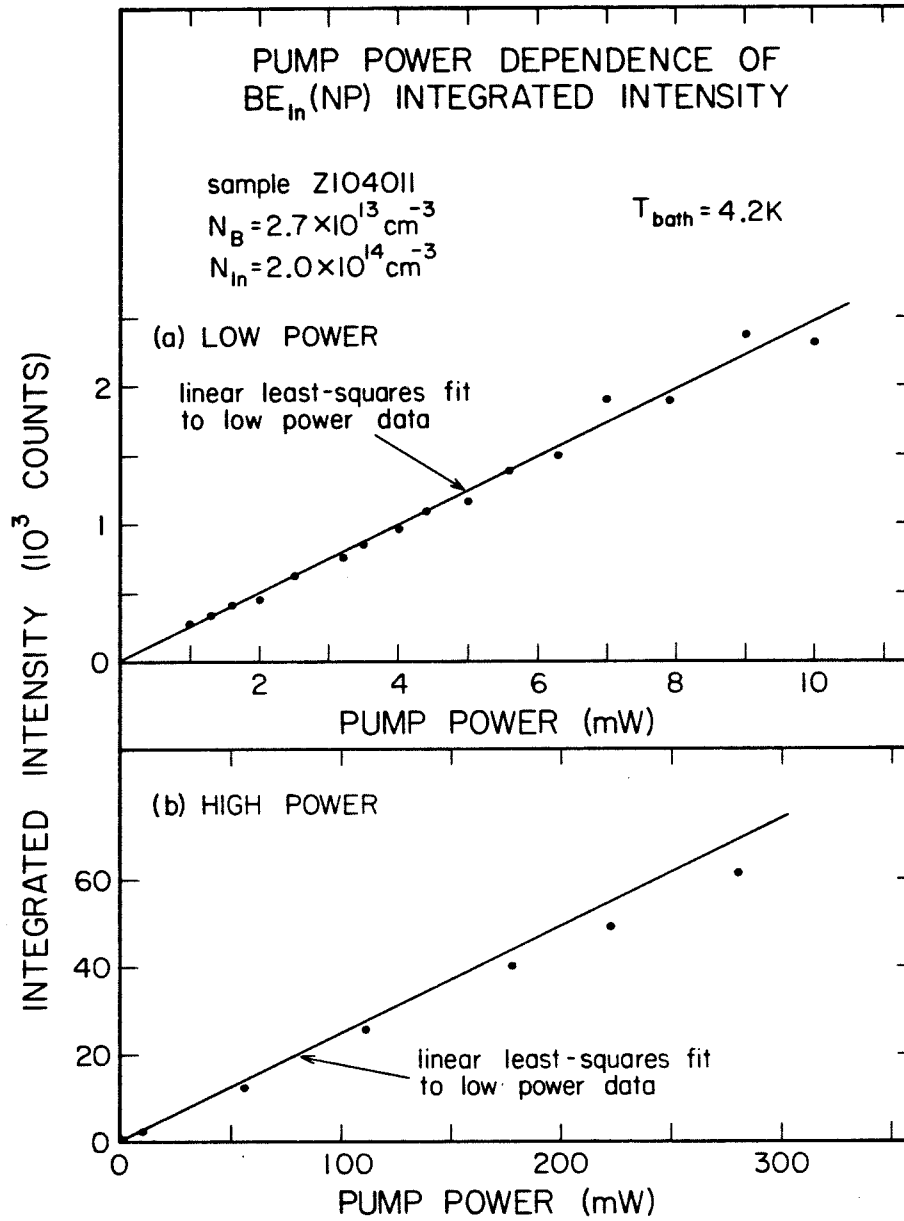


Figure 2.6. Pump power dependence of the NP BE_{In} luminescence intensity in sample Z104011.
 (a) The low pump power regime, where the luminescence intensity is proportional to pump power.
 (b) The high pump power regime, where moderate saturation effects are observed.
 The same linear least-squares fit is shown in both cases.

Fig. 2.5 shows the pump power dependence of the TO BE_B line for sample Z104011. As this figure demonstrates, the intensity varies linearly with the pump power for pump powers ranging from 1 to 10 mW and varies sublinearly for pump powers greater than 10 mW. This sublinear deviation is due to saturation of the B centers with excitons. Also shown in Fig. 2.5 is the straight line least squares fit to the low power points from which α_B was obtained.

Similar measurements for the BE_{In} line are presented in Fig. 2.6. In this case the intensity variation is only slightly sublinear at high pump powers. It is much more difficult to saturate the In line in these samples because of the higher concentration of In centers and the short lifetime of the In bound exciton ($\tau_{In} \approx 3ns$ ⁽⁸⁾ as compared to $\tau_B \approx 1.0 \mu s$ ⁽⁷⁾). Also shown is the straight line least squares fit to the low power data, from which α_{In} was obtained.

2.3.4 The Dependence of R_{BIn} on In Concentration

The procedure described above was employed to determine luminescence intensity ratios for all samples in which B and In luminescence could be observed. The results of the low pump power straight line fits and the consequent intensity ratios are listed in Table 2.2. This information, together with the results of the Hall effect measurements summarized in Table 2.1, has enabled us to investigate the dependence of the ratio

Table 2.2 Results of the determination of I_{B0}/I_{NP} in the unsaturated regime, using the procedure described in the text. The errors quoted for the slope values are obtained from the expression (16)

$$\sigma_{\alpha} = \frac{|\alpha|}{\sqrt{n-2}} \sqrt{\frac{1}{r} - 1}$$

which gives the standard error in the slope, σ_{α} , in terms of the slope, α , the correlation coefficient, r , and the number of data points, n .

SAMPLE	NUMBER OF POINTS IN FIT		CORRELATION COEFFICIENT		SLOPE		I_B/I_{In}
	n_B	n_{In}	r_B	r_{In}	α_B	α_{In}	
Z163.S	21	21	.9989	.9943	3240 ± 110	336 ± 8.3	$9.64 \pm .57$
Z163.T	18	19	.9977	.9980	2790 ± 47	779 ± 12	$3.59 \pm .12$
Z104011	16	16	.9976	.9936	$38.8 \pm .72$	246 ± 7.5	$(1.58 \pm .077) \times 10^{-1}$
Z20601A	23	22	.9923	.9978	$19.6 \pm .53$	687 ± 10	$(2.86 \pm .12) \times 10^{-2}$
C120A	10	11	.9647	.9994	$0.601 \pm .058$	$61.6 \pm .73$	$(9.77 \pm 1.1) \times 10^{-3}$

$$R_{\text{BIn}} = \left(\frac{I_{\text{B}}^{\text{TO}}}{I_{\text{In}}^{\text{NP}}} \right) \left(\frac{N_{\text{In}}}{N_{\text{B}}} \right) \quad (2.14)$$

on the In concentration. As demonstrated by the rate theory presented in Section 2.2, the use of photoluminescence as a tool for semiconductor analysis depends on R_{ij} being independent of N_i and N_j . The range of concentrations for which this is the case has now been determined for the Si:(B,In) model system. The result of this analysis is summarized in Fig. 2.7, which is a plot of R_{BIn} versus N_{In} . As can be seen from Fig. 2.7 within experimental error R_{BIn} is independent of N_{In} for N_{In} between $6 \times 10^{12} \text{ cm}^{-3}$ and about 10^{15} cm^{-3} . However, for $N_{\text{In}} > 10^{15} \text{ cm}^{-3}$, we observe that R_{BIn} decreases with increasing N_{In} . For $N_{\text{In}} > 2 \times 10^{16} \text{ cm}^{-3}$, we were not able to observe BE_{B} luminescence in any of our samples, and therefore no points are plotted in Fig. 2.7. It appears, therefore, that the simple theory presented in Section 2.2 breaks down and R_{BIn} becomes dependent on N_{In} , for $N_{\text{In}} > 10^{15} \text{ cm}^{-3}$.

2.4 DISCUSSION OF THE EXPERIMENTAL RESULTS

2.4.1 The Low Concentration Result

The experimental results for the Si:(B,In) system presented in Section 2.3 show that the behaviour expected on the basis of the theory of Section 2.2 is obtained in the low concentration regime. That is, for $N_{\text{In}} < 10^{15} \text{ cm}^{-3}$ we observe that R_{BIn} is independent of

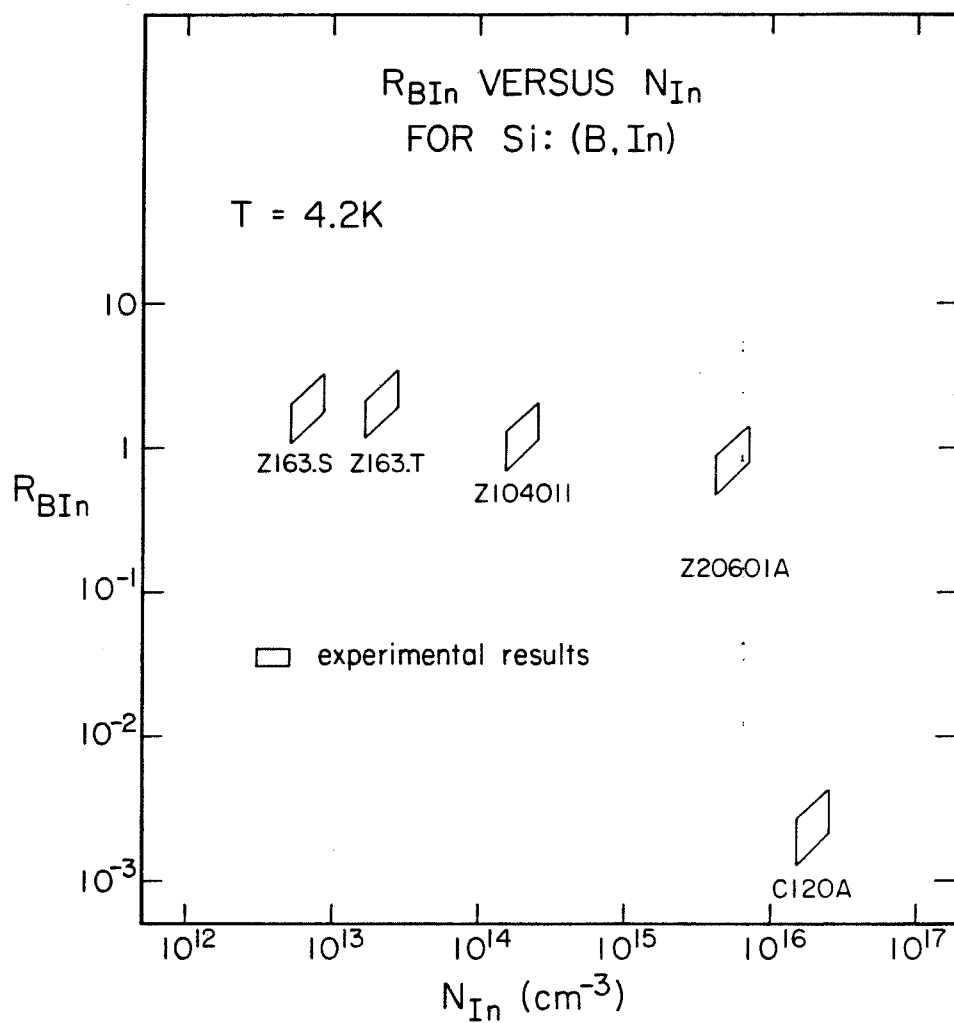


Figure 2.7. The ratio $R_{BIn} = \left(\frac{I_{B}^{TO}}{I_{In}^{NP}} \right) \left(\frac{N_{In}}{N_B} \right)$ as a function of N_{In} . The experimental results are shown. The parameters for the various samples are given in Table 2.1. For $N_{In} > 2 \times 10^{16} cm^{-3}$, B luminescence was not observed, and hence, no points are plotted. The error regions for the experimental points are based on estimates of the error in N_B , N_{In} , I_B and I_{In} .

N_{In} , as predicted by Eq. (2.11),

The experimental results also show that $1.0 < R_{BIn} < 3.5$ in the low concentration regime. We can show that this result is consistent with the theory presented in Section 2.2 by estimating R_{BIn} from Eq. (2.11). We take $f_B = 2.8 \times 10^{-5}$ (17) for the TO BE_B and $f_{In} = 8.5 \times 10^{-5}$ (18) for the NP BE_{In} . Also, at 4.2 K $(\nu_B + \rho_B) = 1.27 \times 10^6 \text{ sec}^{-1}$ (10) and $(\nu_{In} + \rho_{In}) = 3.7 \times 10^8 \text{ sec}^{-1}$ (8). The ratio of capture cross sections is only known approximately. We take $0.025 < \sigma_B / \sigma_{In} < 0.11$ (10) for this estimate. Finally, our detection system is approximately twice as sensitive at the NP BE_{In} energy as it is at the TO BE_B energy. On the basis of these estimates, Eq. (2.11) results in $1.2 < R_{BIn} < 5.3$, which is consistent with the experimentally observed result.

2.4.2 The Effect of Increasing In Concentration

On the basis of the experimental results presented in Section 2.3, it is clear that the simple theory obtained in the low concentration limit becomes inapplicable at even moderately increased concentrations. In order to model the behaviour observed at higher concentrations, we propose that some direct interaction begins to occur between a B bound exciton and its nearest-neighbour neutral In atom, which results in a transfer of the exciton from the B atom to the In atom.

A quick estimate will show that it is not unreasonable to expect a process of this nature to begin occurring at In concentrations in the neighbourhood of 10^{16}cm^{-3} . First, we calculate the probability that the nearest-neighbour In atom is between r and $r+dr$ from a given B atom, $P(r)dr$. We obtain

$$P(r)dr = 4\pi r^2 dr N_{\text{In}} \exp\left(-\frac{4}{3}\pi r^3 N_{\text{In}}\right) \quad (2.15)$$

where

$4\pi r^2 dr N_{\text{In}}$ = the probability that an In atom is between r and $r+dr$ of a given B atom

and

$\exp\left(-\frac{4}{3}\pi r^3 N_{\text{In}}\right)$ = the probability that there is no In atom between the B atom and r (obtained from the Poisson distribution).

Note that

$$\int_0^{\infty} P(r) dr = 1$$

as expected. Now we calculate the average value of r to be

$$\begin{aligned} \langle r \rangle &= \int_0^{\infty} r P(r) dr \\ &= \left(\frac{3}{4\pi N_{\text{In}}} \right)^{1/3} \Gamma\left(\frac{4}{3}\right) \end{aligned} \quad (2.16)$$

For $N_{\text{In}} = 10^{16} \text{cm}^{-3}$ we find $\langle r \rangle = 250 \text{ \AA}$. Considering that the Si FE Bohr radius is 43 \AA , the suggestion that direct interaction effects become important at these concentrations is reasonable.

2.4.3 Rate Model Including Exciton Transfer

The rate theory presented in Section 2.2 can be modified to include the effects of this exciton transfer process. We introduce a distance dependent transfer rate, $\Omega(r)$, for the exciton transfer from a B atom to an In atom at a distance r . Then Eqs. (2.1) and (2.2) are modified as follows:

$$\frac{dn_{\text{FE}}}{dt} = g - (v_{\text{FE}} + \gamma_{\text{B}} + \gamma_{\text{In}}) n_{\text{FE}} + \rho_{\text{B}} n_{\text{B}} + \rho_{\text{In}} n_{\text{In}} \quad (2.17)$$

$$\frac{\partial n_{\text{B}}(r)}{\partial t} = \gamma_{\text{B}}(r) n_{\text{FE}} - [v_{\text{B}} + \rho_{\text{B}} + \Omega(r)] n_{\text{B}}(r) \quad (2.18)$$

$$\frac{dn_{\text{In}}}{dt} = \gamma_{\text{In}} n_{\text{FE}} - (v_{\text{In}} + \rho_{\text{In}}) n_{\text{In}} + \int_0^{\infty} \Omega(r) n_{\text{B}}(r) dr \quad (2.19)$$

where

$n_{\text{B}}(r)dr$ = the density of BE_{B} with a nearest-neighbour In between r and $r+dr$

$\gamma_B(r)$ = the rate of FE capture by B atoms with a nearest-neighbour In atom between r and $r+dr$.

Then it follows from Eq. (2.3) that

$$\gamma_B(r) = \sigma_B v_{th} [N_B(r) - n_B(r)] \quad (2.20)$$

where

$N_B(r)dr$ = the density of B atoms with a nearest-neighbour In between r and $r+dr$.

It also follows that

$$P(r)dr = \frac{N_B(r)dr}{N_B} \quad (2.21)$$

so that

$$\int_0^{\infty} N_B(r) dr = \int_0^{\infty} N_B P(r) dr = N_B \quad (2.22)$$

as expected.

In the absence of saturation, when $n_B(r) \ll N_B(r)$, we can write Eq. (2.20) as

$$\begin{aligned} \gamma_B(r) &= \sigma_B v_{th} N_B P(r) \\ &= \gamma_B P(r) \quad . \end{aligned} \quad (2.24)$$

In this limit, we can obtain the steady state solution to Eqs.

(2.17) - (2.19) as

$$n_{FE} = \frac{g}{v_{FE} + v_B \int_0^{\infty} \xi_B(r) dr + \left[1 + \frac{1}{\gamma_{In}} \int_0^{\infty} \omega(r) \xi_B(r) dr \right] v_{In} \xi_{In}} \quad (2.25)$$

$$n_B(r) = \xi_B(r) n_{FE} \quad (2.26)$$

$$n_{In} = \left[1 + \frac{1}{\gamma_{In}} \int_0^{\infty} \omega(r) \xi_B(r) dr \right] \xi_{In} n_{FE} \quad (2.27)$$

where we have defined

$$\xi_B(r) = \left[\frac{P(r)}{1 + \omega(r)} \right] \xi_B \quad (2.28)$$

and

$$\omega(r) = \frac{\Omega(r)}{v_B + \rho_B} \quad (2.29)$$

From Eqs. (2.26) and (2.27) we obtain an expression analogous to Eq. (2.10),

$$\frac{N_B}{N_{In}} = \frac{1}{R_{BIn}} \frac{I_B}{I_{In}} \quad (2.30)$$

but where R_{BIn} now includes the effects of exciton transfer;

$$R_{BIn} = \left\{ \frac{\int_0^{\infty} \frac{P(r)}{1 + \omega(r)} dr}{1 + \frac{\sigma_B}{\sigma_{In}} \frac{N_B}{N_{In}} \int_0^{\infty} \frac{\omega(r) P(r)}{1 + \omega(r)} dr} \right\} R_{BIn}^0 \quad (2.31)$$

In this expression, R_{BIn}^0 is the value of R_{BIn} in the absence of exciton transfer, as expressed by Eq. (2.11). This expression for R_{BIn} must now be compared with the experimental results obtained in Section 2.3.

2.4.4 The Exciton Transfer Rate

Before the solution of the modified rate theory can be compared with the experimental results, we must determine an appropriate form for $\Omega(r)$, the exciton transfer rate. The general topic of excitation transfer in solids has been considered extensively in the literature. The original work by Förster ⁽¹⁹⁾ and Dexter ⁽²⁰⁾ considered excitation transfer in the context of "host-sensitization" or "impurity-sensitization" of material doped with specific "activator" impurities. In this case, the rate of energy transfer from an excited sensitizer to an activator in its ground state is

$$W = \frac{2\pi}{\hbar} |\langle \psi_F | H_{int} | \psi_I \rangle|^2 \rho_F \quad (2.32)$$

where Ψ_I is the wavefunction of the initial state in which the sensitizer is excited and the activator is in its ground state, Ψ_F is the wavefunction of the final state in which the activator is excited and the sensitizer is in its ground state, H_{int} is the Coulomb interaction Hamiltonian, and ρ_F is the density of final states. Dexter ⁽²⁰⁾ expanded H_{int} in powers of r , the distance between the sensitizer and activator, and examined the dipole-dipole and dipole-quadrupole terms. The exchange integrals, which result when Ψ_I and Ψ_F are properly antisymmetrized, were also considered. In particular, the spatial dependences for these transfer rates were obtained. These spatial dependences reside in the matrix element in Eq. (2.32). Dexter found that the transfer rates for the dipole-dipole, dipole-quadrupole and exchange processes have the following spatial dependences:

$$W_{dd}(r) \propto r^{-6} \quad (2.33)$$

$$W_{dq}(r) \propto r^{-8} \quad (2.34)$$

$$W_{ex}(r) \propto \exp\left(-\frac{r}{r_0}\right) \quad (2.35)$$

Of course, Eq. (2.32) refers to a resonant energy transfer process, in which the initial and final state energies are equal. Subsequent work by Orbach ⁽²¹⁾ extended Dexter's theory to include non-resonant

energy transfer, in which phonon emission results in energy conservation. These calculations show that the phonon assisted transfer rates can be written as the product of the resonant transfer rate and a factor which accounts for the effect of phonon assistance. In our application of the rate theory, we assume that phonon assistance introduces only a negligible change in the spatial dependence of the transfer rate. That is, we assume Dexter's results, Eqs. (2.33) to (2.35).

In our comparison of theory and experiment, we have considered both the dipole-dipole and exchange interactions. For the dipole-dipole interaction, the transfer rate was assumed to be

$$\Omega(r) = \Omega_{dd} \left(\frac{r_{dd}}{r} \right)^6 \quad (2.36)$$

For the exchange interaction, the transfer rate was assumed to be

$$\Omega(r) = \Omega_{ex} \exp \left(- \frac{r}{r_{ex}} \right) \quad (2.37)$$

2.4.5 Comparison of Modified Rate Model with Experimental Results

The prediction of the rate model including exciton transfer,

Eq. (2.31), has been compared with the experimental results obtained in Section 2.3. The exciton transfer rates given by Eqs. (2.36) and (2.37) were considered. Also, at 4.2 K the capture cross section ratio was taken to be $\sigma_B/\sigma_{In} = 0.1$ ⁽¹⁰⁾ and the total BE_B decay rate was taken to be $(\nu_B + \rho_B) = 1.27 \times 10^6 \text{ sec}^{-1}$ ⁽¹⁰⁾. Then Eq. (2.31) was fit to the experimental data shown in Fig. 2.7.

The result of this procedure is shown in Fig. 2.8. As this figure demonstrates, the best fit is obtained when we assume the exchange mechanism. In this case, good agreement has been obtained for $R_{BIn}^0 = 1.8$, $\Omega_{ex} = 10^{13} \text{ sec}^{-1}$ and $r_{ex} = 27 \text{ \AA}$. The dipole-dipole interaction produces a fit which is not quite as good. The best results were obtained for $R_{BIn}^0 = 1.8$ and $\Omega_{dd} r_{dd}^0 = 2 \times 10^{22} \text{ \AA sec}^{-1}$. On the basis of these results, then, it appears that the exchange mechanism dominates the transfer process.

There are a number of features associated with this conclusion which should be mentioned. First, our result, which indicates that the dipole-dipole interaction is not particularly strong in Si, is reasonable. The dipole-dipole transition rate is proportional to the BE oscillator strengths, which are very small in indirect gap materials like Si. Second, an effect which appears to be the result of exciton tunneling has been observed in GaP:N ⁽²²⁾. In this work, a transfer rate with the form of Eq. (2.35) was found to be consistent with the data. However, a transition rate with the form of Eq. (2.33) was not

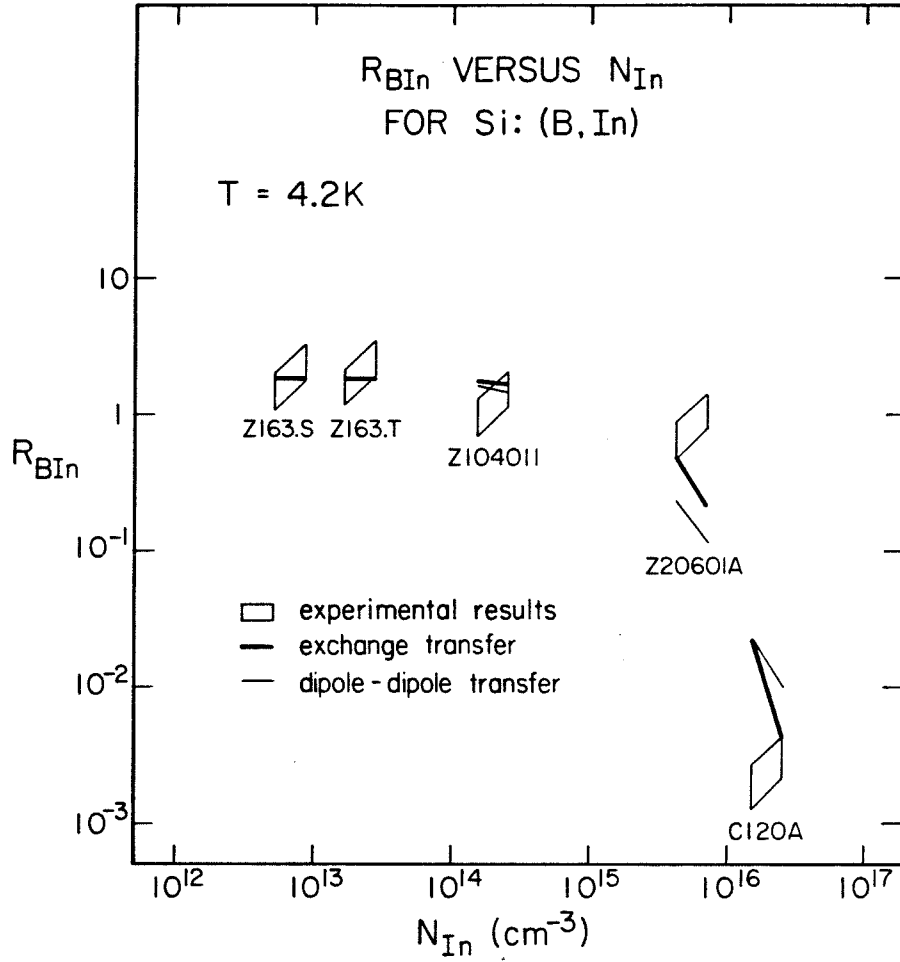


Figure 2.8. Comparison of exciton transfer model with experimental results. Model results for both exchange transfer and dipole-dipole transfer are presented. The variation in the calculated experimental result for each sample is primarily a result of the uncertainty in N_{In} .

consistent. Furthermore, the parameters obtained from the exchange interaction fit in the present study are consistent with those obtained in the GaP:N work. Third, the value of R_{BIn}^O obtained from the fits is consistent with our estimate of R_{BIn}^O in the absence of transfer based on Eq. (2.11), which was $1.2 < R_{BIn}^O < 5.3$. These considerations all support the proposal that the exchange interaction is the dominant transfer mechanism for exciton transfer in Si.

2.5 SUMMARY AND CONCLUSION

In this chapter the use of photoluminescence as a technique for determining impurity concentrations in semiconductors was investigated. The results obtained can be summarized as follows:

(i) A model for photoluminescence from doped Si was developed in the limit of low laser pump power and low impurity concentrations. A steady-state solution was obtained, and examined in various limits. Based on this model, a procedure was developed for interpreting the photoluminescence spectrum in terms of impurity concentrations.

(ii) This procedure was tested on a particular system which is of technological interest, the Si:(B,In) system. A careful and systematic study of B bound exciton luminescence intensity as a function of increasing In concentration was made, and limits on the applicability of the model were obtained. In particular, it was observed that B bound exciton luminescence was quenched for In concentrations greater than

10^{15}cm^{-3} . For In concentrations greater than approximately $2 \times 10^{16} \text{cm}^{-3}$, B bound exciton luminescence was not observed in any sample studied. Since technologically interesting material has In concentrations above 10^{17}cm^{-3} , it appears that the photoluminescence technique will not be useful for determining the concentration of residual B impurities in technologically useful Si:In.

(iii) The results of the systematic study enabled us to examine in detail the behaviour of the Si:(B,In) system as the In concentration was increased. In particular, the model was modified to include a new process which we propose becomes active at high In concentrations. This process is transfer of excitons from B to In impurities. Again, a steady-state solution was obtained and compared to the experimental results. Two transfer mechanisms were considered; the dipole-dipole interaction and the exchange interaction. When the exchange interaction was assumed, a good fit to the experimental results was obtained, and it was concluded that exchange is the dominant transfer mechanism for excitons in Si.

REFERENCES

1. J. R. Haynes, Phys. Rev. Lett. 4, 361 (1960).
2. See, for example, P. J. Dean, J. R. Haynes and W. F. Flood, Phys. Rev. 161, 711 (1967); K. Kosai and M. Gershenzon, Phys. Rev. B9, 723 (1974); M. A. Vouk and E. C. Lightowers, J. Lumin. 15, 357 (1977); S. A. Lyon, D. L. Smith and T. C. McGill, Phys. Rev. B17, 2620 (1977).
3. M. Tajima, Appl. Phys. Lett. 32, 719 (1978).
4. H. Nakayama, T. Nishino and Y. Hamakawa, Jpn. J. Appl. Phys. 19, 501 (1980).
5. See, for example, S. A. Lyon, D. L. Smith, and T. C. McGill, Phys. Rev. B17, 2620 (1977); M. L. W. Thewalt, Can. J. Phys. 55, 1463 (1977).
6. G. C. Osbourn and D. L. Smith, Phys. Rev. B16, 5426 (1977).
7. S. A. Lyon, G. C. Osbourn, D. L. Smith and T. C. McGill, Solid State Commun. 23, 425 (1978).
8. W. Schmid, Phys. Status Solidi B 84, 529 (1977).
9. R. B. Hammond and R. N. Silver, Appl. Phys. Lett. 36, 68 (1980).
10. R. M. Feenstra and T. C. McGill, Solid State Commun. 36, 1039 (1980).
11. K. R. Elliott, D. L. Smith, and T. C. McGill, Solid State Commun. 24, 461 (1977).

12. G. S. Mitchard, S. A. Lyon, K. R. Elliott, and T. C. McGill, *Solid State Commun.* 29, 425 (1979).
13. U. O. Ziemelis, R. R. Parsons, and M. Voos, *Solid State Commun.* 32, 445 (1979).
14. U. O. Ziemelis and R. R. Parsons, submitted to *Can. J. Phys.*
15. K. R. Elliott, S. A. Lyon, D. L. Smith, and T. C. McGill, *Phys. Lett.* 70A, 52 (1979).
16. See, for example, E. L. Crow, F. A. Davis, and M. W. Maxfield, *Statistics Manual*, (Dover Publications, New York, N.Y. 1960) p. 160.
17. P. J. Dean, W. F. Flood, and G. Kaminsky, *Phys. Rev.* 163, 721 (1967).
18. G. C. Osbourn and D. L. Smith, *Phys. Rev.* B16, 5426 (1977).
19. T. Förster, *Ann. Physik* 2, 55 (1948).
20. D. L. Dexter, *J. Chem. Phys.* 21, 836 (1953).
21. R. Orbach, *Optical Properties of Ions in Crystals*, (Interscience Publishers, New York, N.Y., 1967), H. M. Crosswhite and H. W. Moos, Eds.
22. P. J. Wiesner, R. A. Street, and H. D. Wolf, *Phys. Rev. Lett.* 35, 1366 (1975).

CHAPTER 3

ISOELECTRONIC COMPLEXES IN Si-
THE "P,Q,R" LINES IN Si:In

3.1 INTRODUCTION

The photoluminescence spectrum of Si:In has recently been the subject of a great deal of attention. This interest stems primarily from the fact that the Si:In is technologically useful as an IR detector material, and also from the fact that the photoluminescence technique is a powerful and relatively accessible method for examining the properties of such materials. In particular, the presence of certain impurities and impurity complexes in Si:In can affect the performance of devices made from the material. An example of this type of complex is the "X-level", a shallow acceptor which is thought to be an In-C pair. As another example, in this chapter we present the results of a study of luminescence which is attributed to the presence of an isoelectronic complex in Si:In.

The first examinations of the Si:In photoluminescence spectrum were made by Dean et al. ⁽¹⁾ In this original study only the major spectral features were observed. Specifically, luminescence due to no-phonon (NP) recombination of In bound excitons (BE_{In}) was observed, as well as a replica involving the assistance of transverse optical (TO) phonons. Only very weak luminescence was obtained in this study, which can be attributed to the high temperatures (30 K and 100 K) at which the spectra were recorded. The lack of detail was probably a result of the large slit widths therefore employed and the consequent poor spectral resolution.

More recently, the Si:In spectrum has been examined by Vouk and Lightowlers ^(2,3). In this study, transverse acoustic (TA) and longitudinal optical (LO) phonon assisted BE_{In} luminescence was observed, as well as a splitting of the NP and TO assisted BE_{In} lines. This splitting of the BE_{In} luminescence was attributed to the presence of a low-lying excited state of the BE_{In} complex. In addition, several lines of unknown origin were observed, which were labelled U1 to U5. The increased spectral detail revealed by this study is probably a result of the relatively intense low temperature luminescence observed and the small slit widths which were therefore employed.

Since these original studies, BE_{In} luminescence has been examined in great detail ⁽⁴⁻⁶⁾. In particular, the BE_{In} doublet structure has been measured in very high resolution experiments, and the splitting has been accurately determined to be 3.1 meV ⁽⁴⁾. Also, the line labelled U1 by Vouk and Lightowlers has been examined in detail, and is thought to be due to a BE_{In} transition which leaves the neutral In acceptor in a 4.1 meV excited state ⁽⁵⁾.

Finally, certain properties of the BE_{In} have been deduced as a result of detailed examination of the BE_{In} luminescence. The decay mechanisms for BE_{In} have been identified ⁽⁶⁾ and the decay rates have been measured ^(7,8). In addition, the In FE capture cross sections have been determined as a function of temperature ^(9,10).

In this chapter, we present the measurement of very detailed, high-resolution spectra of Si:In. In addition to the lines previously reported ⁽¹⁻⁵⁾, many other spectral features have been observed. In particular, three intense luminescence lines in the Si:In spectrum, the "P,Q,R" lines, have been studied in detail. Time-resolved measurements show that these lines have lifetimes which are orders of magnitude longer than those measured for the other features in the spectrum. For this reason they are of considerable interest. The remainder of the chapter deals with a systematic study of the properties of these lines.

3.2 THE Si:In SAMPLES

Measurements of the photoluminescence of Si:In were made on crystals grown by the float-zone and Czochralski techniques. The samples were grown and characterized at Hughes Research Laboratories in Malibu, California. Hall effect measurements performed there resulted in a determination of the impurity concentrations in these samples, and these results are summarized in Table 3.1.

3.3 EXPERIMENTAL RESULTS AND DISCUSSION

3.3.1 Typical Si:In Photoluminescence Spectrum

A typical Si:In photoluminescence spectrum is shown in Fig. 3.1. As indicated, the measurement temperature was 20 K. The spectrum clearly shows luminescence features due to NP BE_{In} recombination, as well as transverse acoustic (TA) phonon and TO + LO phonon replicas. The TO + LO phonon replica of FE recombination luminescence is also

Table 3.1. Si:In samples investigated in this study. The samples were grown and characterized at Hughes Research Laboratories. The In concentration (N_{In}) and concentration of uncompensated donors ($N_D - N_B$) were determined by Hall effect measurements. The O concentration (N_O) and C concentration (N_C) were determined by IR absorption measurements.

SAMPLE	N_{In} (cm^{-3})	$N_D - N_B$ (cm^{-3})	N_O (cm^{-3})	N_C (cm^{-3})
C117A	2.1×10^{16}	-5.6×10^{13}		
C20102	6.0×10^{16}	9.0×10^{13}	9.6×10^{17}	3.4×10^{16}
C014.1	1.2×10^{17}	4.6×10^{13}	1.4×10^{18}	1.9×10^{16}
C014.3	1.5×10^{17}	5.4×10^{13}	1.3×10^{18}	3.0×10^{17}
C025.A1	1.5×10^{17}	4.8×10^{13}	1.3×10^{18}	3.6×10^{16}
C008.T	2.6×10^{17}	5.7×10^{14}	1.4×10^{18}	6.0×10^{16}

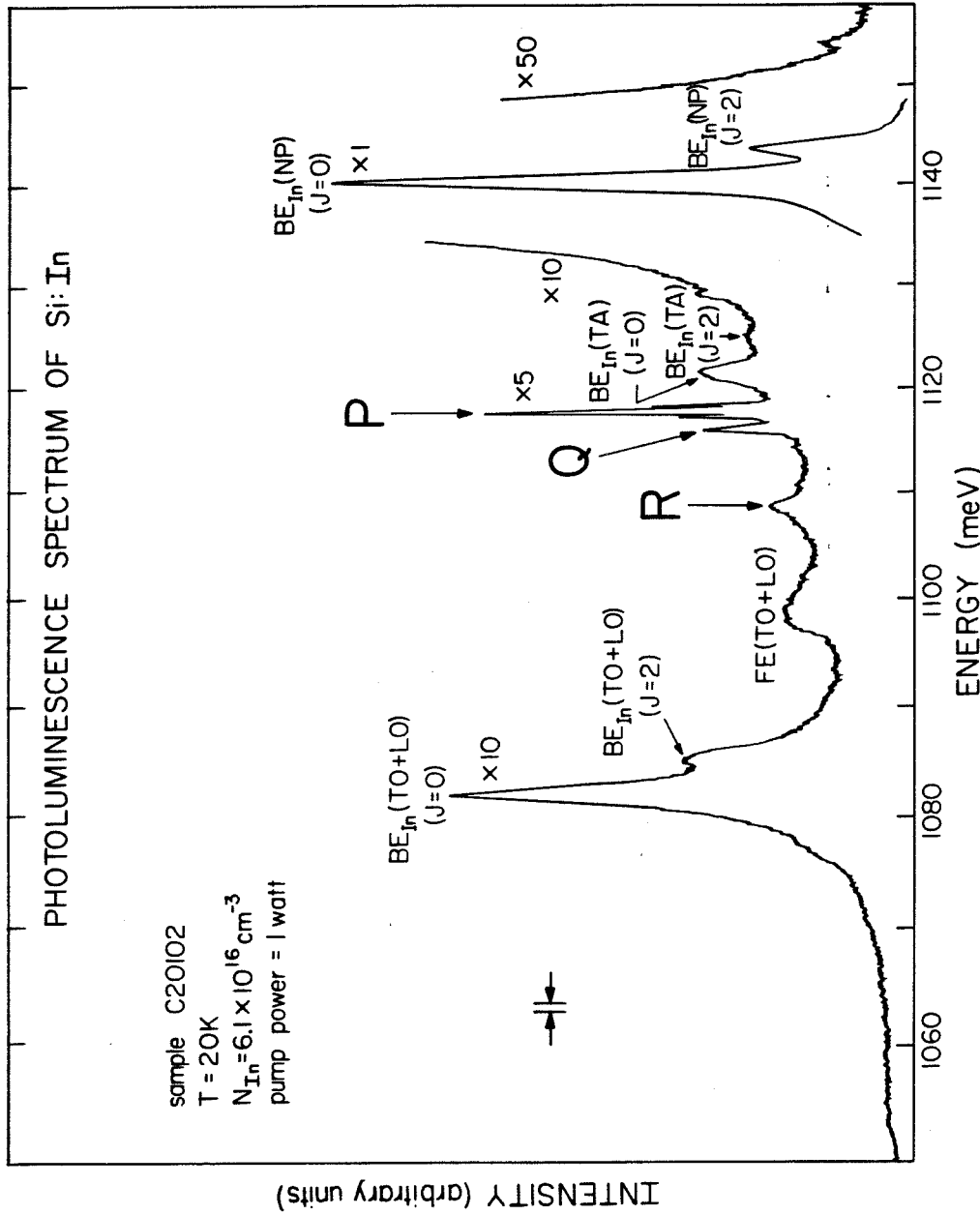


Figure 3.1. The photoluminescence spectrum of Si:In sample C20102 at 20 K. The lines labelled BE are associated with the In bound exciton, and the line labelled FE is associated with the free exciton. The lines labelled P, Q and R are the long lifetime lines discussed in the text. The scale factors (e.g., "X50") give the relative intensity magnification.

shown. In addition to these lines, many other features in the Si:In spectrum have been observed. These features are listed in Table 3.2, where peak positions and some identifications are indicated. Three of the Si:In luminescence lines have been labelled P,Q,R in Fig. 3.1 and Table 3.2. We now consider in detail the properties of these lines.

3.3.2 General Systematics of P,Q,R Luminescence

To begin with, it should be mentioned that P,Q,R luminescence has only been observed in Si:In. The only previous report of this luminescence was in the work of Vouk and Lightowers, who observed lines P and R and labelled them U2 and U3. P,Q,R luminescence has not been observed in undoped Si, or in Si doped with other impurities. As an illustration of this, Fig. 3.2 shows the luminescence from undoped Si at 20 K. Only intrinsic luminescence features due to FE and electron-hole droplet (EHD) recombination are observed. The P,Q,R line positions are indicated, but the lines are not present. In addition, the P,Q,R lines are only observed together. It appears, therefore, that the P,Q,R lines are related and that P,Q,R luminescence is associated with the presence of In.

3.3.3 Temperature Dependence of P,Q,R Luminescence

In this section, we consider the temperature dependence of the P,Q,R line luminescence intensities.

Table 3.2. The energy and assignment of some of the lines observed in this study of the photoluminescence spectrum of Si:In. Energies are accurate to ± 0.2 meV.

PEAK ENERGY (meV)	IDENTIFICATION
1077.6	
1082.0	TO + LO phonon BE_{In} (J = 0)
1085.1	TO + LO phonon BE_{In} (J = 2)
1093.3	
1098.4	TO + LO phonon FE
1101.1	
1105.7	
1108.6	R
1110.7	
1114.4	
1115.9	Q
1117.6	P
1121.5	TA phonon BE_{In} (J = 0)
1125.1	TA phonon BE_{In} (J = 2)
1129.2	
1136.5	
1140.3	BE_{In} (J = 0)
1143.7	BE_{In} (J = 2)
1154.3	

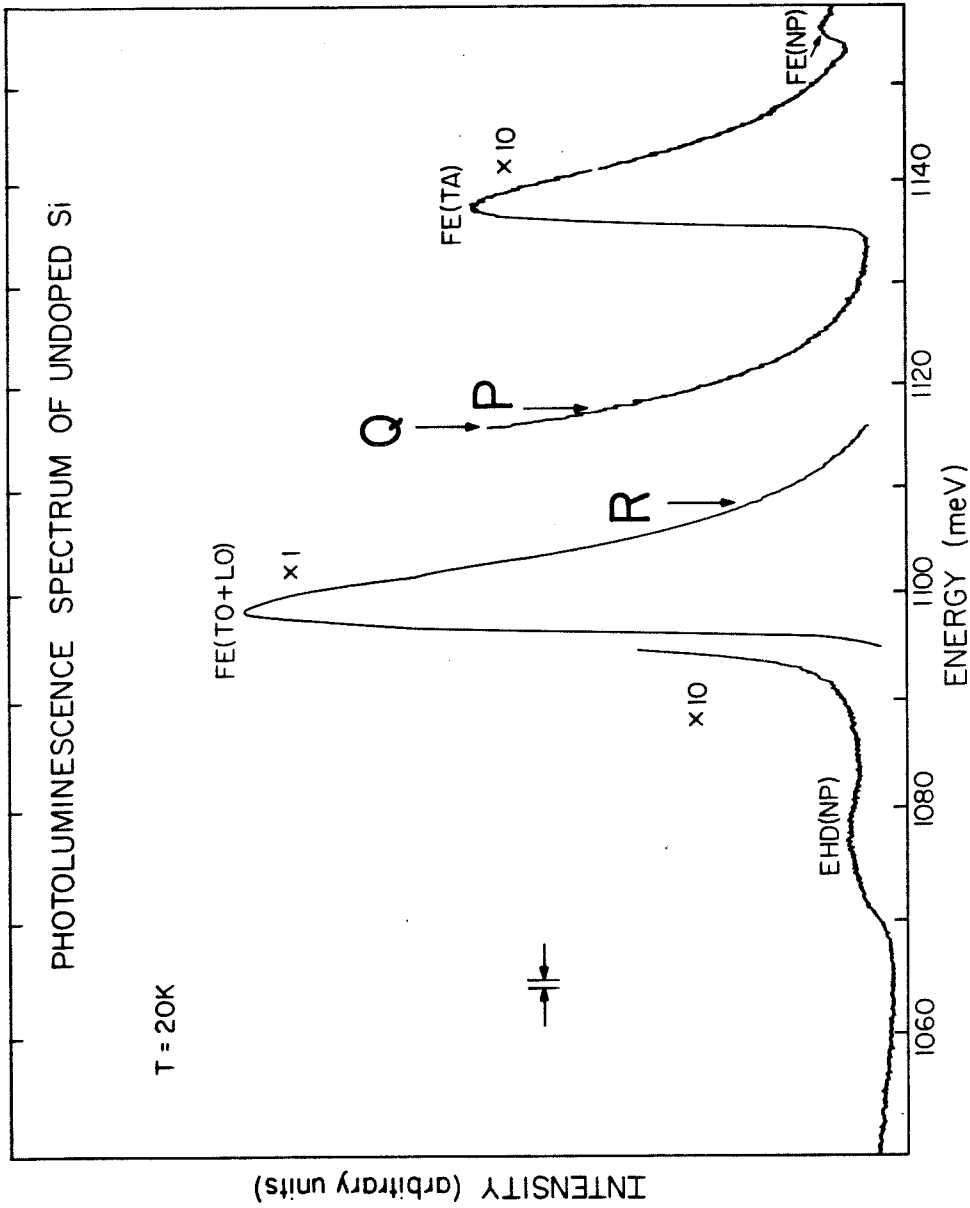


Figure 3.2. The photoluminescence spectrum of undoped Si at 20 K. Only intrinsic luminescence is observed. The lines labelled FE are associated with the free exciton. The line labelled EHD is associated with electron-hole droplet luminescence. The scale factors (e.g., "x10") give the relative intensity magnification.

3.3.3.1 Temperature-Resolved Spectra

In Fig. 3.3 spectra taken at various temperatures from 5 K to 25 K are shown. For purposes of comparison, in these spectra the BE_{In} intensity has been set to 1. These spectra show that line Q is present only at relatively high temperatures. Its intensity becomes appreciable at 15 K and increases with increasing temperature. This result suggests that line Q may be due to a transition from an excited state.

3.3.3.2 Temperature Dependence of P,Q,R Luminescence Intensity Ratios

From the spectra presented in Fig. 3.3, measurements of the P,Q,R line intensity ratios have been made as a function of temperature. The results are shown in Fig. 3.4. This figure shows that the Q/P intensity ratio increases with increasing temperature, as mentioned in the previous section. Fig. 3.4 also shows that the R/P intensity ratio remains constant, independent of temperature. This result suggests that lines P and R are related, and possibly due to transitions from the same initial state but to different final states. The difference in luminescence energy, 9.0 meV, is not equal to that of any bulk Si phonon with a wavevector which will conserve momentum, but may be due to the excitation of a local vibrational mode of the system responsible for the P luminescence. This suggestion is supported by the observed width of the R line, and measurements of the pump power dependence of the R/P intensity ratio. These measurements show

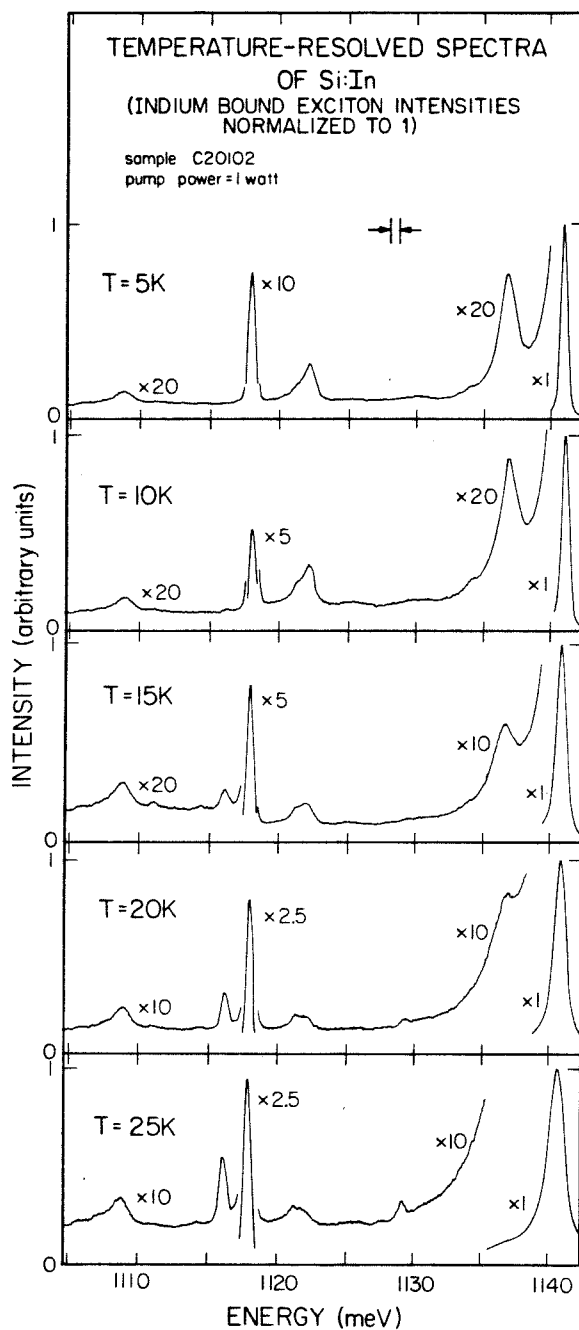


Figure 3.3. Photoluminescence spectra of Si:In sample C20102, taken at temperatures from 5 K to 25 K. In each spectrum, the In bound exciton intensity has been normalized to 1. Note that line Q appears only at higher temperatures. The scale factors (e.g., "X20") give the relative intensity magnification.

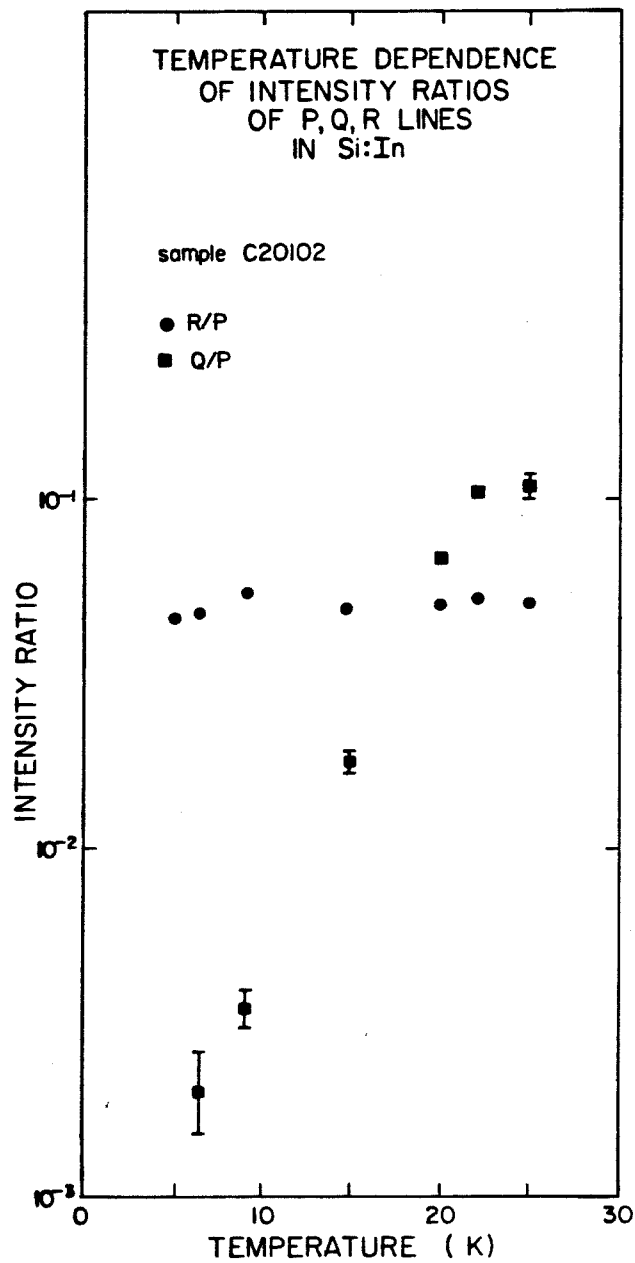


Figure 3.4. The temperature dependence of the intensity ratios of the P,Q,R lines in Si:In sample C20102. Note that the R/P intensity ratio is independent of temperature, while the Q/P intensity ratio increases with temperature.

that the R/P intensity ratio is independent of pump power, which is the behaviour expected for a local mode replica.

3.3.4 Time Dependence of P,Q,R Luminescence

In addition to these temperature dependence measurements, we have also examined the time dependence of P,Q,R luminescence. The pulsed GaAs laser diode was used as the excitation source, and the time resolution was accomplished by gating the output signal at the desired time after the end of the laser pulse. For measurement of the long decay times in question here, the gate width used was 20 μ sec.

3.3.4.1 Time-Resolved Spectra

Time-resolved spectra obtained in this manner at 20 K are shown in Fig. 3.5. As this figure illustrates, the P,Q,R lines have extremely long lifetimes, and we observe complete temporal isolation of P,Q,R luminescence.

3.3.4.2 Lifetimes of P,Q,R Luminescence

From the time-resolved spectra presented in the previous section, decay characteristics for the P,Q,R lines were obtained. Since entire time-resolved spectra were available, it was possible to subtract out the background contribution from each point to obtain accurate decay curves. The result at 20 K is shown in Fig. 3.6. An exponential decay of intensity with time was assumed, and the indicated lifetimes were determined from an exponential least

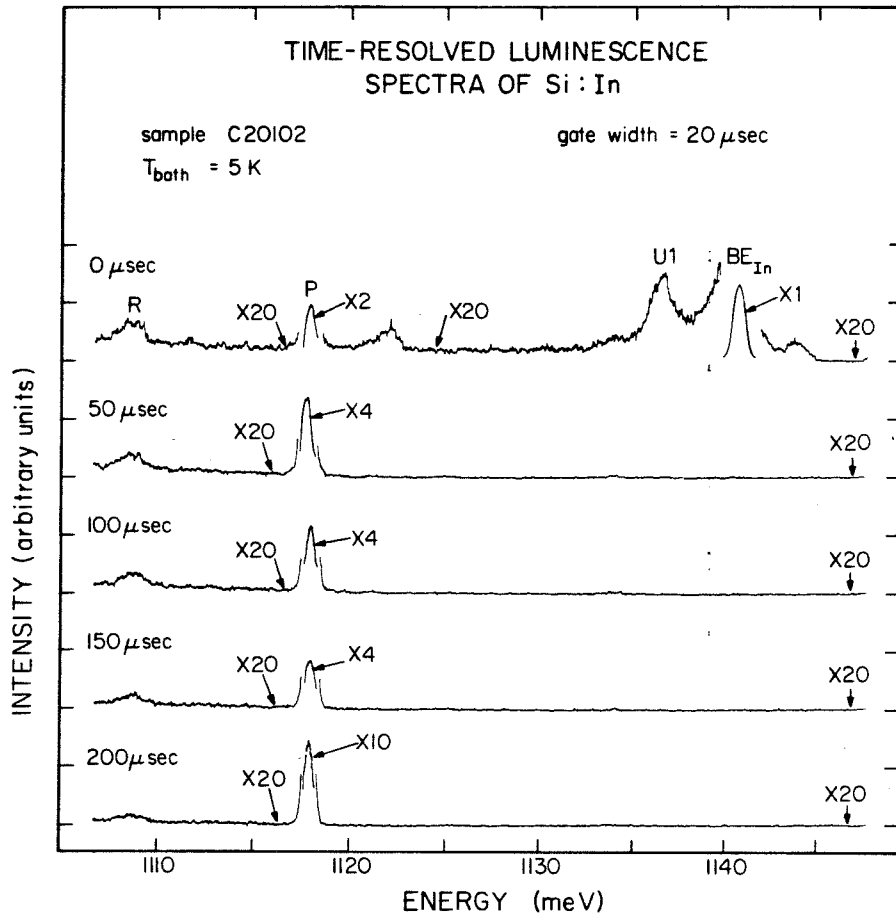


Figure 3.5. Time-resolved spectra of Si:In sample C20102 at 5 K. We observe complete temporal isolation of the P,Q,R lines. The scale factors (e.g., "X20") give the relative magnification.

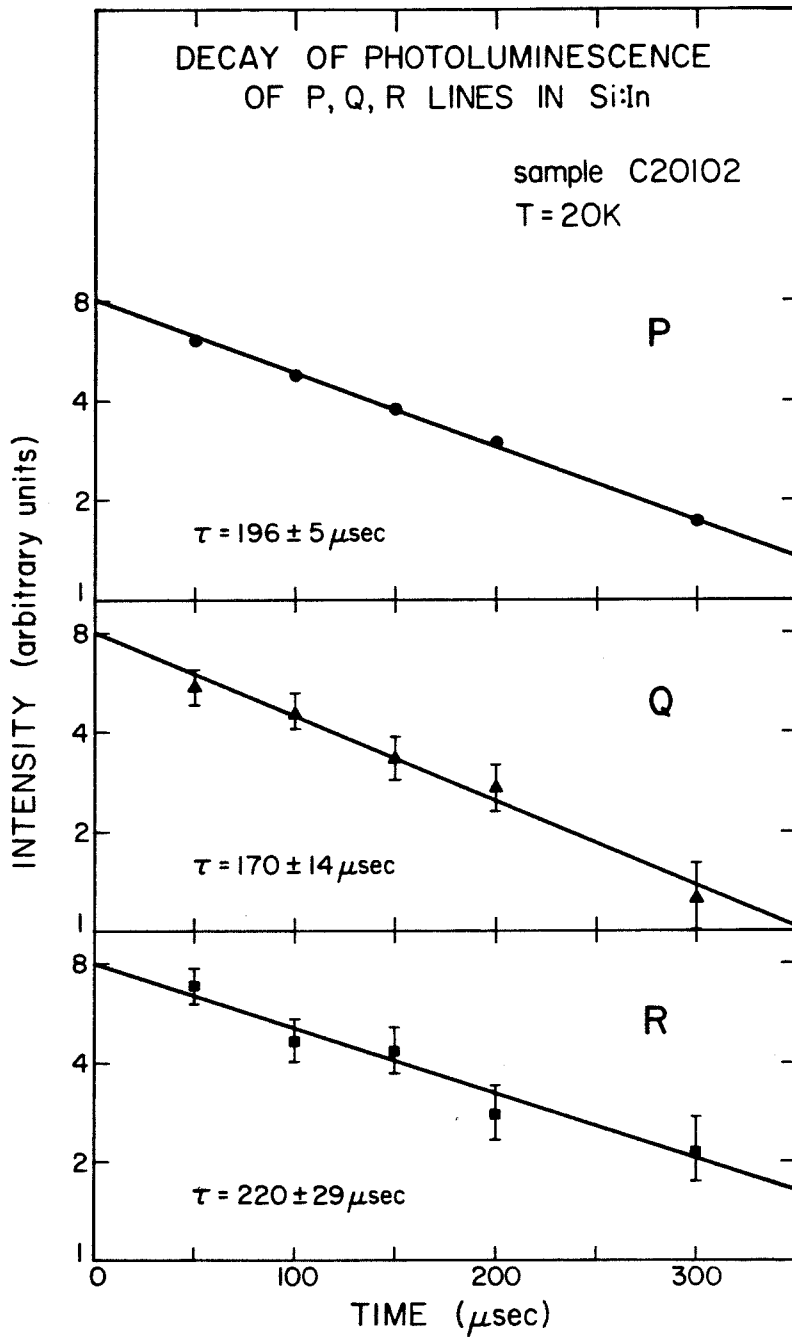


Figure 3.6. Typical decay curves for the P,Q,R lines in Si:In sample C20102 at 20 K. The intensities were normalized to the same initial value. The slopes are inversely proportional to the lifetimes, which are given on the figure.

squares fit to the measured data points. As shown in Fig. 3.6, the lifetimes obtained in this manner for the P,Q,R lines are 196 ± 5 μ sec, 170 ± 14 μ sec, and 220 ± 29 μ sec, respectively, at 20 K.

3.3.5 Isoelectronic Impurities

The lifetimes measured for P,Q,R luminescence in the previous section are orders of magnitude greater than the lifetimes measured for donor or acceptor BE luminescence in Si, where the Auger recombination mechanism dominates ⁽⁶⁾ and results in decay times which range from 1006 nsec for B to 2.7 nsec for In ^(7,8). The measured P,Q,R lifetimes indicate that the dominant decay mechanism for these lines is radiative recombination ⁽¹¹⁾, which suggests that the lines result from recombination of excitons bound to isoelectronic centres (BE_I) where the additional Auger carrier is not present.

Isoelectronic centres in semiconductors have been the subject of considerable study since the first realization that isoelectronic impurities can produce discrete BE states ⁽¹²⁾. The review article by Dean ⁽¹³⁾ provides a discussion of the topic. It is sufficient to note that while simple substitutional impurities are the most common form of isoelectronic trap observed, more complex isoelectronic centres can also produce BE states, although often their identity is difficult to establish ⁽¹³⁾. On the basis of these

previous observations, then, our proposal that P,Q,R luminescence results from BE_T recombination in Si:In is not unreasonable. Furthermore, it seems reasonable to suppose that the isoelectronic centres involved are impurity and/or defect complexes, which involve In as well as other impurities and/or defects. If this is the case, our work is the first observation of isoelectronic centres in Si. Subsequent to this work, what appears to be isoelectronic luminescence from heavily C doped Si has been reported by Weber et al ⁽¹⁴⁾. The P,Q,R lines are not associated with this Si:C luminescence, however.

3.3.6 Temperature Dependence of P,Q,R Lifetimes

The lifetime measurements described above were repeated at a number of different temperatures. The result of these measurements is shown in Fig. 3.7, in which the measured lifetimes are plotted as a function of temperature. Fig. 3.7 shows that the lifetimes of all three lines exhibit roughly the same dependence on temperature. At temperatures below about 5 K, the P,R lifetimes appear to remain relatively constant, independent of temperature. Of course, line Q is not observed at these low temperatures. As the temperature increases, the lifetimes of all three lines increase, reach a maximum value, and then decrease as thermalization becomes important.

The increase observed in the measured lifetimes suggests that

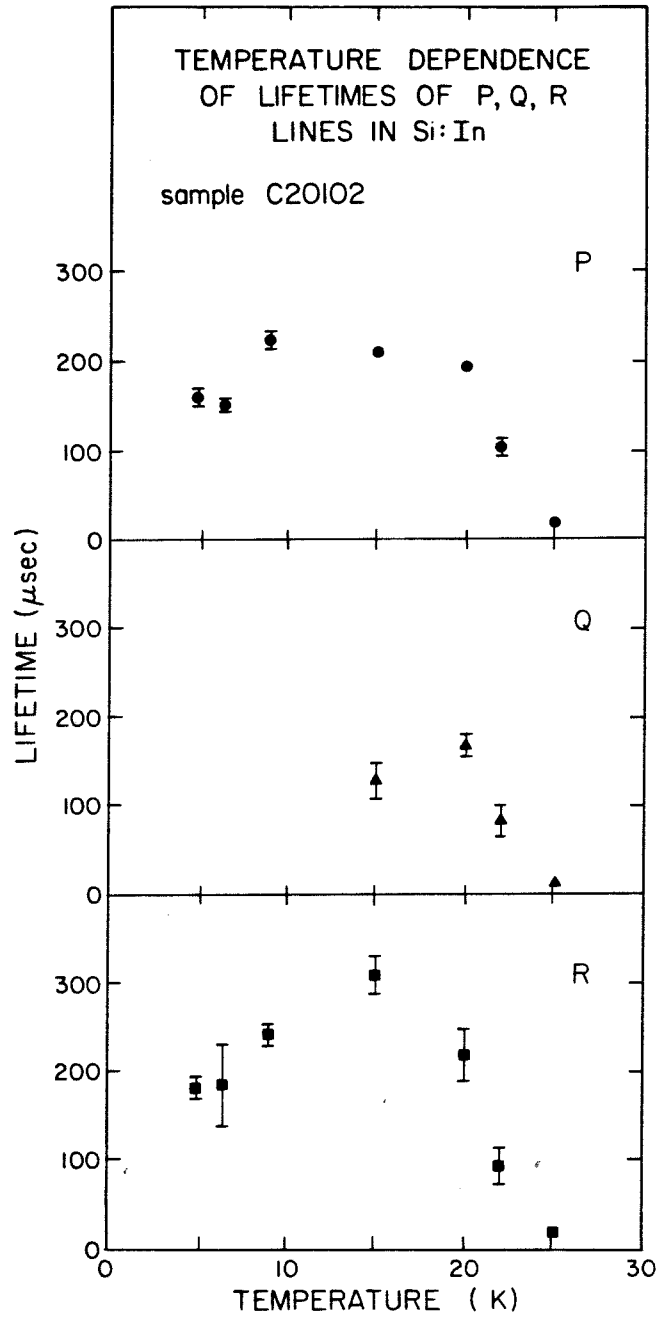


Figure 3.7. The P,Q,R line lifetimes as a function of temperature for Si:In sample C20102. The lines show the same general lifetime temperature dependence.

excited states are involved which have a somewhat longer lifetime than the ground state. As the temperature increases, these excited states will be thermally populated, which will increase the measured lifetimes. This feature of the observed P,Q,R lifetime temperature dependence will be discussed in detail below.

3.4 MODEL FOR P,Q,R LUMINESCENCE

3.4.1 Qualitative Features of the Model

The results which have been presented so far lead us to propose a model for P,Q,R luminescence, which has certain qualitative features. First, the observed very long lifetimes strongly suggest that P,Q,R luminescence is the result of recombination of excitons bound to isoelectronic centres (BE_T) in Si. Second, the lines appear to be related, insofar as they always appear together, and it is reasonable to suggest that the same centre is responsible for all three lines. Third, the lines only appear in Si:In, and so it appears that the centre is some complex which involves In. Fourth, line Q appears to be the result of a transition from an excited state of the BE_T complex, since it is only observed at high temperatures where an excited state is thermally populated. Fifth, the observed lifetime temperature dependence suggests that this excited state has a longer lifetime than the ground state. Finally, the observed width of the R line and the independence of the R/P intensity ratio on temperature and pump power suggests that lines P and R are the result of transitions from the same state, and that line R is a local phonon mode replica of

line P.

On this basis, we propose that P,Q,R luminescence is the result of recombination of excitons bound to a single isoelectronic centre (BE_I), which has the level scheme schematically illustrated in Fig. 3.8. As shown in Fig. 3.8, we assume that line P is the result of the no-phonon recombination of an exciton bound to the isoelectronic complex, where the initial state of the transition is the ground state of the bound exciton and the final state is the ground state of the isoelectronic complex. Line R is a 9 meV local phonon mode replica of line P. Finally, line Q is the result of a transition from an excited state of the bound exciton to an excited state of the isoelectronic complex.

3.4.2 The Rate Equations

The qualitative features of the model described in the previous section can be incorporated in a set of rate equations. We assume that the long optical pumping pulse produces FE, which can decay or be captured to form BE_I or BE_{In} . These BE can subsequently decay or be thermally released. We further assume that the BE_I have two states which are in thermal equilibrium and that BE_I decay or thermalization can occur from either state. Application of detailed balance leads to the following set of rate equations:

$$\frac{dn_{FE}}{dt} = - (v_{FE} + \sum_i \gamma_i) n_{FE} + \sum_i \rho_i n_i \quad (3.1)$$

ENERGY LEVEL SCHEME FOR P,Q,R LUMINESCENCE

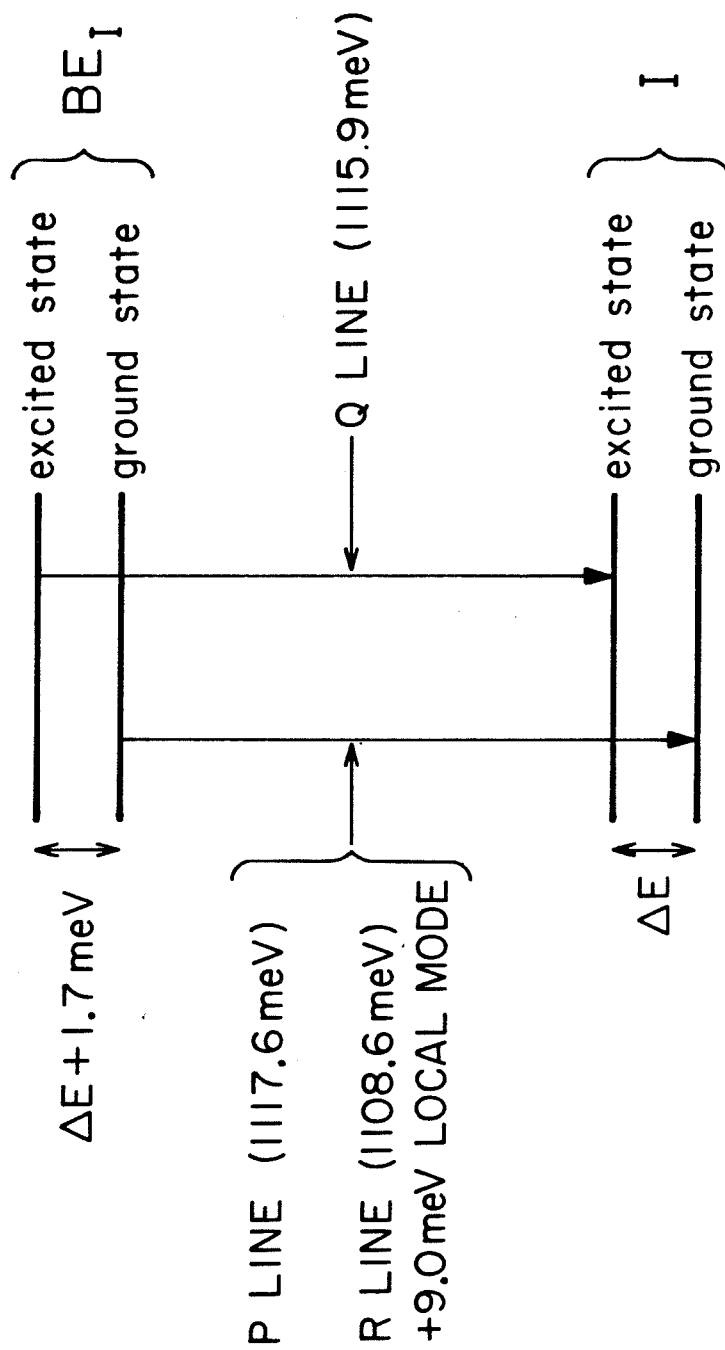


Figure 3.8. Schematic representation of the energy levels involved in P,Q,R luminescence. The symbol "I" refers to the isoelectronic complex.

$$\frac{dn_i}{dt} = \gamma_i n_{FE} - (v_i + \rho_i) n_i \quad (3.2)$$

where the variables are defined as for Eqs. (2.1) and (2.2). We assume that the optical pumping pulse is long enough that steady-state conditions are obtained. Then the boundary conditions at $t = 0$ are:

$$\begin{aligned} \left. \frac{dn_{FE}}{dt} \right|_{t=0} &= g - (v_{FE} + \sum_i \gamma_i) n_{FE} \Big|_{t=0} \\ &+ \sum_i \rho_i n_i \Big|_{t=0} = 0 \end{aligned} \quad (3.3)$$

$$\left. \frac{dn_i}{dt} \right|_{t=0} = \gamma_i n_{FE} \Big|_{t=0} - (v_i + \rho_i) n_i \Big|_{t=0} = 0 \quad (3.4)$$

Now, any term in Eqs. (3.1) to (3.4) for which $i = I$ is to be interpreted as being the sum over ground state and excited state contributions. That is

$$n_I = n_g + n_x \quad (3.5)$$

$$\rho_I n_I = \rho_g n_g + \rho_x n_x \quad (3.6)$$

$$\gamma_I = \gamma_g + \gamma_x \quad (3.7)$$

$$(v_I + \rho_I)n_I = (v_g + \rho_g)n_g + (v_x + \rho_x)n_x \quad (3.8)$$

in an obvious notation. To proceed, we assume thermal equilibrium between the ground state and excited state populations. We let

$$\frac{n_x}{n_g} = K(T) \quad (3.9)$$

where

$$K(T) \propto \exp\left(-\frac{\Delta E}{k_B T}\right) \quad (3.10)$$

and

ΔE = the energy splitting between the ground state and the excited state.

Since $K(T)$ is independent of time, we can use this relation to eliminate n_x from Eqs. (3.5) to (3.8). The sums collapse, and we can define the "effective rates"

$$\rho_I = \frac{\rho_g + \rho_x K(T)}{1 + K(T)} \quad (3.11)$$

$$v_I = \frac{v_g + v_x K(T)}{1 + K(T)} \quad (3.12)$$

We are then left with the problem of obtaining the time-dependent solution of Eqs. (3.2) to (3.5) for n_{FE} , n_I and n_{In} .

3.4.3 The Rate Estimates

Now, Eqs. (3.2) and (3.3) are fairly completely coupled. An exact analytical solution is tedious to obtain, and not particularly enlightening. Considerable simplification results if we can make the assumption that

$$(v_{FE} + \sum_i \gamma_i) (v_i + \rho_i) \gg (\gamma_i) (\rho_i) \quad (3.13)$$

We can estimate these quantities over the temperature range of interest by applying Eq. (2.3) for γ_i and Eq. (2.4) for ρ_i . First, we have $v_{FE} \sim 5 \times 10^5 \text{ sec}^{-1}$. The FE thermal velocity, v_{th} , is calculated assuming a Boltzmann distribution for the FE kinetic energies to be

$$v_{th} = \left(\frac{8 k_B T}{\pi m_{ex}} \right)^{\frac{1}{2}} \quad (3.14)$$

We take $m_{ex} = 0.6 m_o$ ⁽⁹⁾ and obtain

$$v_{th} = (8 \times 10^5)^{\frac{1}{2}} T^{\frac{1}{2}} \text{ cm/sec} \quad (3.15)$$

for T in K. The thermally averaged FE density of states is

$$N_{FE} = 2 \left(\frac{m_{ex} k_B T}{2\pi \hbar^2} \right)^{\frac{3}{2}} \quad (3.16)$$

which results in

$$N_{FE} = (2 \times 10^{15}) T^{\frac{3}{2}} \text{ cm}^{-3} \quad , \quad (3.17)$$

again for T in K. For $i = I_n$, we take $\sigma_{In} = (1.3 \times 10^{-9}) T^{-4} \text{ cm}^2$ (10) and $N_{In} = 6 \times 10^{16} \text{ cm}^{-3}$. Then we obtain

$$\gamma_{In} = (6.2 \times 10^{13}) T^{-3.5} \text{ sec}^{-1} \quad , \quad (3.18)$$

Also, we take $E_{In} = 13.7 \text{ meV}$, which results in

$$\rho_{In} = (2.2 \times 10^{12}) T^{-2} \exp \left[-\frac{159}{T} \right] \text{ sec}^{-1} \quad . \quad (3.19)$$

Since Auger decay is so effective for BE_{In} , ν_{In} is very large. We take $\nu_{In} = 3.7 \times 10^8 \text{ sec}^{-1}$ (8).

The situation for $i = I$ is less precise. To begin with, we assume that $\sigma_g \sim \sigma_x \equiv \sigma_I$ (10). Now, σ_I will depend sensitively on what assumption we make regarding the highly excited state structure of BE_I . For instance, BE_{In} highly excited states have been observed (15) and this is thought to lead to the rapid temperature dependence which is observed for σ_{In} (10). On the other hand, highly excited states have not been observed for BE_B (1-4), and σ_B exhibits a relatively mild temperature dependence (10). We have no reason to assume that BE_I highly excited states exist, and so we take $\sigma_I \sim \sigma_B = (2.5 \times 10^{-13}) T^{-1} \text{ cm}^2$ (10). Also, on the basis of Eqs. (2.10) and (2.11) we estimate N_I from

$$N_I = \left(\frac{\sigma_{In} \eta_{In} I_I}{\sigma_I \eta_I I_{In}} \right) N_{In} \quad (3.20)$$

where the η are radiative efficiencies defined as

$$\eta_i = \frac{f_i}{\nu_i + \rho_i} \quad (3.21)$$

We assume that $f_I = f_{In}$, and consider the low temperature region where $\nu_i + \rho_i \sim \nu_i$. Then

$$\frac{\eta_{In}}{\eta_I} \sim \frac{\nu_I}{\nu_{In}} \quad (3.22)$$

From our previous estimates, we finally obtain $N_I \sim 8 \times 10^{11} \text{ cm}^{-3}$ for $I_I \sim I_{In}$. On the basis of these estimates, we have

$$\gamma_I = (1.6 \times 10^5) T^{-\frac{1}{2}} \text{ sec}^{-1} \quad (3.23)$$

To estimate ρ_I , we assume that the BE_I ground state and excited state have equal degeneracies. Then Eqs. (2.4) and (3.11) combine to give

$$\rho_I = \frac{2 \sigma_I \nu_{th} N_{FE} \exp \left(-\frac{E_g}{k_B T} \right)}{1 + \exp \left(-\frac{\Delta E}{k_B T} \right)} \quad (3.24)$$

where E_g is the thermalization energy of BE_I from the ground state. To estimate we take $\Delta E \sim 1$ meV, which is typical of BE in Si (4,16) and $E_g \sim 37.81$ meV, which corresponds to the observed P line position in the Si:In spectrum. We obtain

$$\rho_I = \frac{(8 \times 10^8) T \exp \left[-\frac{430}{T} \right]}{1 + \exp \left[-\frac{11.6}{T} \right]} \quad (3.25)$$

Finally, we assume that $\nu_g \sim \nu_x = 5 \times 10^3 \text{ sec}^{-1}$ as observed for the P line. Then Eq. (3.12) results in $\nu_I = 5 \times 10^3 \text{ sec}^{-1}$.

3.4.4 The Approximations

The rate estimates obtained in the previous section have been plotted in Fig. 3.9 for the temperature range of interest. We see that, in general, the FE decay rate, ν_{FE} , and the isoelectronic complex capture rate, γ , are orders of magnitude smaller than the In capture rate, γ_{In} . This is basically a result of the large In concentration. So we can assume $\nu_{FE} + \Sigma \gamma_i \sim \gamma_{In}$, and then Eq. (3.13) for $i = I$ because $\gamma_{In} \gg \gamma_I$.

In addition, the BE_{In} Auger rate, ν_{In} , and the In capture rate, γ_{In} , are very large compared to the BE_{In} thermalization rate, ρ_{In} , over the temperature range of interest. Therefore, $\nu_{In} + \rho_{In} \sim \nu_{In}$. So Eq. (3.13) also holds for $i = In$ because $\gamma_{In} \gg \rho_{In}$. We can there-

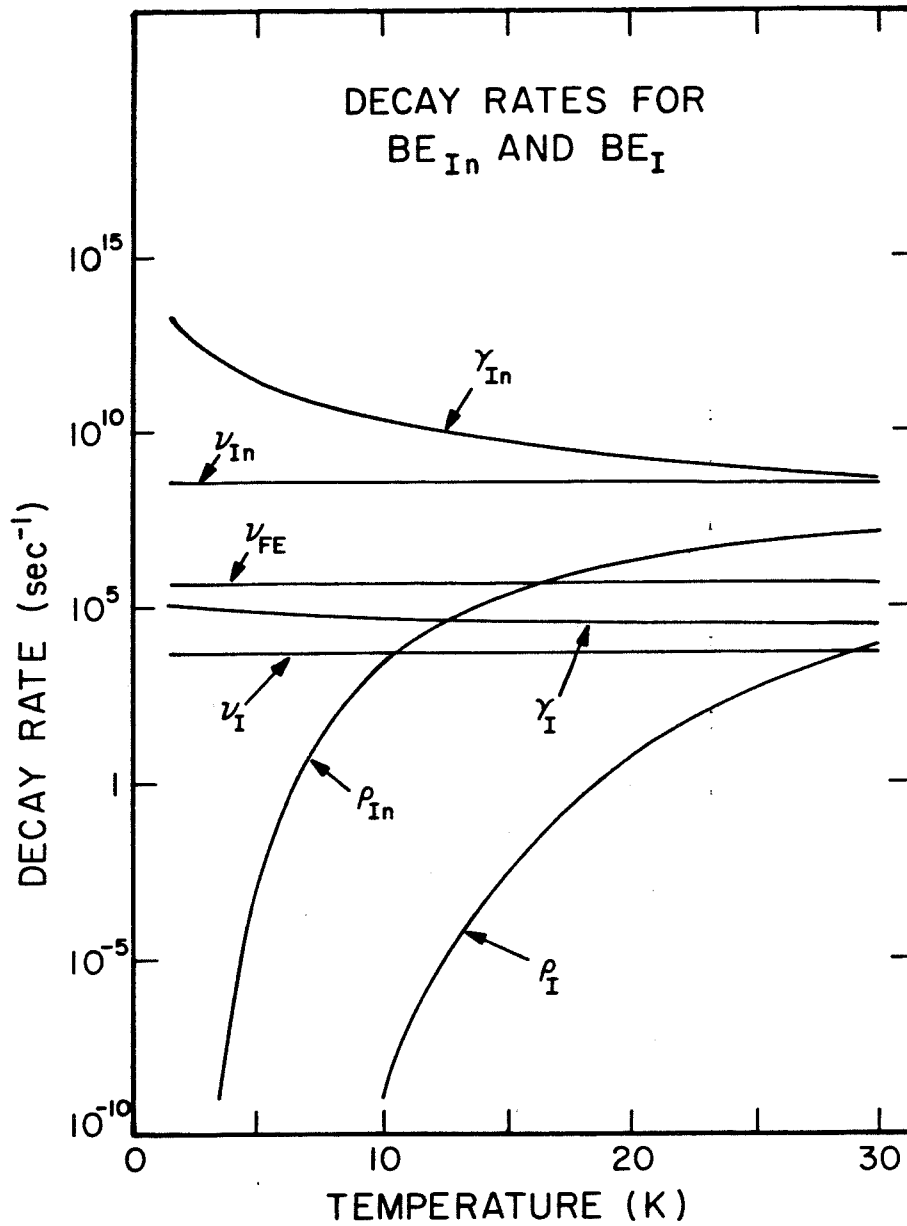


Figure 3.9. Estimated decay rates for BE_{In} and BE_I in Si:In. The assumptions which yield these estimates are discussed in detail in the text. The symbol "I" refers to the isoelectronic complex. "In" refers to the In impurity and "FE" refers to the free exciton. The ν are the decay rates, the γ are capture rates and the ρ are thermal release rates.

fore assume Eq. (3.13) and proceed with the solution of Eqs. (3.1) to (3.4).

3.4.5 The Approximate Solution

In the limit of Eq. (3.13), the solutions to the model presented in Eqs. (3.2) to (3.5) are straightforward. We obtain:

$$n_{FE} = \frac{g}{(v_{FE} + \Sigma \gamma_i)} \exp \left[- (v_{FE} + \Sigma \gamma_i) t \right] \quad (3.26)$$

$$n_i = \frac{g \gamma_i}{(v_{FE} + \Sigma \gamma_i) - (v_i + \rho_i)} \left\{ \frac{1}{(v_i + \rho_i)} \exp \left[-(v_i + \rho_i) t \right] - \frac{1}{(v_{FE} + \Sigma \gamma_i)} \exp \left[-(v_{FE} + \Sigma \gamma_i) t \right] \right\} \quad (3.27)$$

3.4.6 Comparison With The Experimental Results

To examine the proposed model for P,Q,R luminescence in more detail, we can compare the behaviour of the approximate solution obtained in the previous section with the observed behaviour of the P,Q,R system.

3.4.6.1 Lifetime Temperature Dependence

In particular, the behaviour of the approximate solution can be compared with the observed lifetime temperature dependence data. The behaviour of the approximate solution is quite clear. In the presence of large In concentrations, $\nu_{FE} + \sum \gamma_i \sim \gamma_{In}$. Further, $\gamma_{In} > (\nu_i + \rho_i)$, so the long-time decay rate is dominated by $(\nu_i + \rho_i)$ for both BE_I and BE_{In} decay. The measured lifetime, τ , will therefore be given by

$$\tau = \frac{1}{\nu_i + \rho_i} \quad (3.28)$$

In the low temperature regime where thermalization is not important, $(\nu_i + \rho_i) \sim \nu_i$. For $i = I$, ν_I is given by Eq. (3.12). At very low temperatures, $\nu_I \sim \nu_g$. As the temperature increases, ν_I takes on a value between ν_g and $\frac{1}{2}(\nu_g + \nu_x)$. So for $\nu_x < \nu_g$, we expect to see the lifetime increase as we observe in Fig. 3.7. In the high temperature region, where thermalization dominates, $(\nu_i + \rho_i) \sim \rho_i$. For $i = I$, ρ_I is given by Eq. (3.11), which reduces to Eq. (3.24) with the appropriate assumptions. Eq. (3.24) predicts a rapid decrease in the lifetime when thermalization dominates. This effect is also observed in Fig. 3.7.

However, there is one characteristic of the approximate solution which is not consistent with the observed lifetime temperature dependence

data. The approximate solution predicts that, at a given temperature, the P,Q,R lines should all have the same lifetime. Nevertheless, the lifetime temperature dependence data presented in Fig. 3.7 shows that this is not observed at temperatures below 20 K. At these temperatures, the detailed shape of the lifetime temperature dependence curve is different for each line. The lifetime of line R appears to peak sharply at about 15 K, while the lifetime of line P exhibits a much lower, broader maximum centred at about 15 K. The lifetime of line Q also appears to peak sharply, but the lifetime reached is lower than for either line P or line R, and the peak does not occur until about 20 K.

It is possible that this inconsistency is the result of certain assumptions on which the model is based. The model assumes that the bound exciton ground state and excited state are in thermal equilibrium. This leads to Eqs (3.9) and (3.10). We can check this assumption by noting that the luminescence intensity ratios are related to the ratio of bound exciton populations by oscillator strengths which are independent of temperature. Therefore, the model predicts that the Q/P luminescence intensity ratio should vary with temperature according to Eqs. (3.9) and (3.10). In Fig. 3.10, we present an Arrhenius plot of the Q/P intensity ratio, and we see that the expected straight line is not obtained. This suggests that Eqs. (3.9) and (3.10) are not strictly justified in this case.

However, there is another possible source for the inconsistency

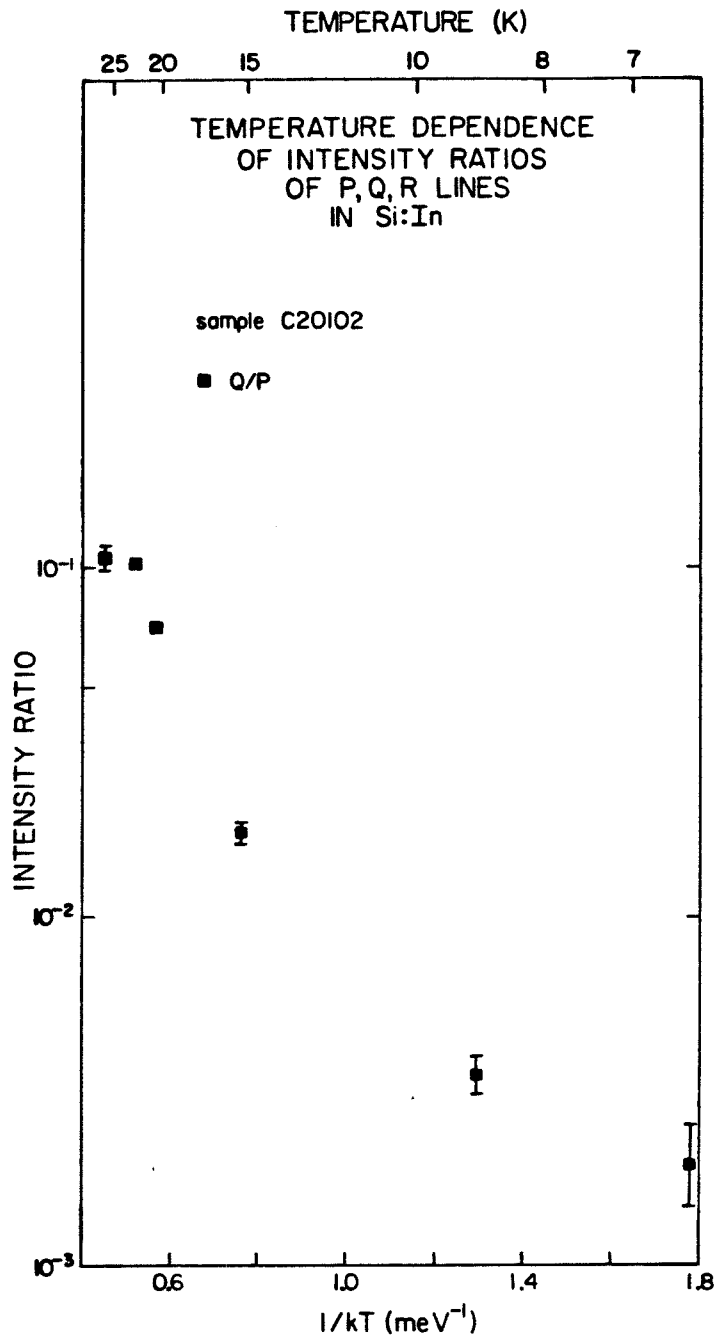


Figure 3.10. Arrhenius plot of the Q/P intensity ratio for Si:In sample C20102. Note that the Q/P intensity ratio does not produce a straight line on the Arrhenius plot.

between the behaviour of the approximate solutions and the observed experimental data. It is possible that this inconsistency is the result of a systematic error in the low temperature experimental data presented in Figs. 3.7 and 3.10. At the high laser pump powers used to obtain this data, both saturation and sample heating effects may be important. These effects are difficult to quantify, and have not been taken into account in our discussion.

3.4.6.2 Thermalization Behaviour

Above 20 K, the P,Q,R line lifetimes decrease abruptly as thermalization becomes important. We can attempt to understand quantitatively the thermalization behaviour by applying the model presented in the previous sections in the high temperature regime. If we assume that ΔE is small enough so that $\exp(-\Delta E/k_B T) \sim 1$ at high temperatures and assume that σ_I is independent of temperature, then the high temperature decay rate given by Eq. (3.24) reduces to

$$\rho_I \propto T^2 \exp\left(-\frac{E_g}{k_B T}\right) \quad (3.28)$$

Fig. 3.11 is an Arrhenius plot of the measured P,Q,R lifetimes multiplied by T^2 in the high temperature regime. We see that the linear variation predicted by Eq. (3.28) is indeed obtained. Linear least-squares fits to the measured data result in values for E_g of 29.4 ± 0.8 meV, 28.3 ± 0.2 meV and 29.5 ± 0.4 meV for lines P,Q and R, respectively.

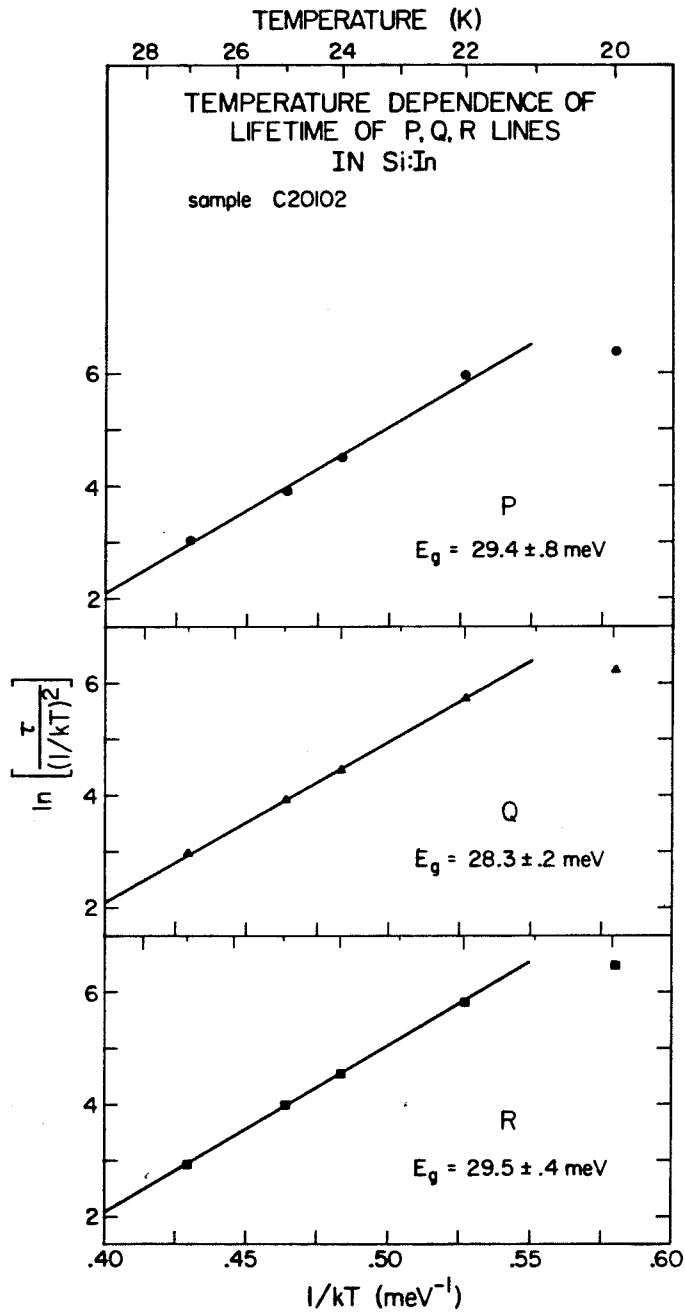


Figure 3.11. Arrhenius plot of the P,Q,R line lifetimes in the thermalization temperature region for Si:In sample C20102. From this plot, thermal bound exciton binding energies are obtained, which are the values for E_g shown in the figure.

There are two features associated with this determination of E_g which should be mentioned. First, the model for P,Q,R luminescence predicts that the same value of E_g should be obtained for each of the P,Q,R lines. The observed values are somewhat different, if the quoted error estimates are taken strictly. However, these estimates reflect only the scatter in the data presented in Fig. 3.11. Systematic errors, such as the sample heating effect described in the previous section, are not taken into account. In fact, an examination of this effect shows that only 1 K of sample heating will shift the values of E_g by approximately 2 meV. So a systematic error due to sample heating could certainly be responsible for the small observed variation in the E_g values.

Second, we note that a value for the exciton binding energy can be determined from the luminescence spectrum. As indicated in Fig. 3.8, we assume that line P is due to the NP recombination of a bound exciton which leaves the binding centre in its ground state. Then the spectroscopic ground state binding energy can be determined as the difference between the NP FE threshold energy, 1154.6 meV, and the energy at which the line appears. The value for E_g obtained in this manner is 37.2 meV for line P.

This result is substantially higher than the thermal binding energy quoted above. A possible explanation for this effect has been proposed by Trumbore *et al.*⁽¹⁷⁾ When an isoelectronic impurity binds an exciton, the binding is thought to occur in two steps. First, one of the

carriers is tightly bound by the short range potential due to lattice distortion about the impurity. Then the second carrier is bound by its Coulomb attraction to the first carrier. When the temperature is increased, the second, weakly bound carrier is thermalized. So it may be the lower binding energy of this second carrier that we obtain with the thermal binding energy measurement. Of course, the spectroscopic measurement will still give the binding energy of the exciton to the centre.

It is possible that this suggestion may explain our results. Of course, a number of approximations were involved in obtaining Eq. (3.28), and it is also possible that these approximations may be affecting the analysis. For instance, the temperature variation of the capture cross section or the influence of excited states may be non-negligible in the temperature range of interest. However, at the present time insufficient information is available for a complete quantitative analysis of these effects.

3.5 ENHANCEMENT OF P,Q,R LUMINESCENCE

3.5.1 Origin of P,Q,R Luminescence

Up to this point, we have considered in detail the behaviour of P,Q,R luminescence in response to changes in the experimental conditions. Results for one sample have been presented, Si:In sample C20102. In addition, some general statements have been made regarding the origin of P,Q,R luminescence. Specifically, it appears that P,Q,R luminescence results from recombination of excitons bound to an isoelectronic complex (BE_T), where the isoelectronic centre in question is probably a complex which undoubtedly involves In. However, no comment has been made regarding the precise nature of the complex and its constituents.

3.5.2 Determination of Origin by Systematic Sample Comparison

One of the most useful techniques for determining the detailed composition of a particular luminescence centre involves the correlation of luminescence intensity with known impurity concentrations for well-characterized samples. In principle, this technique could be applied to P,Q,R luminescence in Si:In. As Table 3.1 indicates, many well-characterized Si:In samples were available for investigation, and an effort to correlate P,Q,R luminescence intensities with the known impurity concentrations could, in principle, be made. However, we have discovered an unusual characteristic of the P,Q,R luminescence which makes it impossible to proceed on such a course.

Application of the technique described above involves the quantitative comparison of luminescence from various samples with different impurity concentrations. As a necessary prerequisite for this comparison, we must ensure that reproducible results can be obtained from a single sample. Of course, the absolute luminescence intensities will depend sensitively on the optical alignments and instrumental responses inherent in the experimental measurement, as well as on the condition of the sample surface. Nevertheless, the relative luminescence intensities should be independent of such influences. This is a central condition necessary for the successful application of the technique.

3.5.3 Reproducibility of P,Q,R Luminescence

In Fig. 3.12 we present various measurements of the photoluminescence spectrum of sample C117A. The experimental conditions were identical for each measurement. The only difference between the spectra is that the sample was removed from and reinserted into the dewar between each spectrum. It is abundantly clear from Fig. 3.12 that the spectra are not reproducible under these conditions. The ratio of P line to BE_{In} luminescence varies by approximately a factor of 2 in Fig. 3.12.

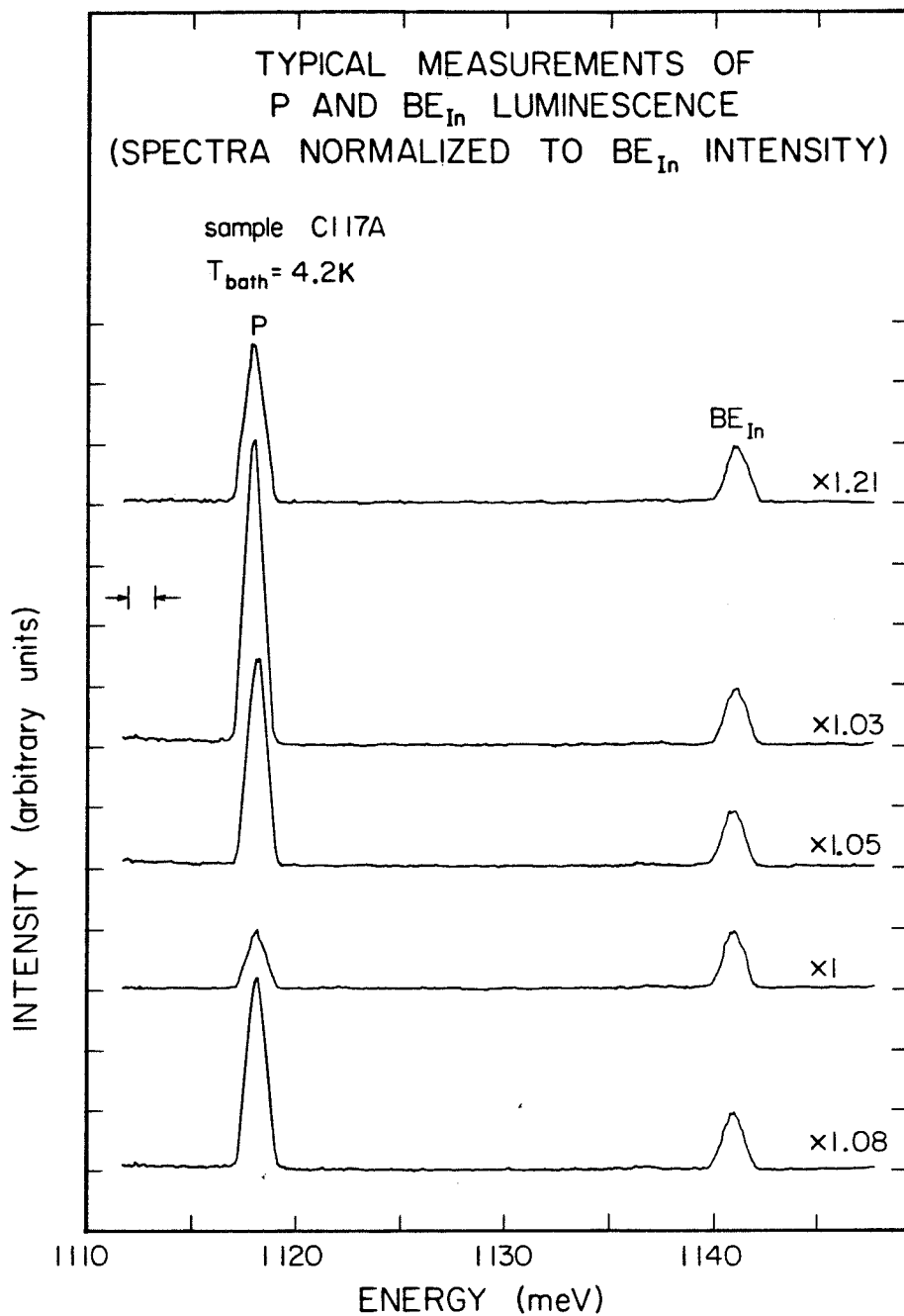


Figure 3.12. Various measurements of the luminescence spectrum of Si:In sample C117A. The spectra are normalized to the BE_{In} intensity, and the scale factors (e.g., "x1.21") give the relative intensity magnifications required to achieve the normalization. Note that the P/BE_{In} intensity ratio varies by over a factor of 2.

3.5.4 Measurement of Sample Homogeneity

One of the most obvious causes of such a lack of reproducibility is sample inhomogeneity. Accordingly, the homogeneity of sample C117A was investigated, and the results are presented in Fig. 3.13. As Fig. 3.13 demonstrates, C117A does not appear to be particularly homogeneous with respect to P line luminescence since the P line to BE_{In} luminescence intensity ratio varies by approximately a factor of 8.

However, such an effect can be accounted for. In the experiments described here, four regions were scribed on the surface of sample C117A. Each region was approximately 4 mm^2 . A particular scribed region could be selected for excitation by observing the laser spot with the aid of a small microscope. When spectra of luminescence from the same region were compared, reproducible results could be obtained independent of changes in laser position, sample position or optical alignment between measurements, providing the sample remained in the dewar at low temperatures. However, reproducible results could not be obtained if the sample was removed from the dewar between measurements even though the spectra were all obtained from the same region. In fact, the spectra shown in Fig. 3.13 are an example of this effect. These results indicate that sample inhomogeneity is not responsible for our inability to obtain reproducible results if care is taken to compare only those spectra which result from excitation of the same scribed region on the sample surface.

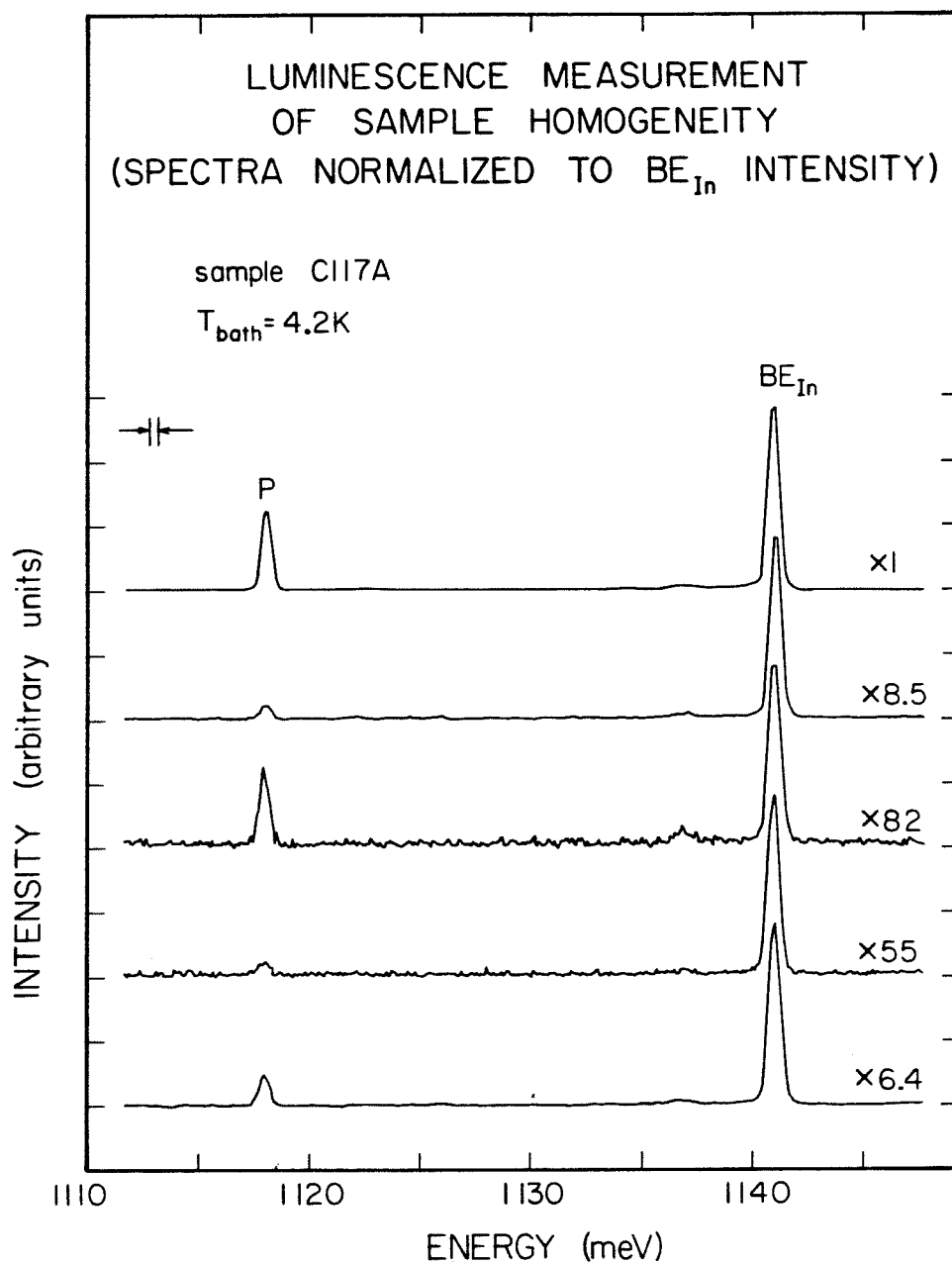


Figure 3.13. Luminescence measurement of the spatial homogeneity of Si:In sample C117A. The spectra are normalized to the BE_{In} intensity, and the scale factors (e.g., "x8.5") give the relative intensity magnifications required to achieve this normalization. Note that the P/BE_{In} intensity ratio varies by over a factor of 8.

3.5.5 Measurement of Luminescence Saturation

A second effect which may cause a lack of reproducibility in relative luminescence intensities is saturation of the centres responsible for the luminescence features. Saturation results in a spatial profile of bound exciton densities, which leads to a dependence of the luminescence intensity on the optical alignment. Of course, as we have already discussed, spectra from the same region were reproducible provided the sample remained in the dewar at low temperatures between measurements. This observation is an indirect indication that saturation effects are not contributing to the observed lack of reproducibility. Nevertheless, measurements of the pump power dependence of P line and BE_{In} luminescence were made explicitly to examine the saturation characteristics of P luminescence. The results are presented in Figs. 3.14 and 3.15. Fig. 3.14 shows the pump power dependence of P line luminescence. As expected on the basis of our estimate for N_I ($\sim 10^{11} \text{ cm}^{-3}$), we observe P line luminescence saturation at very low pump powers. Fig. 3.15 presents the pump power dependence of BE_{In} luminescence, and shows that BE_{In} luminescence saturation does not occur even at the highest pump powers considered here. On the basis of these results, care was taken to ensure that subsequent measurements were made at pump powers for which P line luminescence saturation was not occurring. In spite of this precaution, reproducible results still could not be obtained when the sample was removed from and reinserted into the dewar between measurements.

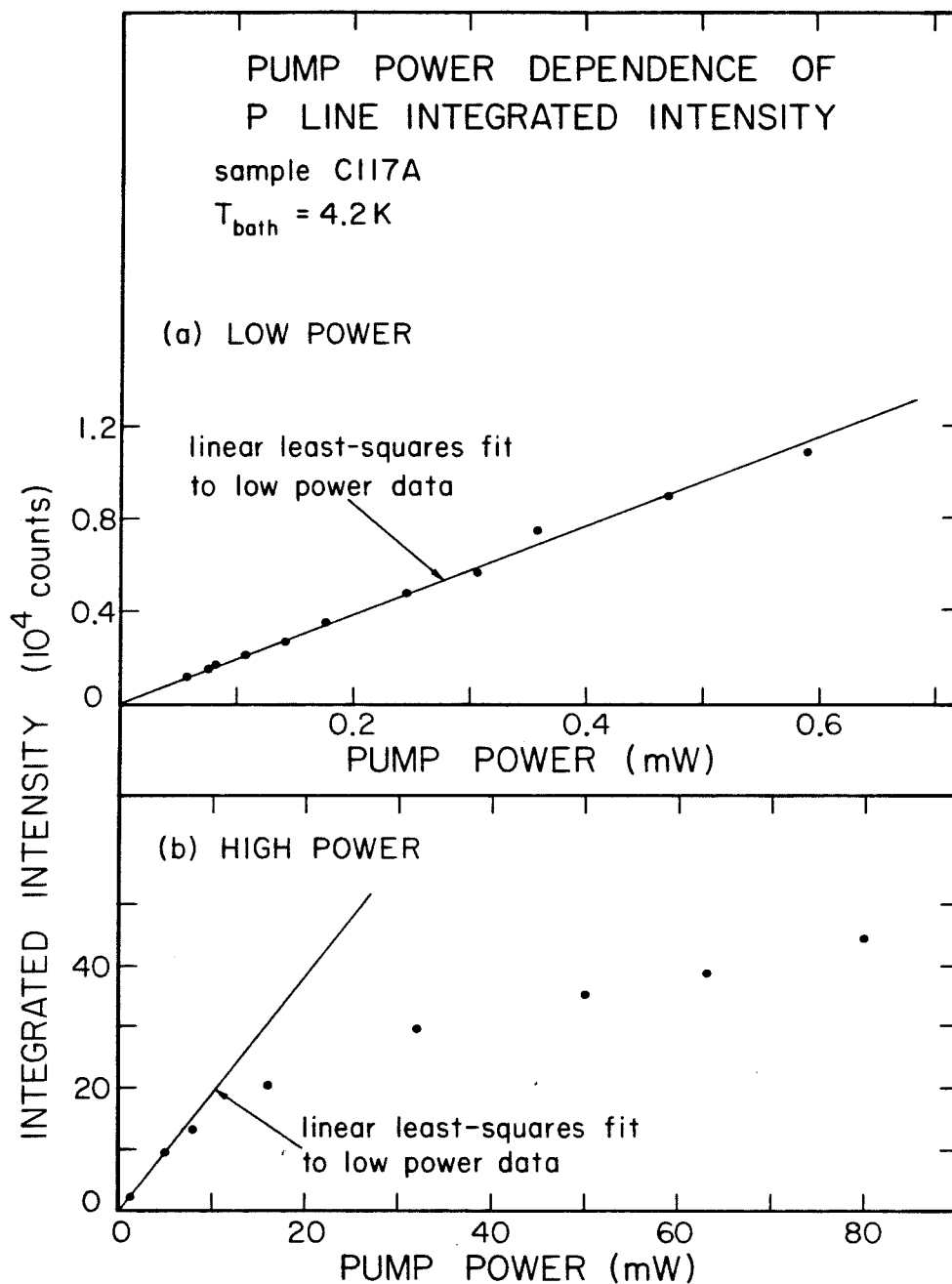


Figure 3.14. Pump power dependence of P line luminescence from Si:In sample C117A.
 (a) Low power region, where saturation effects are not important.
 (b) High power region, where P line saturation is clearly observed.
 The same linear least-squares fit to the low power data is shown in each case.

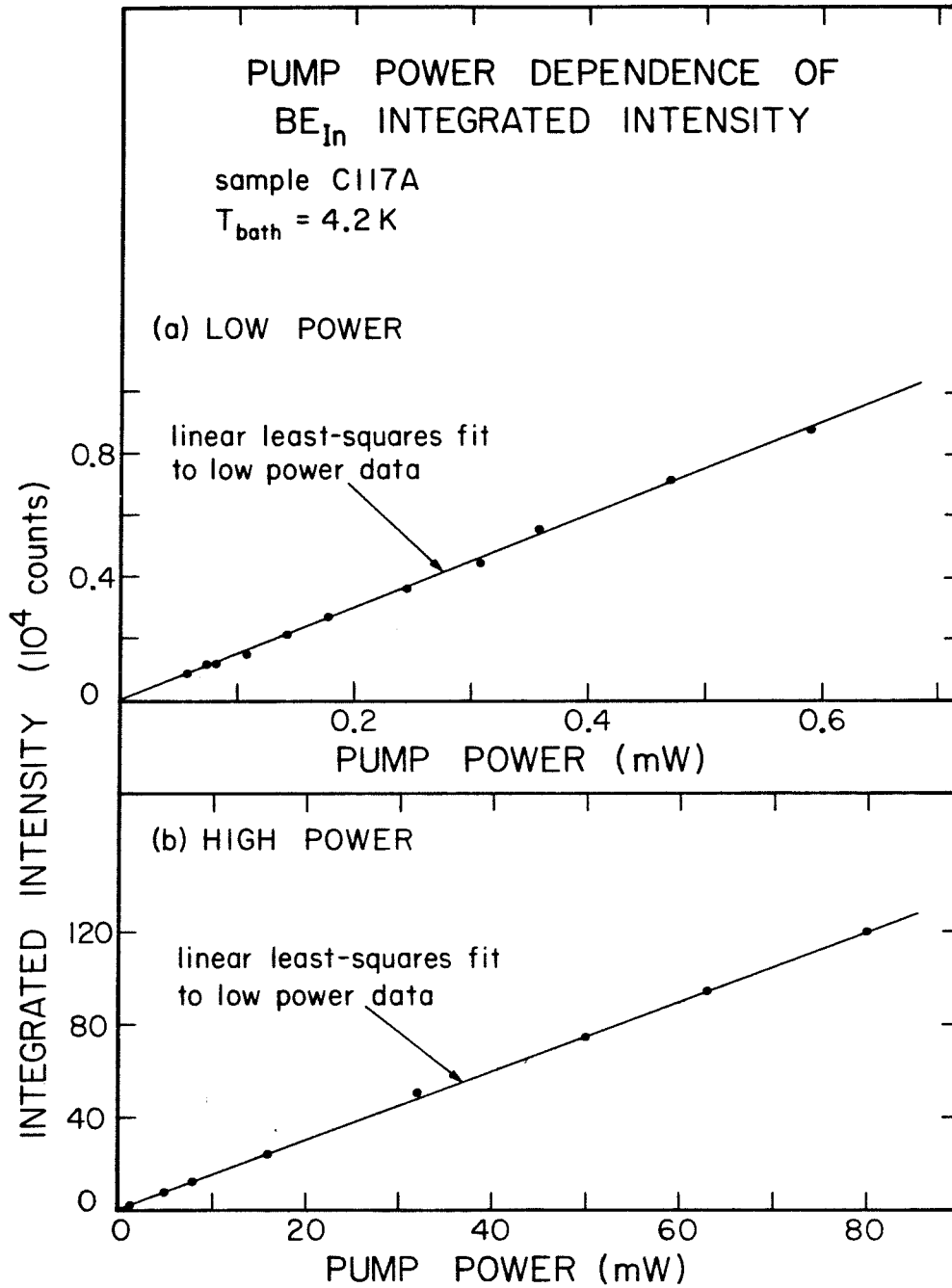


Figure 3.15. Pump power dependence of BE_{In} luminescence from Si:In sample C117A.

(a) Low power region.

(b) High power region.

The same linear least-squares fit to the low power data is shown in each case. Note that BE_{In} saturation is not observed even at the highest pump powers examined here.

3.5.6 Effect of Surface Preparation and the Enhancement of P,Q,R Luminescence

We are led, therefore, to consider our treatment of the sample between luminescence measurements as the source of this lack of reproducibility. As we have mentioned, it is only when the sample is removed from the dewar between measurements that reproducible results cannot be obtained, so we have some reason to suppose that this procedure has some effect on the sample which alters its luminescence characteristics. In particular, we are led to consider the effect of such an operation on the surface characteristics of the sample. Until the present work, the assumption that relative luminescence intensities are insensitive to sample surface conditions has been unquestioned in luminescence measurements. For example, as we discussed in Chapter 2 there is considerable current interest in applying the photoluminescence technique to the characterization of doped Si, and work has been proceeding quite well in this area. The assumption that relative luminescence intensities are independent of sample surface conditions is essential in that work. The successful application of the technique has been indirect confirmation of the validity of the assumption. Indeed, the assumption is quite reasonable if we examine bulk impurities in Si using Ar^+ laser excitation. As indicated in Fig. 1.9, photons at the Ar^+ laser energy of 2.5 eV penetrate approximately 2 μm into Si. This is much deeper than surface effects are thought to extend.

In spite of these considerations, the sensitivity of P line luminescence to sample surface preparation procedures was investigated. As a result, we have determined that P line luminescence is very dependent on the Si surface treatment. In particular, a two-step procedure has been developed which produces extreme P line enhancement. The results of this procedure are illustrated in Fig. 3.16. Fig. 3.16 (a) shows "typical" luminescence from Si:In sample C117A, before the enhancement procedure is applied. In the first step of the procedure, the sample is subjected to a 2-hour anneal at 1000 C in a dry He atmosphere. This step quenches P line luminescence, as shown in Fig. 3.16 (b), but also apparently "primes" the sample for the second step. The second step of the procedure involves lapping the sample with a fine grit lapping compound, 0.03 μm aluminum oxide powder for example. The result of this step is shown in Fig. 3.16 (c), in which we see that the P line luminescence has become almost two orders of magnitude more intense than BE_{In} luminescence.

3.5.7 Characteristics of the Enhancement Procedure

Before we speculate on the nature of the process which produces such unusual behaviour, there are a number of features associated with the enhancement procedure which should be mentioned. First, of course, is the fact that it is a room temperature, surface-specific process which produces the P line luminescence enhancement. Second, this process appears to be quite unique. Other surface-specific processes such as Si or Si oxide etches do not produce the effect. Third, the pre-

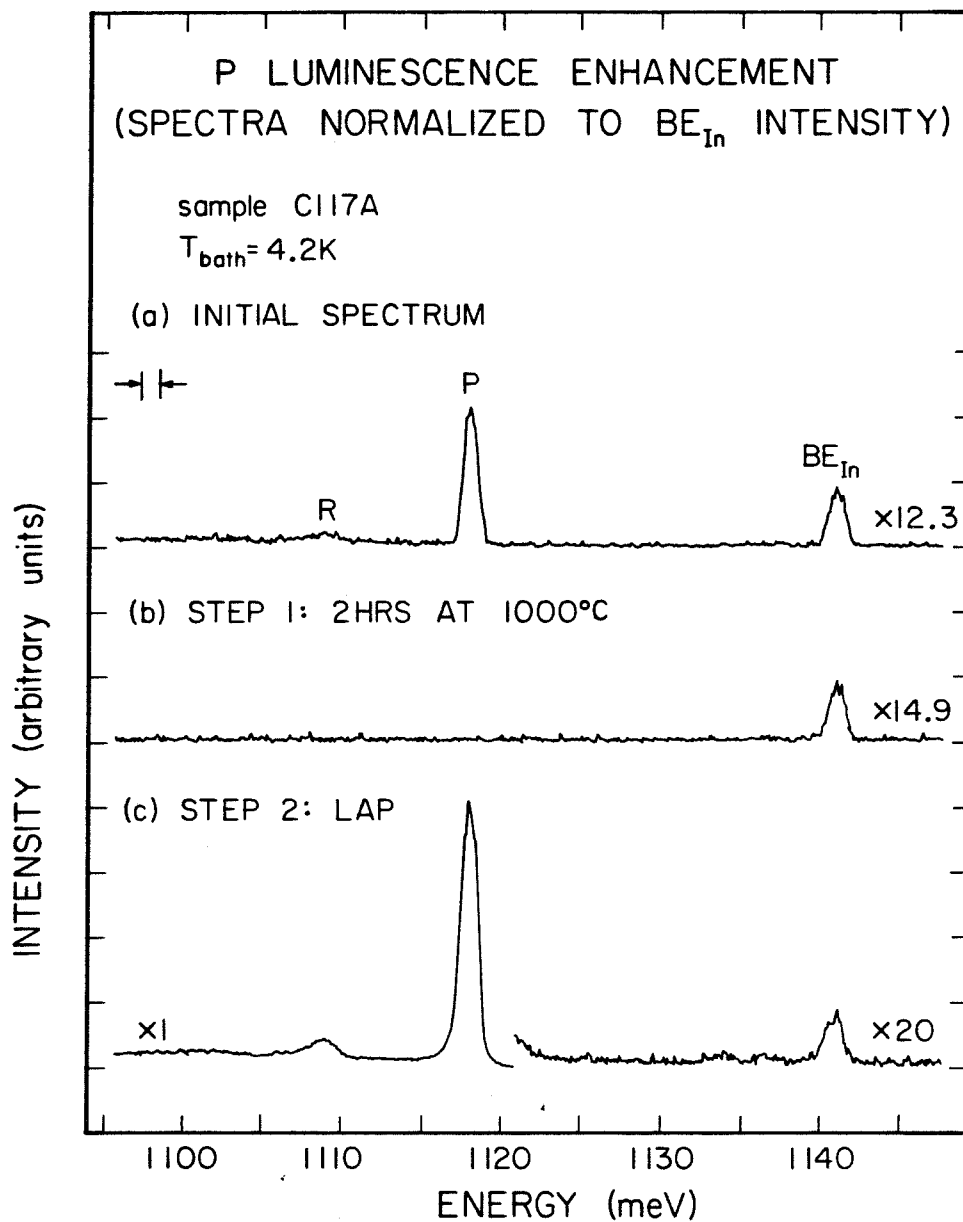


Figure 3.16. P line luminescence enhancement in response to room temperature treatment of the surface of Si:In sample C117A. The spectra are normalized to the BE_{In} intensity, and the scale factors (e.g., "X12.3") give the relative intensity magnifications required to achieve this normalization. We observe P line enhancement by a factor of 50.

sence of the high temperature anneal in an inert atmosphere is crucial. Lapping alone does not produce the effect, and the same is true of the Si or Si oxide etches. Fourth, the enhanced P line luminescence degrades with time spent at room temperature. Quantitative measurements of this effect are not available, but the general time scale is days, rather than hours or weeks. Finally, throughout all these procedures the BE_{In} luminescence intensity remains relatively constant, within approximately a factor of 2.

3.5.8 Models for the Enhancement

There are basically two models which we can construct to explain the observations described above. In the first model, we suppose that P line luminescence is the result of BE_I recombination in the bulk semiconductor material and is associated with an impurity complex involving In. Then the variations we observe in P line luminescence intensity must be due to some surface effect which selectively absorbs or does not absorb P line luminescence as the surface preparation is altered. Furthermore, this effect must be quite specific to P line luminescence. As we have mentioned, the intensity of BE_{In} luminescence and its phonon assisted replicas remains relatively constant while the P line luminescence intensity varies by a factor of 50. The high temperature anneal must enhance this surface absorption effect, as well as increase the concentration of bulk centres responsible for P line luminescence. Subsequent lapping must then interfere with the surface absorption effect, producing P line enhancement.

The second model involves the suggestion that P line luminescence results from recombination which occurs at the surface of the semiconductor and which is, once again, associated with an impurity complex involving In. In this case, the high temperature anneal must produce a high concentration of these surface complexes, but in such a way that the radiative transition responsible for P line luminescence is not active. The subsequent lapping must then activate the radiative transition.

Unfortunately, the experimental results obtained so far do not allow us to determine if P line luminescence originates from the surface or from the bulk. There are difficulties with each interpretation. If the P line luminescence originates from the bulk we are forced to propose a very specific surface absorber, which affects only P line luminescence but not the neighbouring BE_{In} luminescence. If P line luminescence originates from the surface, we have difficulty in reconciling a shallow, highly radiative centre which produces a sharp, well-defined luminescence feature with any type of surface related defect. Such defects are usually deep, non-radiative recombination centres. Even if a highly radiative surface defect did exist, one would expect to observe a broad, poorly-defined luminescence feature as a result of the highly damaged and disordered nature of the surface region.

In spite of these considerations, we can definitely say that sample treatment has a profound effect on the P,Q,R line intensities relative to the BE_{In} luminescence intensity. Just as it stands, this is a significant result. It marks the first observation of surface-dependent photoluminescence, and calls into question the standard assumptions which are applied in the analysis of photoluminescence spectra. Quantitative experimentation under conditions in which controlled surface treatments can be obtained is certainly called for.

3.6 SUMMARY AND CONCLUSION

In this chapter, certain aspects of the photoluminescence spectrum of Si:In were extensively studied. The results that were obtained can be summarized as follows:

(i) High resolution, low temperature spectra of Si:In were obtained. Many new features in the luminescence spectrum were observed for the first time. These features and some identifications are presented in Table 3.1. Three of the most intense features were labelled "P,Q,R" and isolated for further study.

(ii) P,Q,R luminescence only occurs together and has only been observed in Si:In. Examination of undoped Si or Si doped with other shallow impurities does not reveal P,Q,R luminescence.

(iii) Temperature-dependent measurements of P,Q,R luminescence were obtained. These measurements show that line Q appears at high temperatures, greater than approximately 15 K. This result suggests that line Q may be the result of a transition from an excited state. An Arrhenius plot of the P,Q,R line intensity ratios reveals that P,Q,R luminescence is not due to recombination of different BE states of the same centre. However, it does reveal that the P/R luminescence intensity ratio is independent of temperature. This observation suggests that lines P and R are the result of transitions from the same state. Possibly, line R is a local mode replica of line P. This interpretation is supported by the observed width of line R,

(iv) The pump power dependence of P,R luminescence was measured. These results reveal that the P/R luminescence intensity ratio is independent of pump power. This observation supports the interpretation that line R is a local phonon mode replica of line P. Of course, it is also consistent with the interpretation that lines P and R are the result of BE recombination at independent centres, but the temperature dependence measurements effectively rule out this possibility.

(v) The time dependence of P,Q,R luminescence was examined. Decay curves obtained from time-resolved spectra reveal that P,Q,R luminescence has an exceptionally long lifetime. This result indicates that P,Q,R luminescence is the result of recombination of excitons bound to isoelectronic centres where the much faster Auger decay mechanism is not operative.

(vi) Detailed temperature-dependent lifetime measurements were made for the P,Q,R luminescence. The lifetimes exhibit the same general temperature dependence, which can be qualitatively understood if the presence of an excited state with a somewhat longer lifetime is proposed.

(vii) A model for P,Q,R luminescence was proposed which accounts for the bulk of the experimental data. It was suggested that lines P,Q and R originate from the same isoelectronic complex. Line Q is then a transition from an excited state of the complex. Line R is a local phonon mode replica of line P. Rate equations based on this model were solved, and applied in the high temperature regime where thermalization is the dominant decay mechanism. The thermal binding energies obtained in this manner support the interpretation that the P,Q,R lines are the result of isoelectronic bound exciton recombination. In addition, they also support the interpretation that line R is a local mode replica of line P.

(viii) It was determined that the intensity of P,Q,R luminescence is sensitively dependent on the sample surface treatment. This is the first observation of surface-dependent photoluminescence.

REFERENCES

1. P. J. Dean, J. R. Haynes, and W. F. Flood, *Phys. Rev.* 161, 711 (1967).
2. M. A. Vouk and E. C. Lightowers, *J. Luminesc.* 15, 357 (1977).
3. M. A. Vouk and E. C. Lightowers, Proceedings of the Thirteenth International Conference on the Physics of Semiconductors, Rome, 1976, edited by F. G. Fumi, (Tipografia Maves, Rome, 1977), p. 1098.
4. S. A. Lyon, D. L. Smith, and T. C. McGill, *Phys. Rev.* B17, 2620 (1978).
5. K. R. Elliott, S. A. Lyon, D. L. Smith, and T. C. McGill, *Phys. Lett.* 70A, 52 (1978).
6. G. C. Osbourn and D. L. Smith, *Phys. Rev.* B16, 5426 (1977).
7. S. A. Lyon, G. C. Osbourn, D. L. Smith, and T. C. McGill, *Solid State Commun.* 23, 425 (1977).
8. W. Schmid, *Phys. Stat. Solidi* b84, 529 (1977).
9. K. R. Elliott, D. L. Smith, and T. C. McGill, *Solid State Commun.* 24, 461 (1977).
10. R. M. Feenstra and T. C. McGill, *Solid State Commun.* 36, 1039 (1980).
11. G. C. Osbourn, S. A. Lyon, K. R. Elliott, D. L. Smith, and T. C. McGill, *Solid-State Electron.* 21, 1339 (1978).
12. D. G. Thomas, J. J. Hopfield, and C. J. Frosch, *Phys. Rev. Lett.* 15, 857 (1965).

13. P. J. Dean, *J. Lumin.* 7, 51 (1973).
14. J. Weber, W. Schmid, and R. Sauer, *J. Lumin.* 18/19, 93 (1979);
Rev. B 21, 2401 (1980).
15. K. R. Elliott, G. C. Osbourn, D. L. Smith, and T. C McGill,
Phys. Rev. B17, 1808 (1978).
16. M. L. W. Thewalt, *Can. J. Phys.* 55, 1463 (1977).
17. F. A. Trumbore, M. Gershenson, and D. G. Thomas, *Appl. Phys.*
Lett. 9, 4 (1966).

CHAPTER 4
PHOTOLUMINESCENCE PROPERTIES
OF Si-RICH Si-Ge ALLOYS

4.1 INTRODUCTION

The properties of alloy semiconductors have been of general interest for some time. Such alloys provide a convenient system with which to study experimentally and theoretically the effects of disorder, which can be varied with alloy composition. The band gap can also be varied with alloy composition, and for this reason considerable effort has been directed towards the development of intrinsic and extrinsic alloy photodetectors. The study of the luminescence properties of alloy semiconductors can provide useful and relatively easily interpreted information regarding the properties of the alloys and the consequences of their disordered nature. Most attention has been directed towards the III-V ternary alloys, where luminescence processes have been studied extensively ⁽¹⁻³⁾. Luminescence of II-VI ternary alloys has also been studied, most notably $\text{Hg}_{1-x}\text{Cd}_x\text{Te}$ ⁽⁴⁾ where IR detector applications are particularly important.

Another material which has been proposed as a useful IR detector is the binary alloy $\text{Si}_{1-x}\text{Ge}_x$. The luminescence properties of $\text{Si}_{1-x}\text{Ge}_x$ are not particularly well known, although free and bound exciton ⁽⁵⁾, donor-acceptor ⁽⁶⁾ and electron-hole droplet ⁽⁷⁾ recombination has been observed in Ge rich alloys. In this chapter we report the first detailed measurements of luminescence from Si rich alloys, in particular alloys for which $x \approx 0.1$. Intrinsic and

impurity related luminescence is discussed, as well as certain properties of the luminescence which arise as a result of the compositional disorder of the alloy.

4.2 THE Si-Ge ALLOY SAMPLES

In this chapter, the photoluminescence technique was applied to three $\text{Si}_{1-x}\text{Ge}_x$ samples, two of which were not intentionally doped and the third of which was doped with In. The crystals were grown by the Czochralski technique. Impurity concentrations and alloy compositions were determined at Hughes Research Laboratories, where the crystals were grown. Impurity concentrations were established on the basis of Hall effect measurements. These measurements show that residual concentrations of B and P impurities are present in all the samples. Alloy compositions were obtained from a variety of techniques; results of the electron microprobe, density, and X-ray diffraction measurements were in excellent agreement. The samples studied, their impurity concentrations and their alloy compositions are given in Table 4.1.

4.3 EXPERIMENTAL RESULTS AND DISCUSSION FOR UNDOPED $\text{Si}_{1-x}\text{Ge}_x$

In this section, the results of the application of the photoluminescence technique to the undoped samples are reported. Two undoped samples are reported. Two undoped $\text{Si}_{1-x}\text{Ge}_x$ samples were available, C077 ($x=0.11$) and C021-3 ($x=0.067$). As indicated in Table 4.1, these samples have low residual concentrations of B and P

Table 4.1. $\text{Si}_{1-x}\text{Ce}_x$ alloys studied using photoluminescence. The samples were grown and characterized at Hughes Research Laboratories. All samples show residual B and P impurity concentrations.

SAMPLE	N_B (cm^{-3})	N_P (cm^{-3})	N_{In} (cm^{-3})	x		
				electron microprobe	density	x-ray diffraction
C077	3.6×10^{13}	2.8×10^{13}		0.1115	0.113	0.113
C021-3	2.3×10^{14}	4.1×10^{14}		0.0667	0.0685	
C093	5.0×10^{15}	5.3×10^{14}	2.5×10^{16}			0.104

impurities, in spite of not being intentionally doped.

4.3.1 Typical Photoluminescence Spectrum and Identification of Phonon Replicas

A typical low temperature photoluminescence spectrum of sample C077 is shown in Fig. 4.1. Two broad features are visible at the high energy end of the spectrum and are labelled "FE" and "BE_p". Replicas of these lines, labelled "FE(TO)" and "BE_p(TO)", are observed approximately 58 meV lower in energy. Since this is the transverse-optical (TO) phonon energy in Si, the low energy lines are interpreted as being due to TO phonon replicas of the higher energy lines.

4.3.2 Identification of Free Exciton Luminescence

In this section we consider the effect of increasing the sample temperature on the photoluminescence spectrum of sample C077. In Fig. 4.2 we see that as the temperature is increased the BE_p line thermalizes with respect to the FE line. Above 10 K (Fig. 4.3), the BE_p line is no longer visible, and the FE line assumes a shape characteristic of free exciton (FE) recombination in Si. In intrinsic Si, FE recombination luminescence has been fit very accurately with a lineshape ⁽⁸⁾

$$I(E) \propto \sqrt{E-E_0} \exp \left[\frac{E - E_0}{k_B T} \right] \quad (4.1)$$

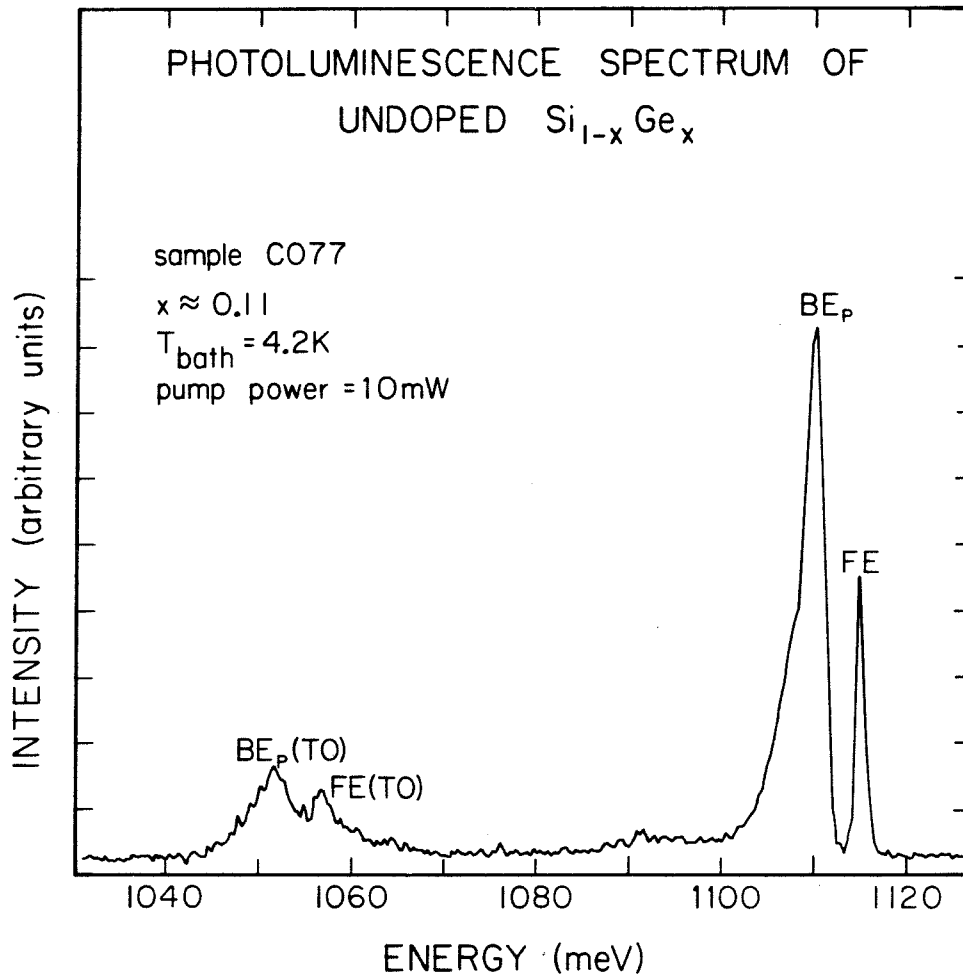


Figure 4.1. Typical photoluminescence spectrum of undoped $\text{Si}_{1-x}\text{Ge}_x$ sample C077. Refer to the text for an explanation of the line assignments.

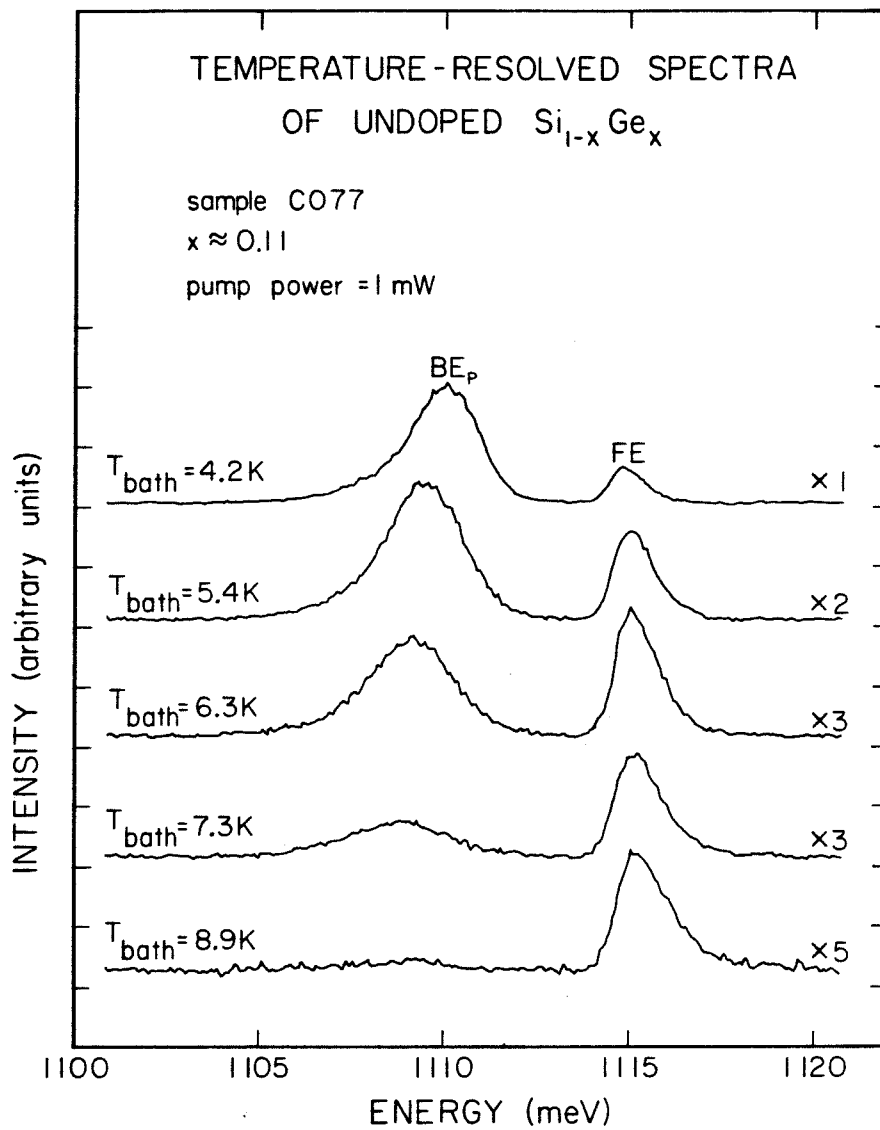


Figure 4.2. Temperature-resolved spectra of undoped $\text{Si}_{1-x}\text{Ge}_x$ sample C077 from 4.2 K to 8.9 K. The scale factors (e.g., "X2") give the relative intensity magnification. Note that BE_p thermalization is observed. In addition, the BE_p peak position shifts to lower energy as the temperature is increased. At high temperatures, the free exciton (FE) luminescence assumes a shape characteristic of free exciton luminescence in Si.

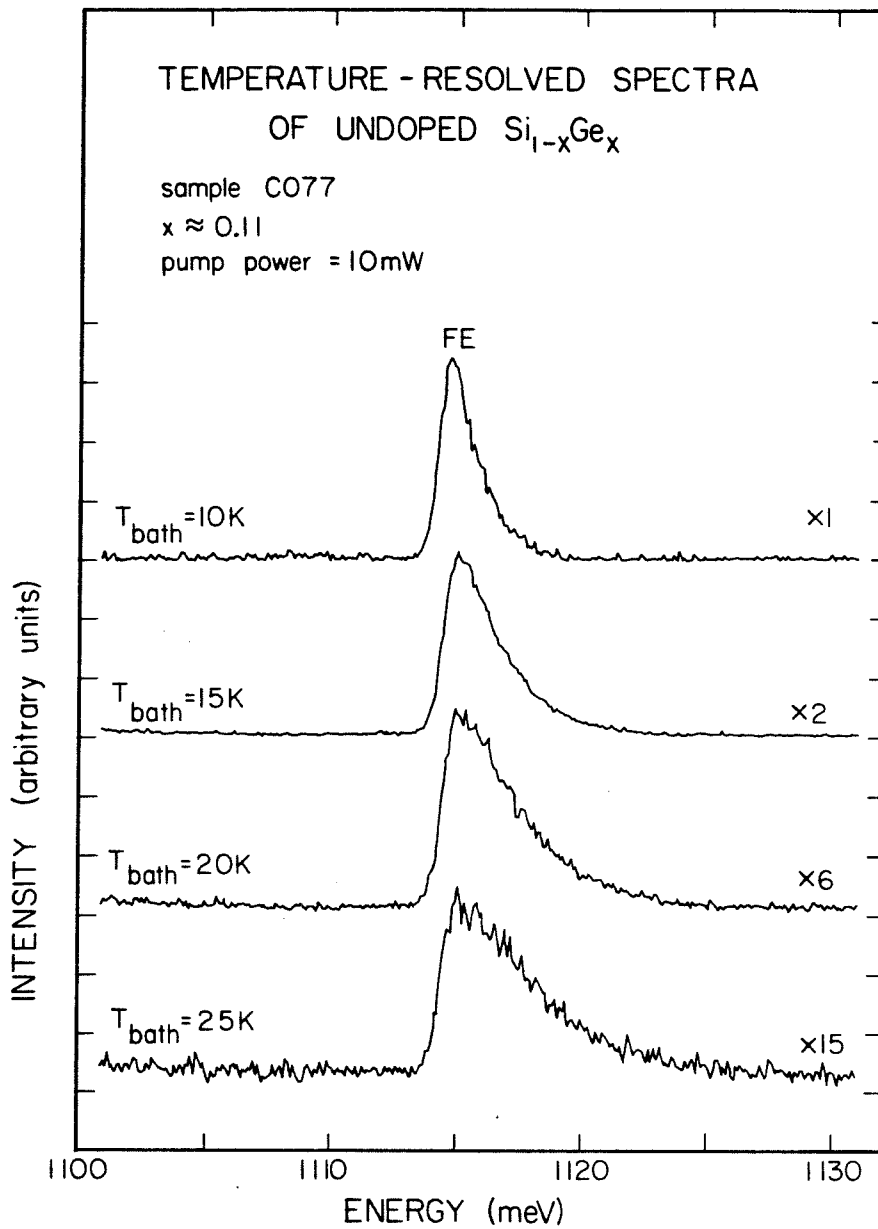


Figure 4.3. Temperature-resolved spectra of undoped $\text{Si}_{1-x}\text{Ge}_x$ sample C077 from 10 K to 25 K. The scale factors (e.g., "X2") give the relative intensity magnification. Note that, at these temperatures, the FE luminescence assumes a shape characteristic of free exciton luminescence in Si.

where

$I(E)$ = the luminescence intensity at photon energy E

E_0 = the FE threshold energy

T = the temperature .

In this expression we assume parabolic FE bands and a Boltzmann distribution of FE centre of mass kinetic energies. The high temperature luminescence from sample C077 can also be fit very well with the lineshape described by Eq. (4.1). An example of this fit is shown in Fig. 4.4. In all cases, the fit temperature obtained in this manner was within 1 K of the measured bath temperature. Also, the threshold energy remained constant within 0.05 meV. On the basis of this analysis, the line labelled FE is identified as resulting from no-phonon (NP) FE recombination. Note that this intrinsic NP luminescence is greatly enhanced in the alloy, since the Ge atoms can act as momentum conserving scattering centres. (5)

4.3.3 Identification of Bound Exciton Luminescence

The identification of the FE line obtained in the previous section, splitting between the FE threshold and BE_p line peak positions, and the thermal behavior shown in Fig. 4.2 suggest that the line labelled BE_p is due to the NP recombination of excitons bound by about 4 meV to a shallow level. The pump power dependence at low power shown in Fig. 4.5 supports this proposal. As this figure

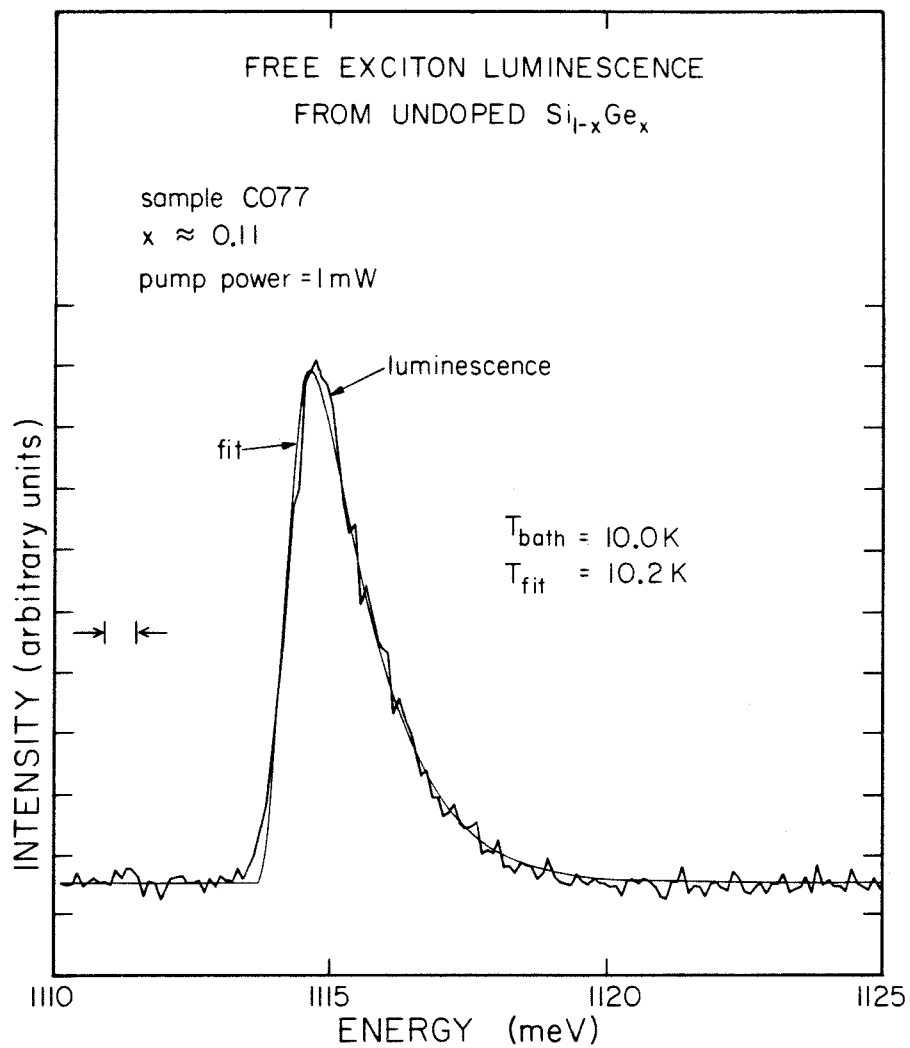


Figure 4.4. Free exciton luminescence from undoped $\text{Si}_{1-x}\text{Ge}_x$ sample C077 and least-squares fit of the theoretical lineshape (Eq. (4.1)). The sample temperature obtained as a result of the fit, T_{fit} , is shown with the measured bath temperature, T_{bath} .

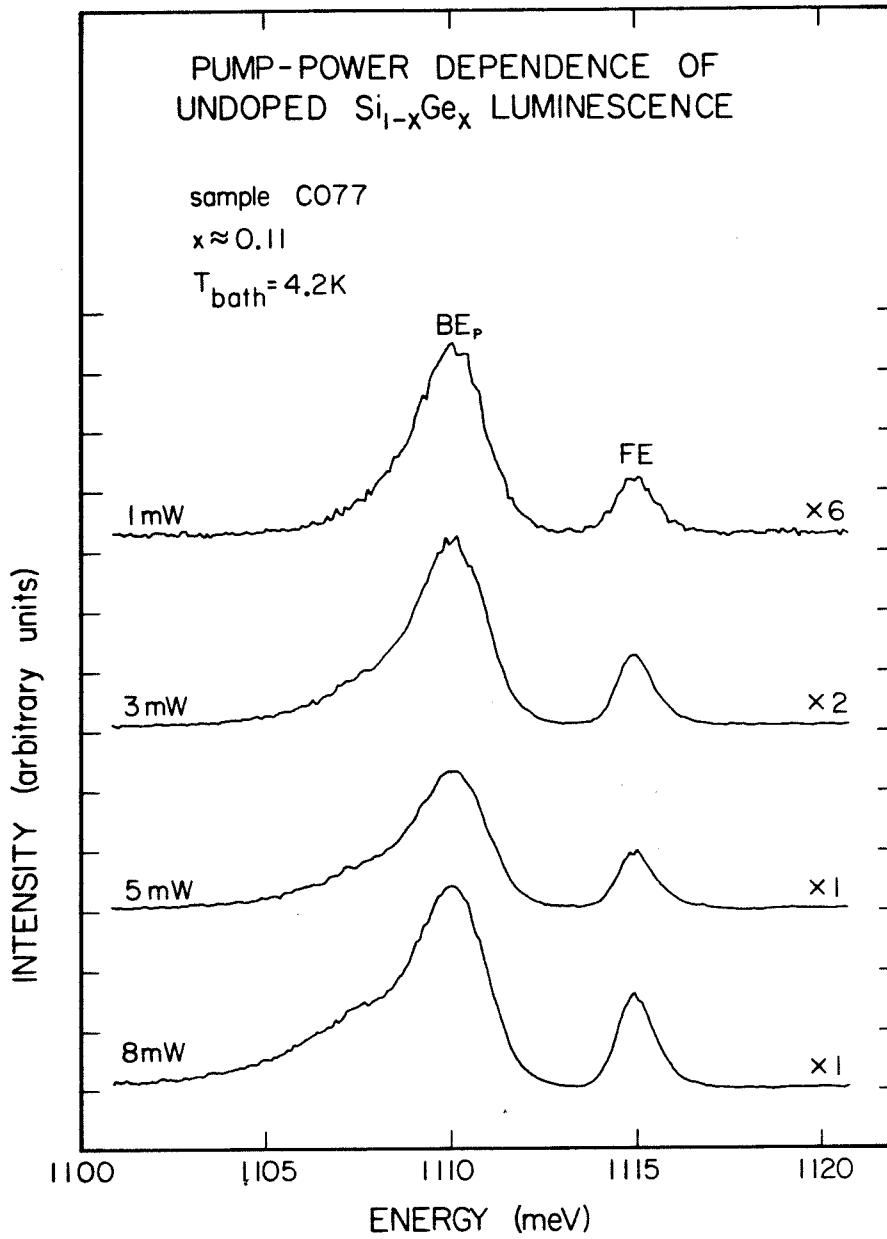


Figure 4.5. Pump power dependence of the luminescence from undoped $\text{Si}_{1-x}\text{Ge}_x$ sample C077 at low pump powers. The scale factors (e.g., "X6") give the relative intensity magnification. Note that the BE_p/FE intensity ratio is independent of pump power at these power levels.

demonstrates, the FE to BE luminescence intensity ratio is independent of pump power. Candidates for such a level are clearly B and P, which have binding energies in the neighborhood of 4 meV in Si (3.9 meV and 4.7 meV, respectively ⁽⁹⁾), and which are the most common shallow impurities in the undoped material. In Fig. 4.6, the NP B bound exciton (BE_B) and P bound exciton (BE_P) luminescence from Si containing approximately equal background concentrations of B and P is presented. This figure shows that BE_P luminescence is more intense than BE_B luminescence in the NP region by at least an order of magnitude. It seems reasonable to conclude, therefore, that the line labelled BE in the luminescence from sample C077 is primarily due to NP BE_P recombination.

The high-power pump power dependence presented in Fig. 4.7 supports this conclusion. In undoped Si, low energy lines due to bound multiexciton complexes (BMEC) appear as the pump power is increased. The splitting between the BE_P line and the first BMEC line is 2.2 meV for B and 3.6 meV for P ⁽⁸⁾. As shown in Fig. 4.7, in the luminescence spectrum of sample C077 the BE_P line develops a low energy shoulder as the pump power is increased, which resolves into a separate line at high pump powers. The separation between this line and the BE_P line is about 3.8 meV, which is consistent with the splitting between the P BE and first BMEC in Si. Since no line is observed which would correspond to B BMEC luminescence, our conclusion regarding the origin of the BE_P line in the alloy seems justified.

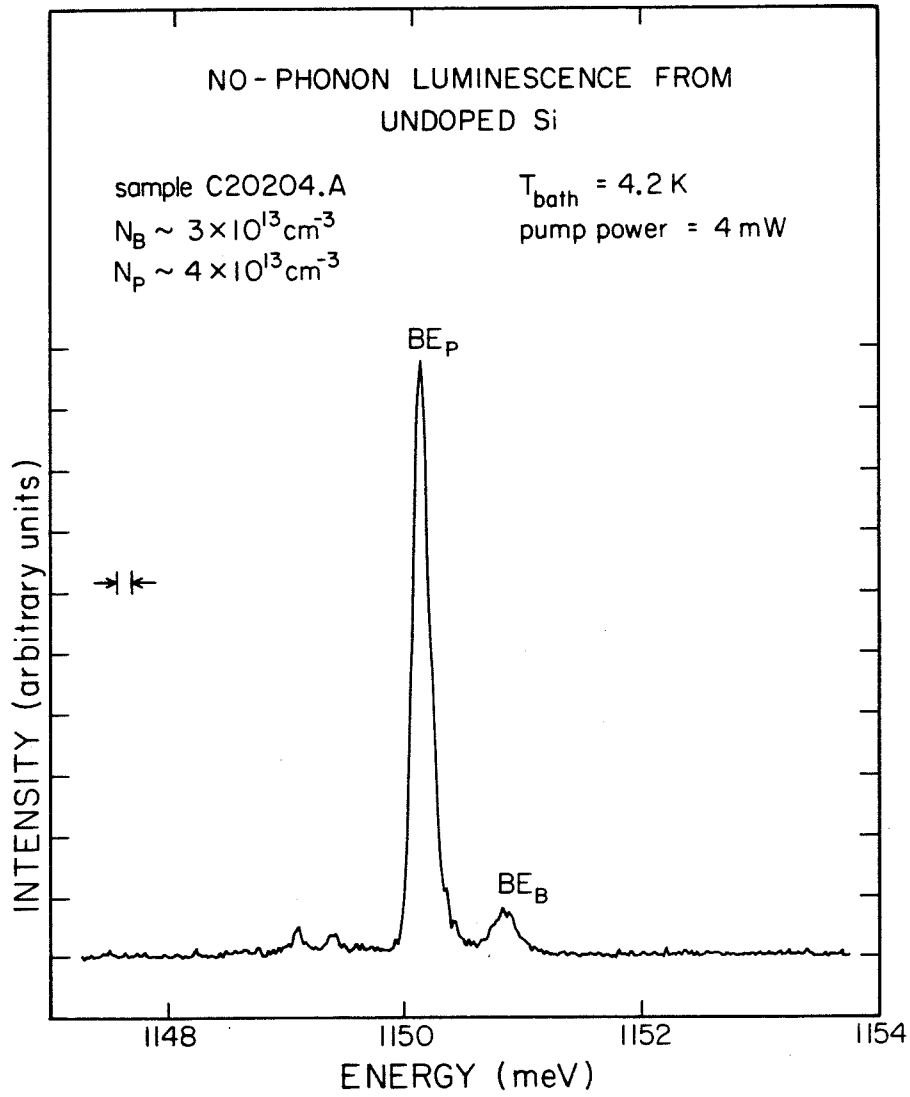


Figure 4.6. Luminescence from undoped Si sample C20204.A in the no-phonon region, showing BE_B and BE_P luminescence. We see that, for the impurity concentrations specified in the figure, the BE_P line is approximately an order of magnitude more intense than the BE_B line.

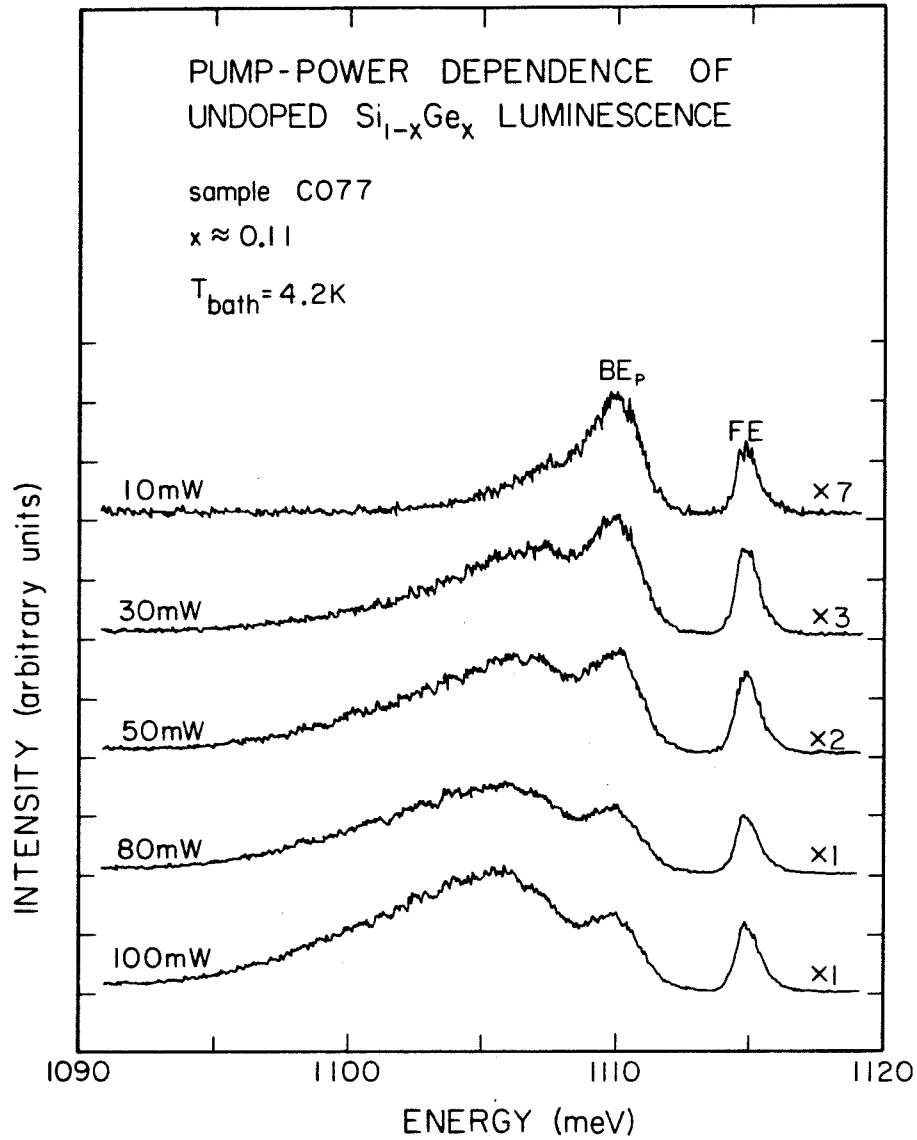


Figure 4.7. Pump power dependence of luminescence from undoped $\text{Si}_{1-x}\text{Ge}_x$ sample C077 at high pump powers. The scale factors (e.g., "X7") give the relative intensity magnification. Note the new feature which appears on the low energy side of the BE_p line at high pump powers. This feature is discussed in the text.

4.3.4 Comparison of Photoluminescence Spectrum of Sample C077 and Sample C021-3

The interpretation of the photoluminescence spectrum of sample C077 developed in the previous sections is consistent with our investigation of the $x = 0.067$ sample, C021-3. In Fig. 4.8, the luminescence spectra of samples C077 and C021-3 are compared. We see that the ratio of BE_p to FE luminescence is considerably greater for sample C021-3. This is consistent with Table 4.1, which indicates that impurity concentrations in sample C021-3 are approximately an order of magnitude higher. In addition, we see that the luminescence spectrum of sample C021-3 is shifted to higher energy. This feature is discussed in detail below.

4.3.5 Models for Bound Exciton Luminescence

Now that the origin of the Si-rich $Si_{1-x}Ge_x$ luminescence lines has been determined, we can consider the effect of alloy compositional disorder on the luminescence features. To begin with, we see that the BE line is considerably broadened in the alloy. In fact, the BE line in the alloy is approximately ten times broader (~ 3 meV) than its counterpart in Si (~ 0.4 meV). We consider two models for the origin of this broadening.

4.3.5.1 Bulk Fluctuation Model

In this model, the BE line broadening is accounted for on the basis of relatively large scale fluctuations in the alloy compo-

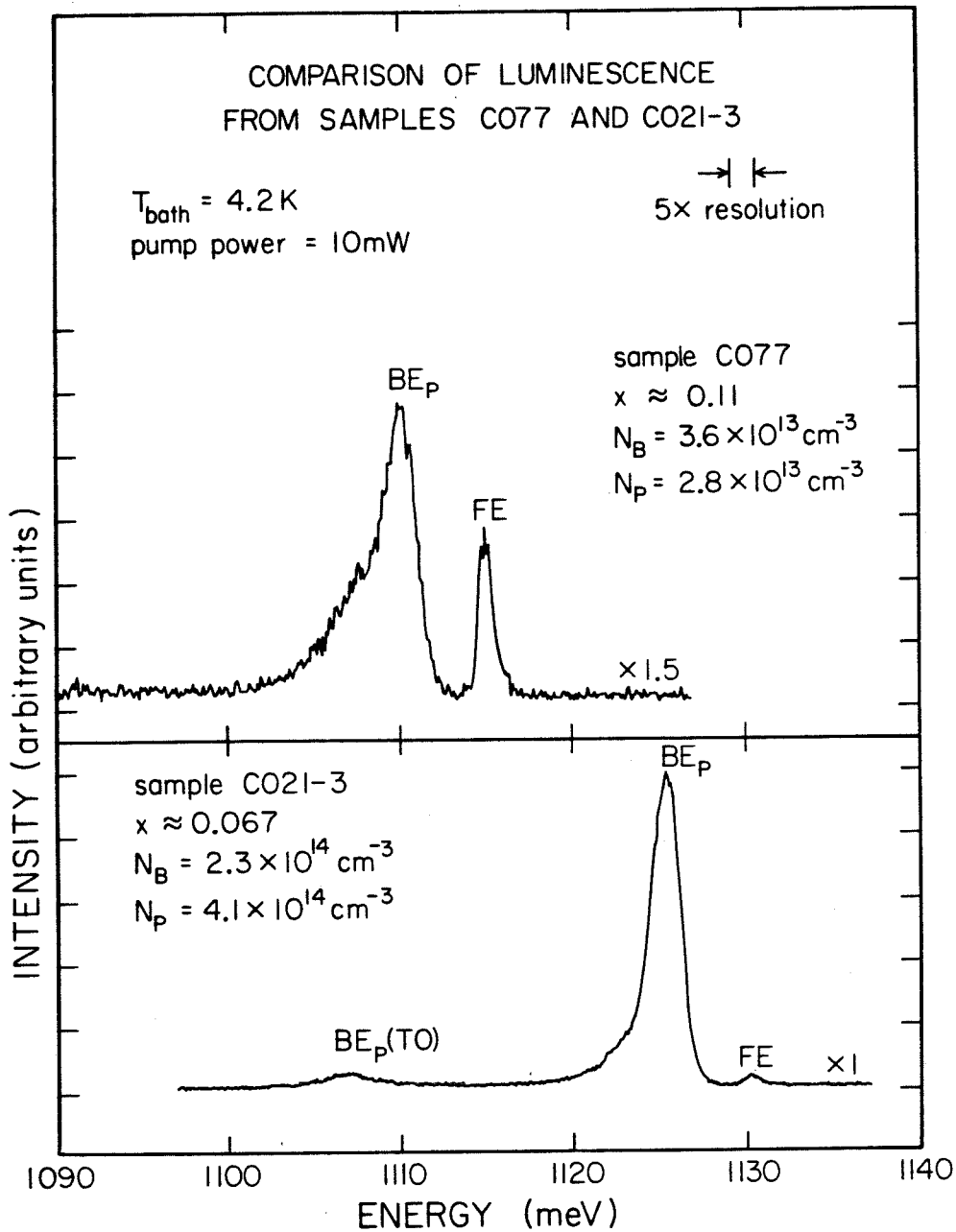


Figure 4.8. Comparison of the luminescence spectra of samples C077 and C021-3. The scale factors (e.g., "×1.5") give the relative intensity magnification. Note that BE_p luminescence is much more from sample C021-3 than from sample C077. Also, note that the luminescence from sample C021-3 is at higher energy than luminescence from sample C077. These features are discussed in the text.

sition, x . This idea was first discussed by Alferov et al. (10)

In this theory, it is the variation in band gap energy produced by these bulk fluctuations in x which results in the BE line broadening.

We can roughly estimate this effect on the basis of the following argument. In a volume a^3 , there will be xNa^3 atoms, where N is the density of lattice sites in the alloy. If the Ge atoms are distributed randomly, the typical fluctuation in the number of Ge atoms in the volume will be $(xNa^3)^{1/2}$. Therefore, the typical fluctuation in the composition parameter x will be

$$\Delta x \sim \frac{(xNa^3)^{1/2}}{Na^3} = \left(\frac{x}{Na^3}\right)^{1/2} \quad (4.2)$$

If $\Delta E = \alpha\Delta x$, where ΔE is the change in gap energy produced by a change in composition Δx , then Eq. 4.2 becomes

$$\Delta E \sim \alpha \left(\frac{x}{Na^3}\right)^{1/2} \quad (4.3)$$

N can be estimated for the alloy from the lattice constant measurements of Dismukes et al. (11). For $x = 0.1$, we find $N \sim 6 \times 10^{21} \text{ cm}^{-3}$.

From the absorption measurements of Braunstein et al. (12) (Fig. 1.7), we can estimate $\alpha \sim 600 \text{ meV}$. Assuming that a is approximately an exciton Bohr radius in Si, i.e., about 40 \AA , we obtain $\Delta E \sim 10 \text{ meV}$, which is reasonable agreement for a crude calculation.

4.3.5.2 Nearest-Neighbour Configuration Model

There is another possible mechanism for the observed broadening of the BE_p line, however. NP donor BE recombination in indirect materials like Si and Ge involve the recombination of a loosely bound hole with one of the two electrons which are tightly bound to the positive donor core. As a result, it is reasonable to suppose that the nearest-neighbour configuration of atoms around an impurity center will have a profound effect on the BE_p binding energy. It is possible, therefore, that the BE_p line is composed of several overlapping luminescence lines from BE_p 's with slightly different binding energies, which are the result of different nearest-neighbour configurations of Si and Ge atoms. We let the nearest-neighbour configuration be specified by an index k , where k is the number of nearest-neighbour Ge atoms which varies between $k=0$ and $k=4$. A P impurity atom or a BE_p with a particular nearest-neighbour configuration k is indicated as $P(k)$ or $BE_p(k)$, respectively. A $BE_p(0)$ will be most like its counterpart in Si, and we expect it to have the highest binding energy. As k increases, the nearest-neighbour configuration becomes more Ge-like. Therefore we expect the binding energy to decrease, producing the broad luminescence feature which is observed.

4.3.6 Experimental Results Which Support the Nearest-Neighbour Configuration Model

There is a considerable amount of evidence which supports the nearest-neighbour configuration model for BE line broadening in the

alloy. This line broadening mechanism is consistent with the photoluminescence measurements reported here, and also with the results of other experiments. In this section, we discuss this evidence.

4.3.6.1 Hopping Conduction and Hall Effect Experiments

To begin with, evidence is available which indicates that the nearest-neighbour configuration plays an important role in determining the fluctuation of impurity ionization energies in alloy materials ⁽¹³⁾. For example, studies of hopping conduction in Ga doped Ge-rich $\text{Si}_{1-x}\text{Ge}_x$ alloys have shown that the activation energy for hopping conduction varies linearly with x for $x > .94$, not with \sqrt{x} as the bulk fluctuation theory would suggest. The linear variation with x can be obtained by assuming that fluctuations in the impurity ionization energy are determined predominantly by the nearest-neighbour configuration, and that only $k = 3$ and $k = 4$ configurations are important for $x \sim 1$ ⁽¹³⁾.

In addition, Hall effect measurements have been performed on undoped Si-rich $\text{Si}_{1-x}\text{Ge}_x$ alloys which show two distinct B impurity levels in the gap. Analysis of the Hall experiment results yields the relative concentration of these levels, which agrees very well with the prediction of a simple model based on the relative probability of $k=0$ and $k=1$ configurations. ⁽¹⁴⁾

These results indicate that the nearest-neighbour configuration of alloy atoms plays a crucial role in determining the ionization energies of impurities in the alloy. It is reasonable to suppose,

therefore, that the nearest-neighbour configuration will play a similar role in determining the BE binding energies, as the nearest-neighbour configuration model suggests.

4.3.6.2 Temperature Dependence of Bound Exciton Luminescence Peak Position

The temperature dependence of the BE_p line peak position also supports the nearest-neighbour configuration model. Fig. 4.2 shows that the BE_p line peak position moves to lower energy as the temperature increases. Measurements in Si show that the band gap variation with temperature over the range considered here is utterly negligible. However, the shift in the BE_p line peak position with temperature is expected on the basis of the nearest-neighbour configuration model, since the higher energy lines will thermalize at lower temperatures. At low temperatures, we will see luminescence from all BE_p 's. As the temperature increases, though, we expect that luminescence from $BE_p(0)$ will dominate, shifting the peak towards the lower energy $BE_p(0)$ position. A theory of BE broadening based on bulk fluctuations in x will not produce this type of thermal behaviour since it does not depend on changes in the BE binding energy.

4.3.6.3 Bound Exciton Luminescence Lineshape

We can reconcile the observed BE_p luminescence lineshape with the nearest-neighbour configuration model as follows. Fig. 4.2 shows that the BE_p luminescence line is reasonably symmetrical. As

previously mentioned, at high temperatures the $BE_p(0)$ luminescence dominates, so a symmetrical line is expected. At low temperatures, however, contributions from all $BE_p(k)$ must be considered. For a given value of k , the $BE_p(k)$ luminescence intensity is given by

$$I_p(k) \propto f_p(k) n_p(k) \quad (4.4)$$

where

$I_p(k)$ = the $BE_p(k)$ luminescence intensity

$f_p(k)$ = the $BE_p(k)$ oscillator strength

$n_p(k)$ = the $BE_p(k)$ density.

Now, the probability of a particular nearest-neighbour configuration k is given by the Binomial distribution

$$B(4,k) = \frac{4!}{(4-k)! k!} (1-x)^{4-k} x^k \quad (4.5)$$

Then we have

$$n_p(k) = n_p B(4,k) \quad (4.6)$$

where

$$n_p = \sum_{k=0}^4 n_p(k) \quad (4.7)$$

is the total BE_p density. Evaluation of Eq. (4.5) shows that $n_p(k)$ decreases rapidly as k increases. These considerations suggest that $I_p(k)$ should be a maximum for $k = 0$ and decrease as k increases,

resulting in a BE_p luminescence line which peaks at the low energy $BE_p(0)$ position and has a high energy shoulder.

In spite of this, the temperature-resolved spectra in Fig. 4.2 show that the low temperature BE_p line is reasonably symmetrical and peaks at a somewhat higher energy than the $BE_p(0)$ position. We can explain this discrepancy by noting that $I_p(k)$ also depends on the oscillator strength, $f_p(k)$. Now, in an indirect semiconductor like Si the no-phonon radiative recombination process requires some mechanism for momentum conservation. Nearest-neighbour Ge atoms provide such a mechanism, since they can act as momentum conserving scattering centres during exciton recombination. As a result, we expect that the presence of nearest-neighbour Ge atoms will increase $f_p(k)$ as k increases. This effect could cause $I_p(k)$ to reach a maximum for some intermediate value of k , and thereby produce the observed BE_p luminescence lineshape.

4.3.6.4 Time-Resolved Spectra

As a final consideration, we note that the time-resolved spectra shown in Fig. 4.9 can also be explained on the basis of the nearest-neighbour configuration model. Fig. 4.9 shows that all components of the BE_p line decay with the same total rate - the lineshape does not change and the peak position remains fixed. To account for this observation, we consider a simple model for the decay of $BE_p(k)$ luminescence following a long optical pumping pulse, in

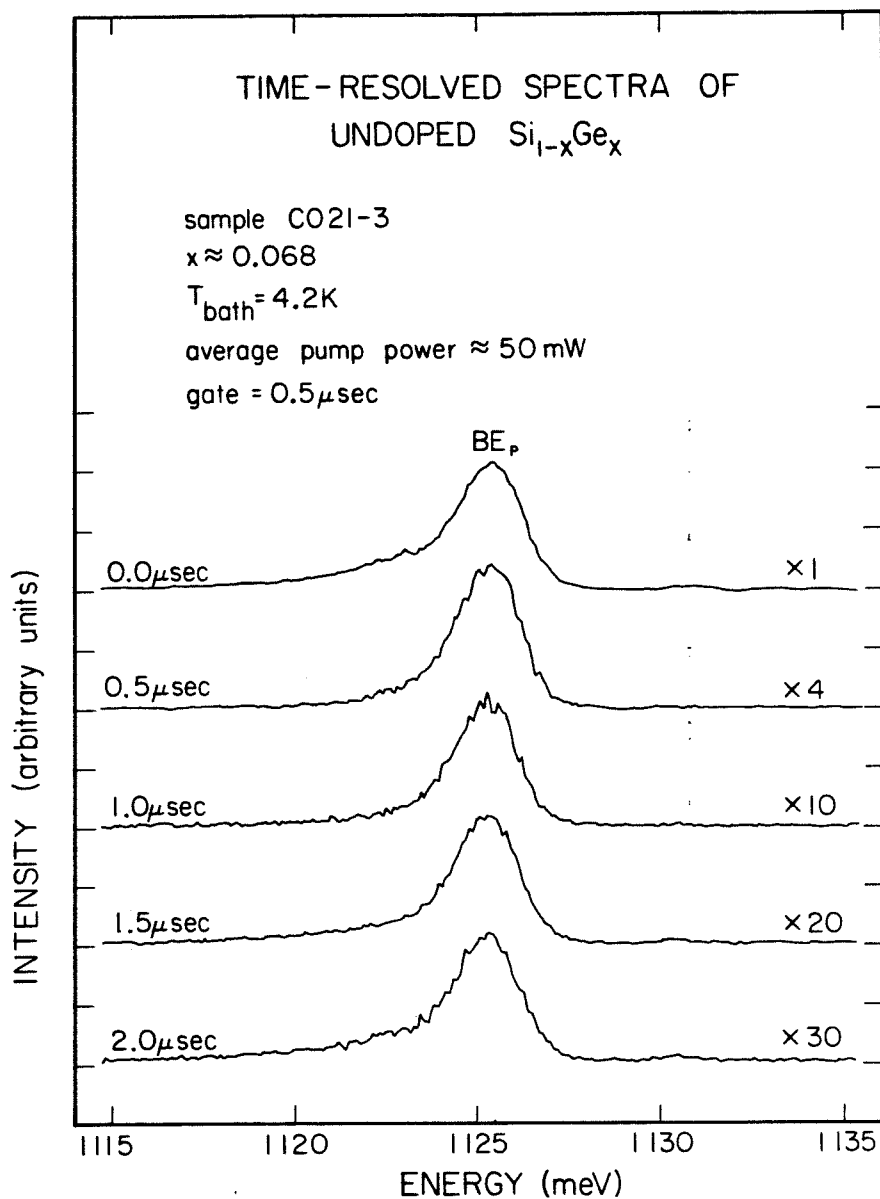


Figure 4.9. Time-resolved spectra of undoped $\text{Si}_{1-x}\text{Ge}_x$ sample C021-3 at LH_eT . The scale factors (e.g., "X4") give the relative intensity magnification. Note that the BE_p lineshape does not change appreciably with time. This feature is discussed in the text.

which the capture of FE by P(k) impurity atoms and their subsequent decay are related by detailed balance. If we assume that thermalization effects are not important, the result is the following set of rate equations:

$$\frac{dn_{FE}}{dt} = -(\nu_{FE} + \gamma_P) n_{FE} \quad (4.8)$$

$$\frac{dn_P(k)}{dt} = \gamma_P(k) n_{FE} - \nu_P(k) n_P(k) \quad (4.9)$$

where

n_{FE} = the FE density

ν_{FE} = the FE decay rate

$\gamma_P(k)$ = the rate of FE capture by P(k) impurity atoms

$\nu_P(k)$ = the BE_P(k) decay rate

and where we have defined

$$\gamma_P = \sum_{k=0}^4 \gamma_P(k) \quad (4.10)$$

We assume that the optical pumping pulse is long enough that steady-state conditions are obtained. Then the boundary conditions at $t = 0$ are

$$\left. \frac{dn_{FE}}{dt} \right|_{t=0} = g - (\nu_{FE} + \gamma_P) n_{FE} \Big|_{t=0} = 0 \quad (4.11)$$

$$\left. \frac{dn_p(k)}{dt} \right|_{t=0} = \gamma_p(k) n_{FE} \Big|_{t=0} - \nu_p(k) n_p(k) \Big|_{t=0} = 0 \quad (4.12)$$

where

g = the FE generation rate.

The solution of Eqs. (4.8), (4.9), (4.11) and (4.12) is easily determined to be

$$n_{FE} = \frac{g}{(\nu_{FE} + \gamma_p)} \exp \left[-(\nu_{FE} + \gamma_p)t \right] \quad (4.13)$$

$$n_p(k) = \frac{g \gamma_p(k)}{(\nu_{FE} + \gamma_p) - \nu_p(k)} \left\{ \frac{1}{\nu_p(k)} \exp \left[-\nu_p(k)t \right] - \frac{1}{(\nu_{FE} + \gamma_p)} \exp \left[-(\nu_{FE} + \gamma_p)t \right] \right\} \quad (4.14)$$

The time evolution of $n_p(k)$ expressed by Eq. (4.14) is governed by the relationship between $\nu_p(k)$ and $(\nu_{FE} + \gamma_p)$. If $\nu_p(k) < (\nu_{FE} + \gamma_p)$, then the long-time decay rate is dominated by $\nu_p(k)$ and we would expect to see some variation in the BE_p lineshape during the decay. On the other hand, if $(\nu_{FE} + \gamma_p) < \nu_p(k)$ for all k , then the long-time decay is governed by $(\nu_{FE} + \gamma_p)$, which is independent of k . In this "capture-limited" case, we would expect to see all components of the BE_p line decay with the same rate.

We can make an estimate of $(\nu_{FE} + \gamma_p)$ as follows. From Eq. (2.3), in the absence of saturation effects we can write

$$\gamma_P(k) = \sigma_P(k) N_P(k) v_{th} \quad (4.15)$$

where

$\sigma_P(k)$ = the P(k) capture cross section for FE

$N_P(k)$ = the P(k) density.

If we assume that all the $\sigma_P(k)$ are equal, $\sigma_P(k) = \sigma_P$, then we note that

$$\gamma_P = \sigma_P N_P v_{th} \quad (4.16)$$

where

$$N_P = \sum_{k=0}^4 N_P(k) \quad (4.17)$$

is the total P density. To estimate γ_P , we assume $\sigma_P \sim \sigma_B$ ⁽¹⁵⁾ and use $\sigma_B = 10^{-13} \text{ cm}^2$ ⁽¹⁶⁾. The FE thermal velocity, v_{th} , is calculated assuming a Boltzmann distribution for the FE kinetic energies to be

$$v_{th} = \left(\frac{8k_B T}{\pi m_{ex}} \right)^{1/2} \quad (4.18)$$

We take $m_{ex} = 0.6 m_o$ ⁽¹⁷⁾ and $T=4 \text{ K}$ to obtain $v_{th} = 2 \times 10^6 \text{ cm/sec}$. For $N_P = 10^{13} \text{ cm}^{-3}$, we finally obtain $\gamma_P = 2 \times 10^6 \text{ sec}^{-1}$. Since $v_{FE} \sim 5 \times 10^5 \text{ sec}^{-1}$, we can assume $(v_{FE} + \gamma_P) \sim \gamma_P$.

To estimate $v_P(k)$, we note that in Si the BE decay rate is dominated by the Auger decay process ^(18,19). This results in an

observed decay rate for BE_p of $4 \times 10^6 \text{sec}^{-1}$ (19). In the $Si_{0.9}Ge_{0.1}$ alloy, we expect that the presence of nearest-neighbour Ge atoms will contribute to enhanced k-space spreading of the wavefunctions and therefore increase the decay rates. So we take $4 \times 10^6 \text{sec}^{-1}$ as a lower limit for the BE_p decay rate in $Si_{0.9}Ge_{0.1}$.

On the basis of these estimates, it seems reasonable to conclude that the $BE_p(k)$ decay is capture-limited. The BE_p luminescence decay characteristic shown in Fig. 4.10 supports this conclusion. Although the initial decay is somewhat non-exponential, the long-time decay rate is measured to be $1.5 \times 10^6 \text{sec}^{-1}$, in reasonable agreement with our estimate of γ_p .

The conclusion that $BE_p(k)$ decay is capture-limited explains our observation that all components of the BE_p line decay with the same rate. In the capture-limited case, the decay rate of all components is $(\nu_{FE} + \gamma_p)$, which is independent of k.

4.3.7 Comparison of Si and Undoped $Si_{1-x}Ge_x$ Luminescence Energies

If we assume that the nearest-neighbour configuration model correctly describes BE luminescence from the Si-rich $Si_{1-x}Ge_x$ alloy, then a procedure for directly comparing Si and $Si_{1-x}Ge_x$ luminescence energies presents itself. Since nearest-neighbour effects are the same for a $BE_p(0)$ in the alloy and a BE_p in Si, we propose that the difference in recombination energy in these two cases is just due

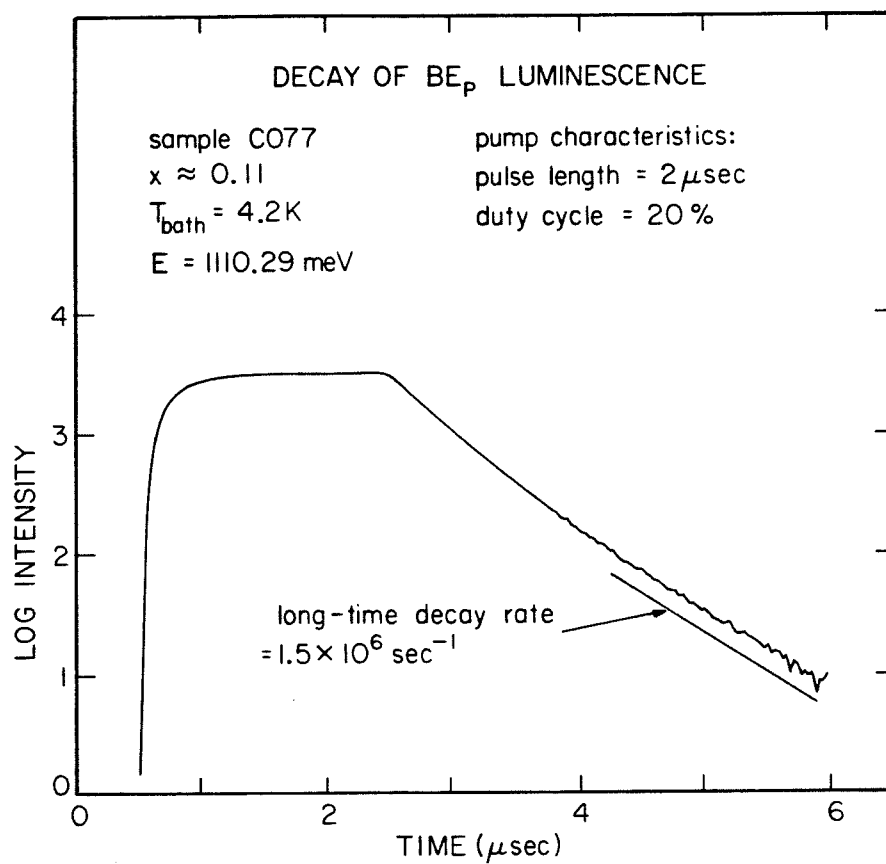


Figure 4.10. Decay characteristic of BE_p , measured at the BE_p 4.2 K peak position of 1110.3 meV. The background, which was measured 8 μsec after the end of the laser pulse, has been subtracted.

to the shift in band gap of the alloy. The consequences of this proposal are discussed in the following sections.

4.3.7.1 Band Gap Decrease for Sample C077 ($x=0.11$)

On the basis of the proposal described above, the Si and $\text{Si}_{1-x}\text{Ge}_x$ sample C077 luminescence energies can be compared. Fig. 4.11 schematically illustrates the comparison. The $\text{BE}_p(0)$ luminescence line position, 1108.71 meV, was obtained from the 8.0 K spectrum. This was the highest temperature at which BE_p luminescence could be reliably observed, and it was assumed that the luminescence was dominated by $\text{BE}_p(0)$. The P luminescence line position in Si, 1150.11 meV, was obtained from direct measurement of lightly doped Si:P. If this change in line position is attributed solely to a change in gap energy, these measurements imply a band gap decrease of 41.4 meV for $x = 0.11$. This value fluctuated by about 0.6 meV due to large scale inhomogeneities in the crystals being examined. If a rough graphical extrapolation of the absorption data published by Braunstein et al ⁽¹²⁾ is attempted, we obtain an alloy band gap shift of approximately 60 meV for $x = 0.11$, which is in reasonable agreement with the luminescence data.

4.3.7.2 Free Exciton Binding Energy for Sample C077 ($x=0.11$)

In addition to the $\text{Si}_{1-x}\text{Ge}_x$ $\text{BE}_p(0)$ and the Si BE_p line positions, Fig. 4.11 also shows the FE threshold and E_{gap} positions

SCHEMATIC COMPARISON OF
UNDOPED Si AND UNDOPED $\text{Si}_{1-x}\text{Ge}_x$
LUMINESCENCE ENERGIES

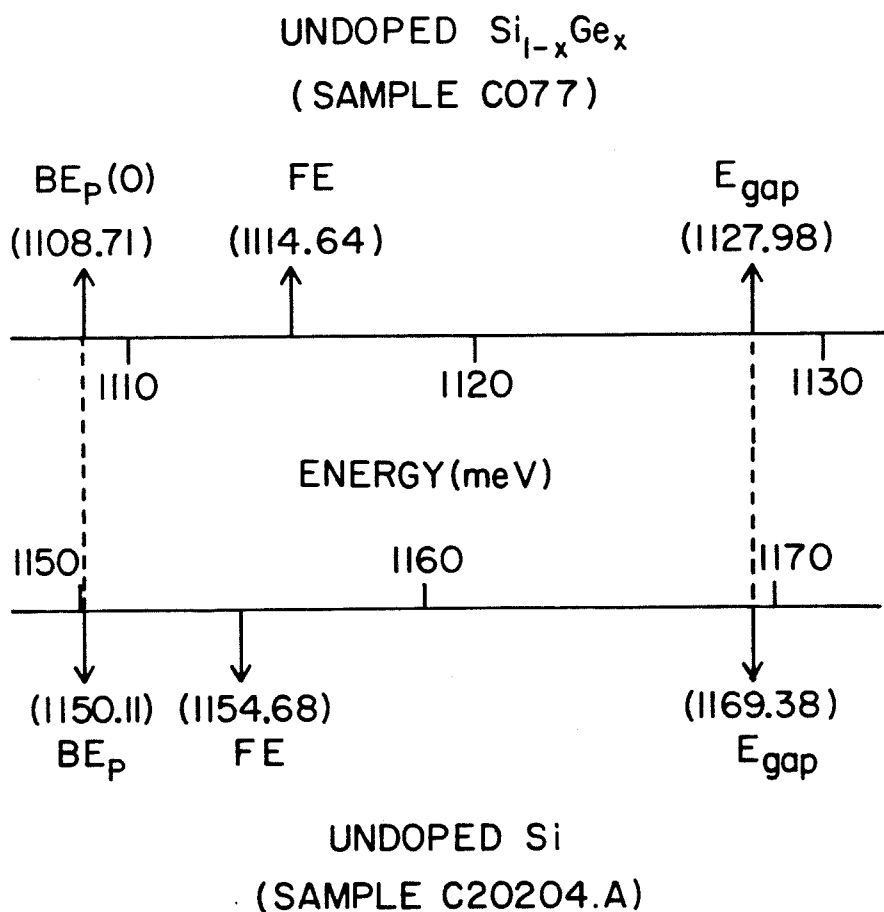


Figure 4.11. Schematic line position comparison between Si and $\text{Si}_{1-x}\text{Ge}_x$ sample C077. This comparison is based on the assumption that the difference between the energy of $BE_p(0)$ luminescence from Si is equal to the difference in band gap energies for Si and $\text{Si}_{1-x}\text{Ge}_x$ sample C077. This fixes the alloy gap energy. The spectra are then compared by lining up the Si and $\text{Si}_{1-x}\text{Ge}_x$ gap energies.

for Si and the $x=0.11$ alloy. The FE threshold position in the alloy, 1114.64 meV, was obtained by fitting Eq. (4.1) to the high temperature FE luminescence spectra (Fig. 4.3), as illustrated in Fig. 4.4. The NP FE threshold position in Si, 1154.68 meV, was obtained by fitting Eq. (4.1) directly to NP FE luminescence from pure Si. An example of this fit is shown in Fig. 4.12. The Si gap energy, 1169.38 meV, was determined from the NP FE threshold energy by subtracting the FE binding energy, which is given in Table 1.2 as 14.7 meV. Then the alloy gap energy, 1127.98 meV, was obtained by subtracting the band gap shift, 41.4 meV, from the Si gap energy.

As indicated in Fig. 4.11, this method implies that the FE dissociation energy in the $x=0.11$ alloy has decreased by 1.36 meV from its value in Si, to 13.34 meV. This compares favourably with a rough estimate based on a linear interpolation between the FE dissociation energies in Si and Ge, which are given in Table 1.2 as 14.7 meV and 4.15 meV, respectively. The linear interpolation results in an estimate of 13.54 meV for the FE dissociation energy in the $x=0.11$ alloy.

4.3.7.3 Band Gap Decrease for Sample C021-3 ($x=0.067$)

A similar analysis has been applied to the $x = 0.067$ sample. C021-3. As shown in Fig. 4.8, compared to sample C077 the luminescence from sample C021-3 is shifted to higher energy by 15.5 meV. This implies a band gap decrease of 25.9 meV for the $x=0.067$ alloy. This

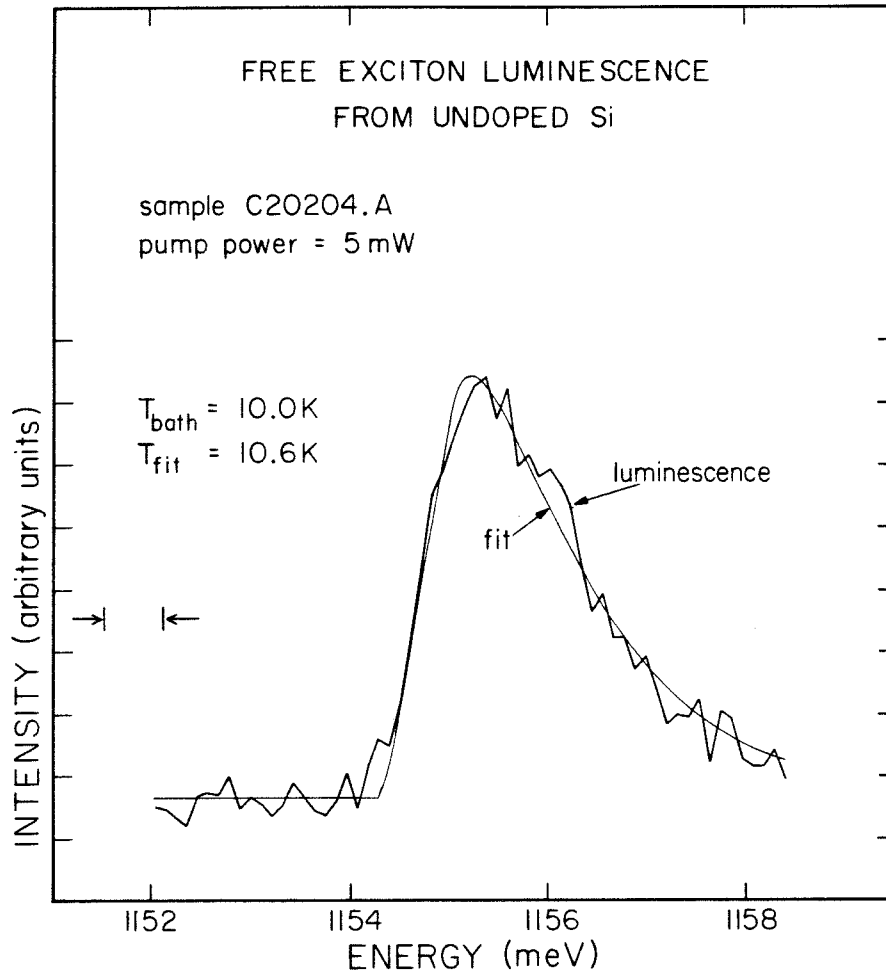


Figure 4.12. Si no-phonon free exciton luminescence and least-squares fit of the theoretical lineshape (Eq. (4.1)). The sample temperature obtained from the fit, T_{fit} , is shown with the measured bath temperature, T_{bath} .

result and the result previously obtained for sample C077 are consistent with the alloy composition measurements presented in Table 4.1 if a linear relationship between the alloy composition and change in band gap is assumed. The composition ratio between the two samples is 0.609 while the ratio of the measured band gap shifts is 0.626,

4.3.8 Excitons Bound to Composition Fluctuations

4.3.8.1 Low Temperature Free Exciton Luminescence

One feature in the luminescence spectrum of sample C077 remains to be discussed. At high temperatures (Fig. 4,3), the FE line assumes a shape characteristic of FE recombination in Si and is well described by Eq. 4.1, as previously discussed. The FE threshold energy obtained by fitting Eq. (4.1) is independent of temperature, as expected. However, at low temperatures this is no longer the case. Spectra taken at various temperatures below 6 K are shown in Fig. 4,13. We see that as the temperature decreases, the line shifts to lower energy and assumes a shape which is no longer characteristic of FE recombination.

4.3.8.2 Fluctuation Bound Excitons

These measurements of low temperature FE luminescence suggest that a low energy shoulder appears on the FE luminescence at low temperatures. This shoulder may be due to the recombination of excitons bound by only about 0.1 meV to a very shallow level. This interpretation is supported by the temperature-resolved spectra, which

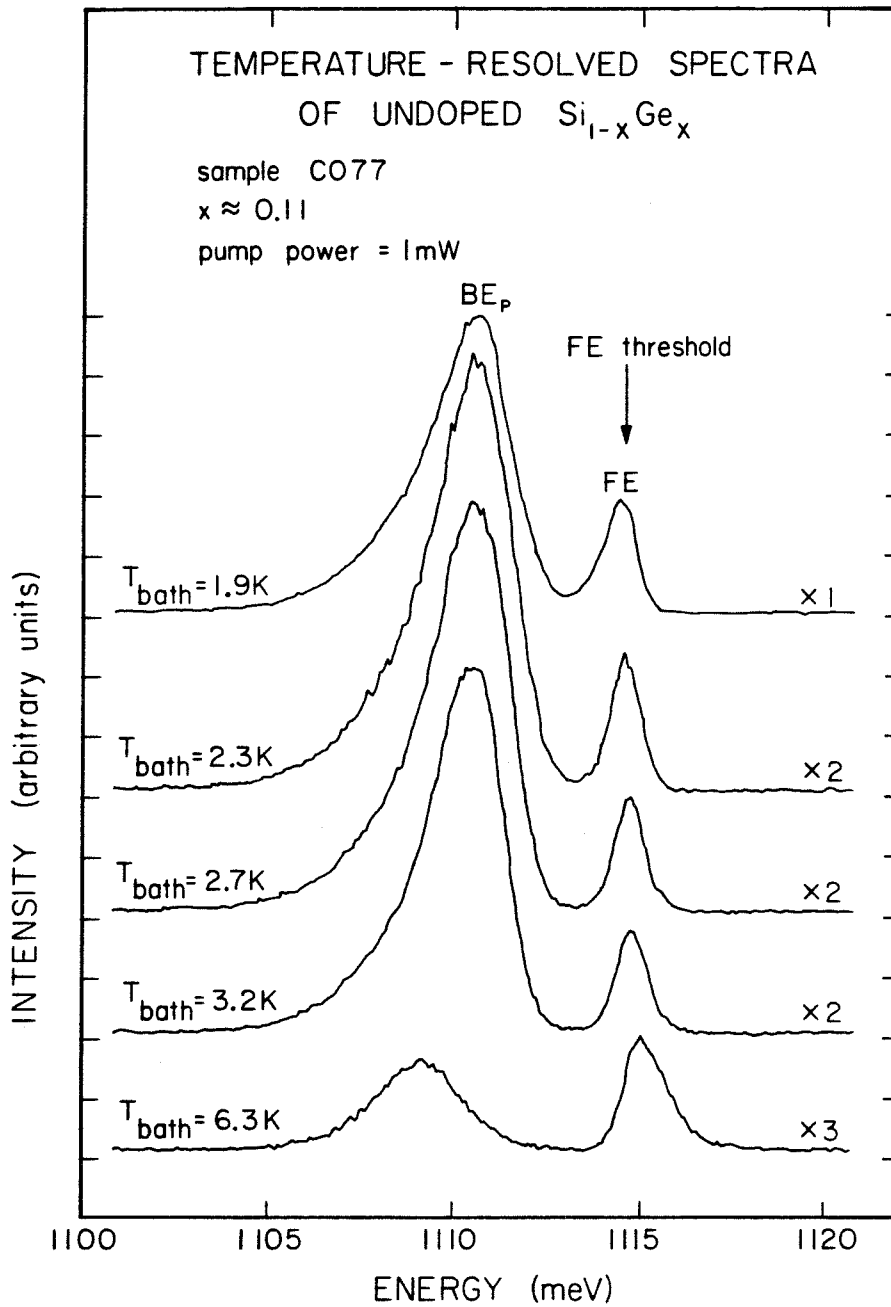


Figure 4.13. Temperature-resolved spectra of undoped $\text{Si}_{1-x}\text{Ge}_x$ sample C077 at low temperatures. The scale factors (e.g., "X2") give the relative intensity magnification. Note that the free exciton line shifts and broadens as the temperature is decreased. For reference, the free exciton threshold energy measured at high temperature is shown.

show that the shoulder has completely thermalized by 6 K. Above 6 K, Eq. (4.1) correctly describes the lineshape, and the threshold energy is independent of temperature. This behaviour is consistent with a binding energy of tenths of meV. Also, the pump power dependence at 1.6 K (Fig. 4.14) shows that the FE to BE_p intensity ratio is independent of pump power, as expected for independent exciton binding centers in the absence of saturation.

These features, and the fact that there is no known defect or impurity in Si which binds an exciton by only 0.1 meV, leads us to suggest that the new feature may be due to the recombination of excitons weakly bound to local fluctuations in the alloy composition (BE_F). The possibility of such a state was first pointed out by Baranovskii and Éfros ⁽²⁰⁾, who extended the bulk fluctuation theory of Alferov et al ⁽⁹⁾ to include excitons. A line which may be due to fluctuation bound excitons has just recently been reported in $GaAs_{1-x}P_x$ ⁽²¹⁾, and has characteristics which are similar to those of the line reported here.

4.3.8.3 Low Temperature Time-resolved Spectra

One of the most important features of this model is the prediction that BE_F luminescence should have a very long lifetime. As indicated during the discussion of BE_p decay, the dominant decay mechanism for donor or acceptor BE's in Si is the Auger process. This results in observed decay rates which can be orders of magnitude

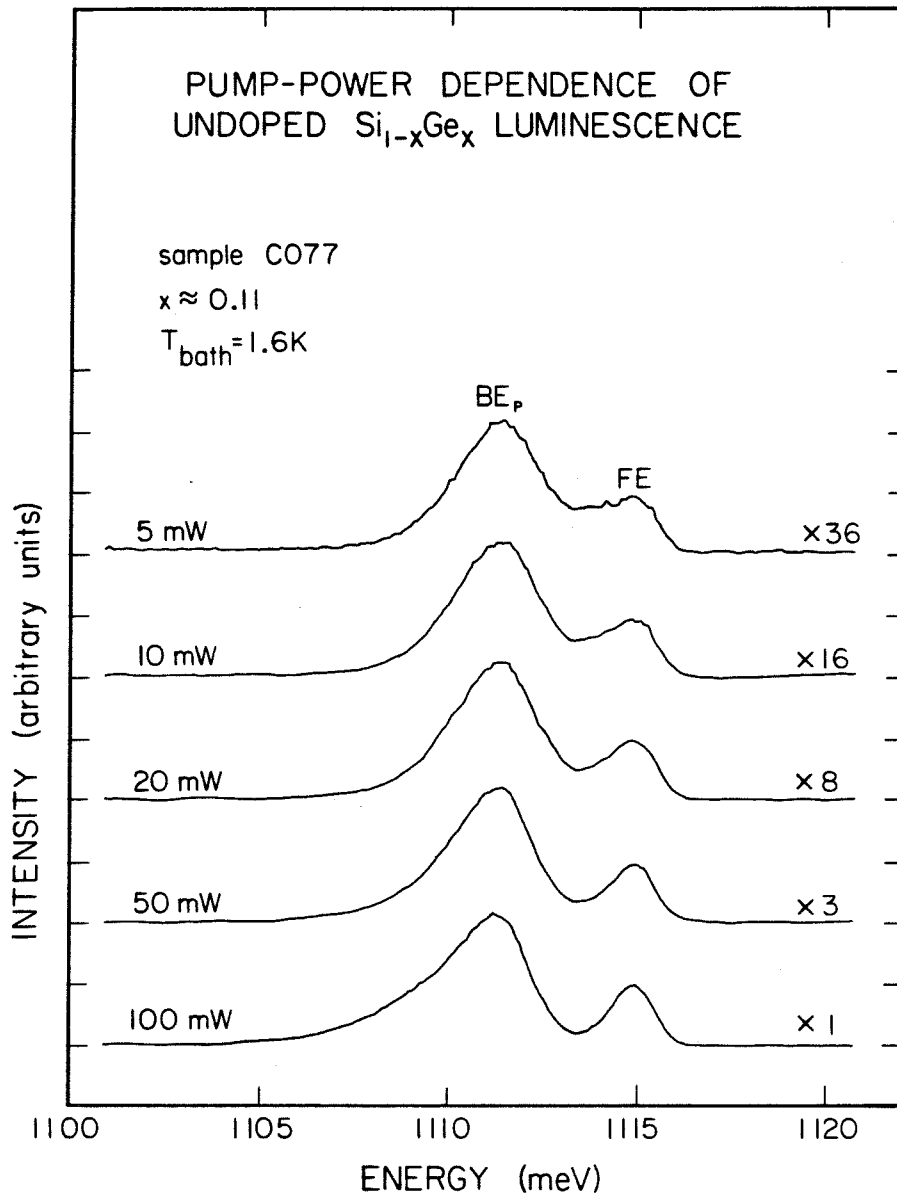


Figure 4.14. Pump power dependence of luminescence from undoped $\text{Si}_{1-x}\text{Ge}_x$ sample C077 at 1.6 K. The scale factors (e.g., "X36") give the relative intensity magnification. Note that the BE_p/FE intensity ratio is independent of pump power.

larger than the radiative rates obtained from measured oscillator strengths (18,19). For instance, the BE_p radiative decay rate is estimated to be $5 \times 10^2 \text{sec}^{-1}$, whereas the observed Auger decay rate is $3.7 \times 10^6 \text{sec}^{-1}$ (19). When an exciton is bound to a local composition fluctuation, however, the Auger process is not possible and long lifetime luminescence is expected. Indeed, this was the case for the luminescence feature observed in $\text{GaAs}_{1-x}\text{P}_x$ (21).

Fig. 4.15 presents the best low-temperature time-resolved spectra available for the $\text{Si}_{0.9}\text{Ge}_{0.1}$ alloy. Although the spectra are somewhat noisy, we see that the BE_F luminescence does not appear to have a particularly long lifetime compared to the BE_p luminescence line. To explain this apparent discrepancy, we return to the rate theory presented in Eqs. (4.8), (4.9), (4.11) and (4.12), but we include a second centre which can bind excitons by tenths of meV. Since this bound state is so shallow, we must include the effects of thermalization between this centre and the FE gas. The resulting set of rate equations are:

$$\frac{dn_{FE}}{dt} = -(\nu_{FE} + \gamma_F + \gamma_P) n_{FE} + \rho_F n_F \quad (4.19)$$

$$\frac{dn_F}{dt} = \gamma_F n_{FE} - (\nu_F + \rho_F) n_F \quad (4.20)$$

$$\frac{dn_P(k)}{dt} = \gamma_P(k) n_{FE} - \nu_P(k) n_P(k) \quad (4.21)$$

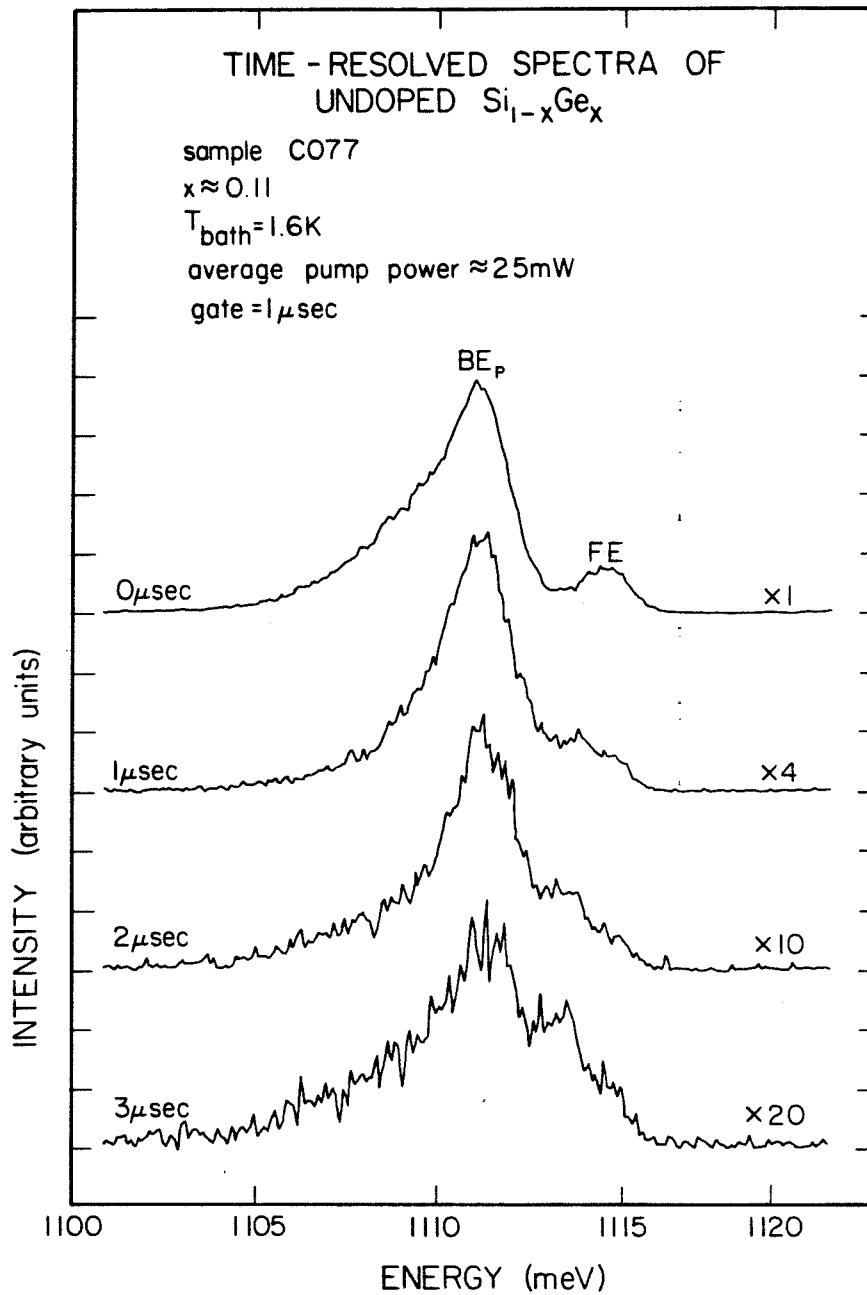


Figure 4.15. Time-resolved spectra of undoped $\text{Si}_{1-x}\text{Ge}_x$ sample C077 at 1.6 K. The scale factors (e.g., "x4") give the relative intensity magnification. Note that BE_F luminescence does not dominate the long time spectrum.

where

n_F = the BE_F density

γ_F = the rate of FE capture by local composition fluctuation

ρ_F = the rate of thermal release by BE_F .

As before, the boundary conditions at $t = 0$ are

$$\left. \frac{dn_{FE}}{dt} \right|_{t=0} = g - (v_{FE} + \gamma_P + \gamma_F) n_{FE} \Big|_{t=0} + \rho_F n_F \Big|_{t=0} = 0 \quad (4.22)$$

$$\left. \frac{dn_F}{dt} \right|_{t=0} = \gamma_F n_{FE} \Big|_{t=0} - (v_F + \rho_F) n_F \Big|_{t=0} = 0 \quad (4.23)$$

$$\left. \frac{dn_P(k)}{dt} \right|_{t=0} = \gamma_P(k) n_{FE} \Big|_{t=0} - v_P(k) n_P(k) \Big|_{t=0} = 0 \quad (4.24)$$

The solution to Eqs. (4.19) - (4.24) is complicated somewhat by the new coupling between Eqs. (4.19) and (4.20). Nevertheless, we can still obtain the solution, which is:

$$n_{FE} = \frac{g}{(\alpha_1 - \alpha_2)} \left[\frac{\alpha_2 + (v_F + \rho_F)}{\alpha_2} \exp(\alpha_2 t) - \frac{\alpha_1 + (v_F + \rho_F)}{\alpha_1} \exp(\alpha_1 t) \right] \quad (4.25)$$

$$n_F = \frac{g \gamma_F}{(\alpha_1 - \alpha_2)} \left[\frac{1}{\alpha_2} \exp(\alpha_2 t) - \frac{1}{\alpha_1} \exp(\alpha_1 t) \right] \quad (4.26)$$

$$n_P(k) = \frac{g \gamma_P(k)}{(\alpha_1 - \alpha_2)} \left[\frac{\alpha_2 + (v_F + \rho_F)}{\alpha_2 [\alpha_2 + v_P(k)]} \exp(\alpha_2 t) - \frac{\alpha_1 + (v_F + \rho_F)}{\alpha_1 [\alpha_1 + v_P(k)]} \exp(\alpha_1 t) \right] + \frac{g \gamma_P(k)}{v_P(k)} \frac{(v_F + \rho_F) - v_P(k)}{[\alpha_1 + v_P(k)] [\alpha_2 + v_P(k)]} \exp[-v_P(k)t] \quad (4.27)$$

where

$$\alpha_{1,2} = \frac{1}{2} \left\{ [(v_{FE} + \gamma_F + \gamma_P) + (v_F + \rho_F)] \pm \sqrt{ [(v_{FE} + \gamma_F + \gamma_P) + (v_F + \rho_F)]^2 - 4 [(v_{FE} + \gamma_F + \gamma_P) (v_F + \rho_F) - \gamma_F \rho_F] } \right\} \quad (4.28)$$

We can simplify considerably if we assume $\gamma_F + \gamma_P \gg \gamma_F$. This is reasonable since we expect that the concentration of these centres, N_F , will be quite low. Then Eq. (4.28) reduces to

$$\alpha_{1,2} = \begin{cases} - (v_{FE} + \gamma_F + \gamma_P) \\ - (v_F + \rho_F) \end{cases} \quad (4.29)$$

and the solution becomes

$$n_{FE} = \frac{g}{(\nu_{FE} + \gamma_F + \gamma_P)} \exp \left[-(\nu_{FE} + \gamma_F + \gamma_P)t \right] \quad (4.30)$$

$$n_F = \frac{g \gamma_F}{(\nu_{FE} + \gamma_F + \gamma_P) - (\nu_F + \rho_F)} \left\{ \frac{1}{(\nu_F + \rho_F)} \exp \left[-(\nu_F + \rho_F)t \right] - \frac{1}{(\nu_{FE} + \gamma_F + \gamma_P)} \exp \left[-(\nu_{FE} + \gamma_F + \gamma_P)t \right] \right\} \quad (4.31)$$

$$n_P(k) = \frac{g \gamma_P(k)}{(\nu_{FE} + \gamma_P + \gamma_F) - \nu_P(k)} \left\{ \frac{1}{\nu_P(k)} \exp \left[-\nu_P(k)t \right] - \frac{1}{(\nu_{FE} + \gamma_F + \gamma_P)} \exp \left[-(\nu_{FE} + \gamma_F + \gamma_P)t \right] \right\} . \quad (4.32)$$

The structure of this solution is quite similar to Eqs. (4.13) and (4.14), and similar considerations apply. On the strength of our previous arguments, we can assume $\nu_{FE} + \gamma_P + \gamma_F \sim \gamma_P$ and $\gamma_P < \nu_P(k)$. So the $n_P(k)$ decay is capture-limited. The n_F decay depends on the relationship between $(\nu_F + \rho_F)$ and γ_P . If $(\nu_F + \rho_F) < \gamma_P$, the long-time decay rate of n_F is dominated by $(\nu_F + \rho_F)$ and we would expect to see the BE_F luminescence have a long lifetime. Conversely, if $\gamma_P < (\nu_F + \rho_F)$ the long-time decay of n_F is determined by γ_P , and the BE_P and BE_F luminescence will decay together. As already

established, we expect ν_F to be small, about $1 \times 10^3 \text{sec}^{-1}$. However, $\gamma_P < (\nu_F + \rho_F)$ can be satisfied if significant BE_F thermalization is occurring. We can estimate the BE_F thermalization rate at 1.6 K by taking Eq. (2.4) for ρ_F :

$$\rho_F = \sigma_F v_{th} N_{FE} \exp\left(\frac{E_F}{k_B T}\right) \quad (4.33)$$

where

$$N_{FE} = 2 \left(\frac{m_{ex} k_B T}{2\pi\hbar^2} \right)^{3/2} \quad (4.34)$$

and v_{th} is given by Eq. (4.18).

To estimate, we take $m_{ex} = 0.6 m_o$ ⁽¹⁷⁾, $T = 1.6 \text{ K}$ and $E_F = 0.1 \text{ meV}$. We assume $\sigma_F \sim \sigma_B$ and take $\sigma_B = 10^{-13} \text{cm}^2$ ⁽¹⁶⁾. Then we

obtain $N_{FE} = 4 \times 10^{15} \text{cm}^{-3}$, $v_{th} = 1 \times 10^6 \text{ cm/sec}$ and finally

$\rho_F \sim 2 \times 10^8 \text{sec}^{-1}$. However, Eq. (4.16) yields $\gamma_P = 1 \times 10^6 \text{ cm/sec}$ at 1.6 K. So we are clearly in a regime where $\gamma_P < (\nu_F + \rho_F)$. The n_F decay is therefore capture-limited, and the time resolved spectra are explained.

It should be mentioned that the observation of long lifetimes for the $\text{GaAs}_{1-x}\text{P}_x$ BE_F is expected on the basis of the above analysis. First, the impurity concentrations in that case were between 10^{16}cm^{-3} and 10^{17}cm^{-3} ⁽²¹⁾, which increased the capture rate by a

factor of about 10^3 to 10^4 . Second, the feature was bound by about 10 meV ⁽²¹⁾, which decreased the 1.6 K thermalization rate by a factor of about 10^5 . As a result, the BE_F decay was not capture-limited, but governed by the radiative decay rate ν_F .

Also, it should be mentioned that the assumption of large BE_F thermalization rates does not necessarily imply a large FE luminescence line in the low temperature spectrum. To demonstrate this, we return to the original equations, Eqs. (4,25) - (4,27), and solve for the steady-state ($t = 0$) solution. We obtain

$$n_{FE} = \frac{g}{(\nu_{FE} + \gamma_F + \gamma_P) - \frac{\gamma_F}{\left(1 + \frac{\nu_F}{\rho_F}\right)}} \quad (4.35)$$

$$n_F = \frac{\gamma_F}{\nu_F + \rho_F} n_{FE} \quad (4.36)$$

$$n_P(k) = \frac{\gamma_P(k)}{\nu_P(k)} n_{FE} \quad (4.37)$$

In the limit of no BE_F thermalization, these results reduce to

$$n_{FE} = \frac{g}{\nu_{FE} + \gamma_F + \gamma_P} \quad (4.38)$$

$$n_F = \frac{\gamma_F}{\rho_F} n_{FE} \quad (4.39)$$

$$n_P(k) = \frac{\gamma_P(k)}{v_P(k)} n_{FE} \quad (4.40)$$

In the limit of infinitely fast BE_F thermalization, we obtain

$$n_{FE} = \frac{g}{v_{FE} + \gamma_P} \quad (4.41)$$

$$n_F = 0 \quad (4.42)$$

$$n_P(k) = \frac{\gamma_P(k)}{v_P(k)} n_{FE} \quad (4.43)$$

If we assume $\gamma_F \ll \gamma_P$ as previously proposed, then comparison of Eqs. (4.38) and (4.41) show that, even in these extreme limits, the FE density remains essentially constant. The FE density is governed primarily by the generation rate, g , and the P capture rate, γ_P .

4.4 EXPERIMENTAL RESULTS AND DISCUSSION FOR In DOPED $Si_{1-x}Ge_x$

The subject of the investigations reported in this section was the In doped $Si_{1-x}Ge_x$ sample C093, for which $x=0.10$.

4.4.1 Typical Photoluminescence Spectra

Typical luminescence spectra obtained from $Si_{1-x}Ge_x$:In sample C093 are shown in Fig. 4.16. Spectra measured at various temperatures

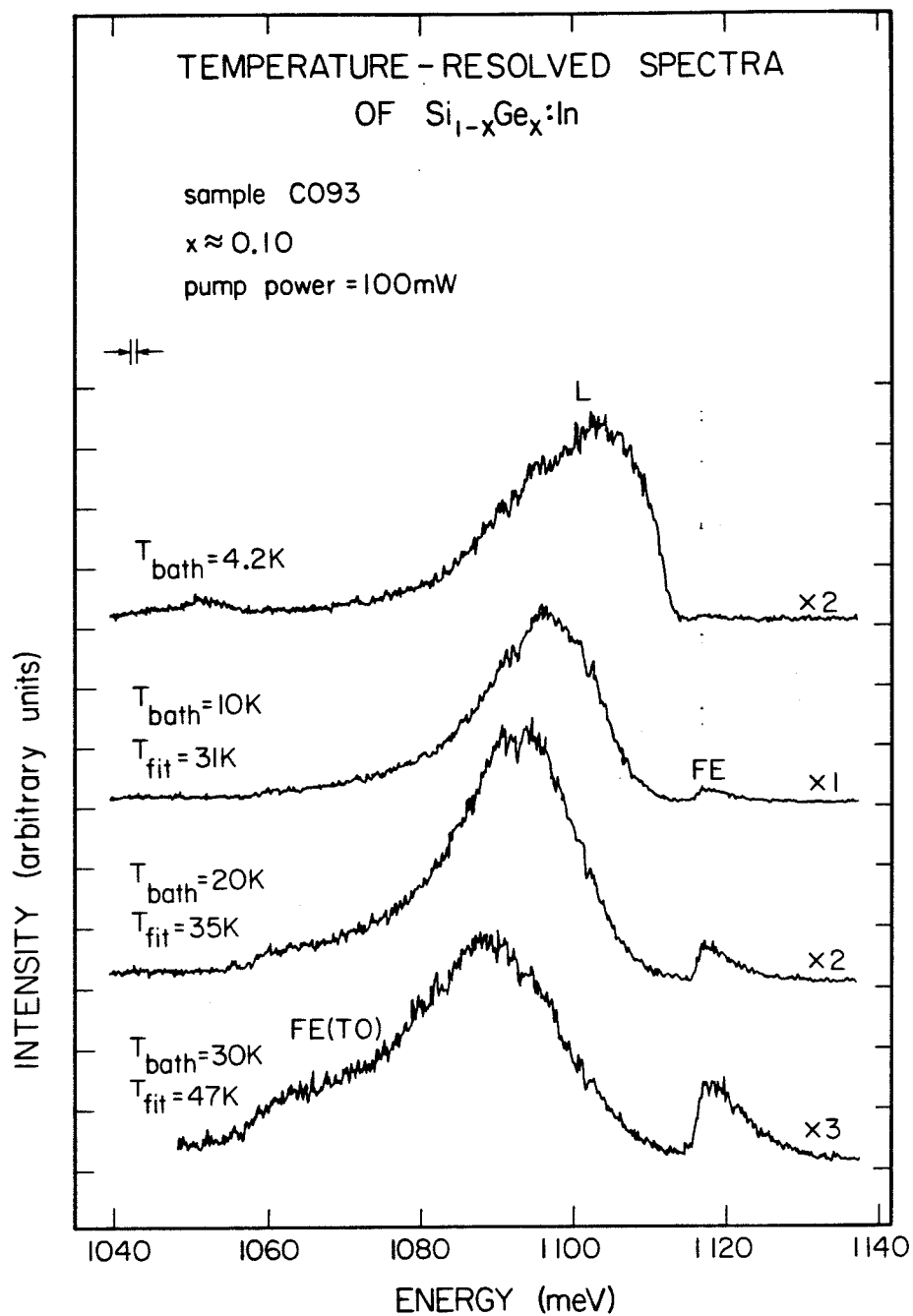


Figure 4.16. Temperature-resolved spectra of $\text{Si}_{1-x}\text{Ge}_x:\text{In}$ sample C093 from 4.2 K to 30 K. The scale factors (e.g., "X2") give the relative intensity magnification. Refer to the text for a discussion of the line assignments shown in the figure. Where free exciton (FE) luminescence is observed, the sample temperature obtained from a least-squares fit to the FE lineshape, T_{fit} , is shown with the measured bath temperature, T_{bath} . The discrepancy between these results is discussed in the text.

are shown. Two features are prominent in the spectra. The higher energy luminescence, labelled "FE", becomes visible only at high temperatures. At somewhat lower energies a broad feature labelled "L" is visible, which moves to lower energy as the temperature is increased. The L luminescence develops a low energy shoulder at high temperatures, which has been labelled "FE(TO)".

4.4.2 Identification of Free Exciton Luminescence

To begin with, we note that the luminescence labelled FE has a lineshape and temperature dependence characteristic of NP FE recombination in Si, as described in detail in the Section 4.3. Eq. (4.1), which describes the NP FE lineshape, can be fit to the FE luminescence from sample C093 very accurately. The FE threshold energy obtained from such fits, 1115.8 meV, remained constant within about 0.3 meV. However, the fit temperatures, T_{fit} , were systematically higher than the measured bath temperatures, T_{bath} . These temperatures are indicated in Fig. 4.16. It seems, therefore, that either the FE luminescence is subject to some broadening as a result of the disordered nature of the alloy, or the sample is being locally heated by the laser pump. Of these two possibilities, the second seems most likely. First, one would expect some broadening mechanism to affect the FE threshold behaviour as well as generally broaden the line. That is, we would expect to see the FE threshold "smear out" and become less abrupt. However, this behaviour is not observed.

As previously mentioned, the lineshape is described by Eq. (4.1) very well. Second, as indicated in Table 4.1 sample C093 has impurity concentrations which are about three orders of magnitude higher than those in sample C077. As a result, much higher pump powers are needed to observe FE luminescence at all in sample C093. At these laser intensities, sample heating must be considered a very likely cause of the observed FE broadening,

If this explanation is accepted, the luminescence labelled FE can be interpreted as resulting from NP FE recombination in the $\text{Si}_{1-x}\text{Ge}_x$:In alloy. Since the feature labelled "FE(TO)" is separated from the FE peak by approximately the Si TO phonon energy, we interpret this shoulder on L as being due to TO phonon assisted FE recombination.

4.4.3 Identification of Bound Exciton Luminescence

Our interpretation of the luminescence labelled L is necessarily considerably more complicated than that of the FE luminescence. There are a number of processes which are undoubtedly contributing to the L line. Primarily, BE_B , BE_P and BE_{In} luminescence must be considered. In, of course, is the majority dopant, and will dominate the NP BE luminescence. The B concentration is about an order of magnitude greater than the P concentration. It follows from our discussion of BE luminescence from undoped $\text{Si}_{1-x}\text{Ge}_x$ that B and P will probably contribute equally to the NP BE luminescence. In addition, the L luminescence is sufficiently broad that transverse-acoustic (TA)

phonon replicas of the FE and BE lines may contribute as well. It is unlikely that NP BMEC or electron-hole droplet (EHD) luminescence will have any significant influence on the spectra presented here. The impurity concentrations in sample C093 preclude the observation of such effects at the pump powers utilized in this study.

4.4.3.1 Time-Resolved Spectra and Isolation of B Bound Exciton Component

In an effort to separate the BE components which produce the L luminescence, the time evolution of the luminescence from sample C093 was measured at low pump power. The time-resolved spectra are shown in Fig. 4.17 for low power laser excitation. As this figure demonstrates, the L luminescence is composed of a relatively sharp high energy component with a long lifetime, and a broad low energy component with a short lifetime. Consideration of the BE_B , BE_P and BE_{In} decay times in Si (1055 nsec, 272 nsec and 2.7 nsec, respectively ⁽¹⁹⁾) leads to the suggestion that the sharp, long lifetime component is primarily a result of BE_B recombination. The broad, short lifetime low energy shoulder is therefore probably due to BE_{In} recombination.

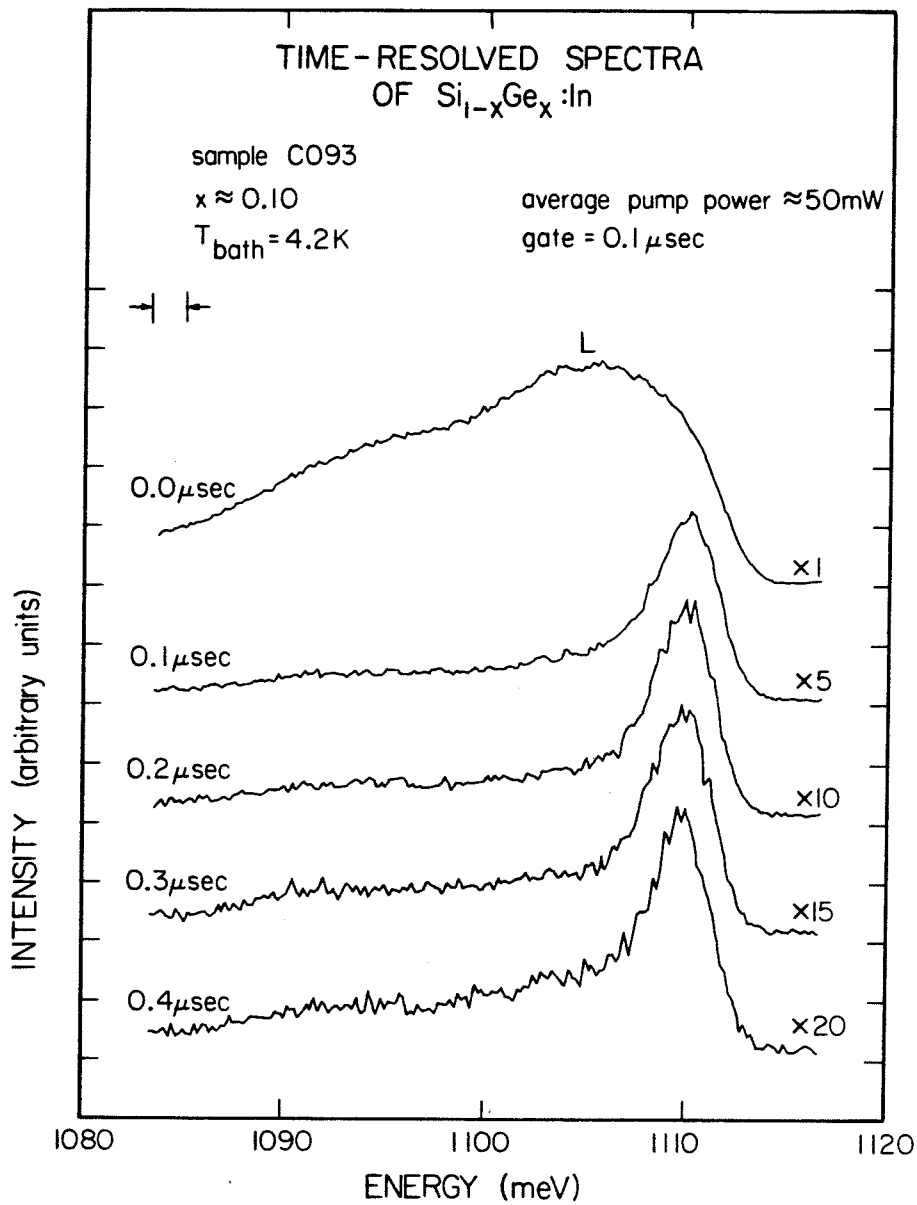


Figure 4.17. Time-resolved spectra of $\text{Si}_{1-x}\text{Ge}_x:\text{In}$ sample C093. The scale factors (e.g., "X5") give the relative intensity magnification. At long times, a sharp, long lifetime component of L luminescence is isolated.

4.4.3.2 Temperature-Resolved Spectra and Isolation of In Bound Exciton Component

A further separation of the BE components which produce the L luminescence can be accomplished by measuring the temperature dependence of the photoluminescence spectrum. This measurement is shown in Fig. 4.16. We see that the high energy side of the L luminescence thermalizes as the temperature is increased. This observation is consistent with the interpretation of L luminescence presented in the previous section. At high temperatures, only the lower energy BE_{In} component is observed. The higher energy BE_B component has thermalized.

This effect is seen clearly in Fig. 4.18, which shows the temperature dependence of L luminescence which is gated in time. At low temperatures, the BE_B peak is reasonably well isolated. At the high pump powers used for this measurement, however, a low energy shoulder is clearly observed. We interpret this shoulder as being due to a BE_{In} component which has not been eliminated by the time resolution. As the temperature is increased, we see the BE_B component thermalize with respect to the BE_{In} component. Above 10 K, only the BE_{In} component remains.

There is one difficulty with this interpretation which should be mentioned. As the temperature is raised above 10 K, the BE_{In} component peak position moves to lower temperature, as expected from the behaviour of BE_P luminescence in undoped $Si_{1-x}Ge_x$. This effect

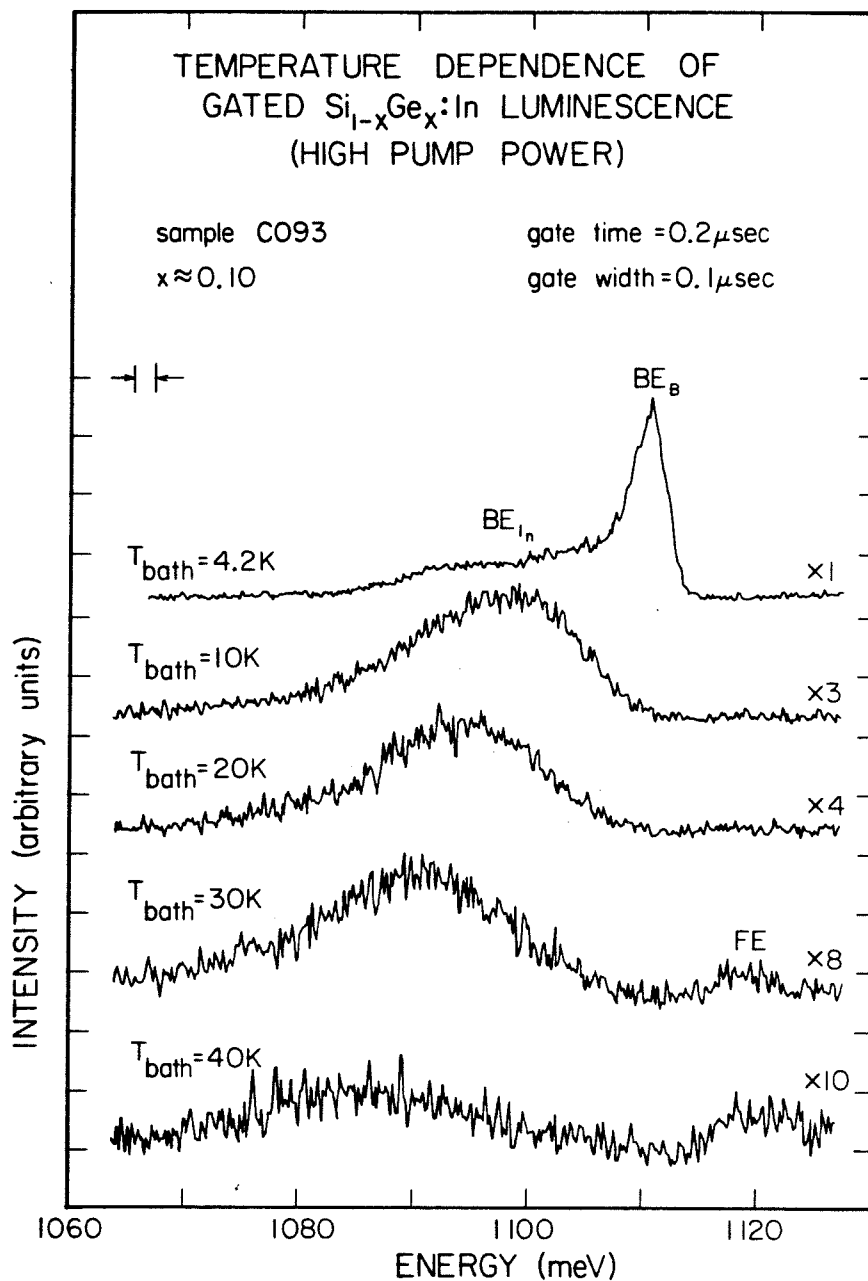


Figure 4.18. Gated, temperature-resolved spectra of $\text{Si}_{1-x}\text{Ge}_x:\text{In}$ sample C093 at high pump power. The scale factors (e.g., "X3") give the relative intensity magnification. At high temperature, the BE_B luminescence component thermalizes, and the BE_{In} component is isolated. At high temperatures, weak free exciton (FE) luminescence is also observed.

is observed in Fig. 4.16 and Fig. 4.18. However, the BE_{In} peak moves too far; by 30 K, it is already approximately 25 meV below the FE threshold, while the BE_{In} binding energy in Si is only 13.7 meV⁽²²⁾. In spite of this, the bulk of the experimental evidence supports the interpretation that this high temperature luminescence is due to BE_{In} recombination in the alloy. It may be that contributions from FE and BE TA assisted luminescence combine to produce the anomalously low high temperature BE_{In} peak position. However, this seems unlikely when the relative intensities of TA and NP luminescence in Si are considered. It is also possible that the $BE_{In}(0)$ binding energy in the alloy is increased as a result of some complicated effect which may involve the unusually large radii of the Ge and In atoms relative to the Si-Si bond length. Of course, this mechanism is also unlikely, practically by definition. Unfortunately, all we can conclude at this point is that the anomalous temperature dependence of the BE_{In} luminescence remains unexplained.

4.4.4 Comparison of Si and $Si_{1-x}Ge_x$:In Luminescence Energies

The separation of the L luminescence components discussed in the previous section leads to the possibility of comparing $Si_{1-x}Ge_x$:In and Si:In spectra by analyzing the $Si_{1-x}Ge_x$:In BE_B line in a manner similar to that employed for BE_p luminescence in the undoped $Si_{1-x}Ge_x$ case. The $Si_{1-x}Ge_x$:In luminescence is gated in time to isolate the BE_B component. Then, as shown in Fig. 4.19, the temperature

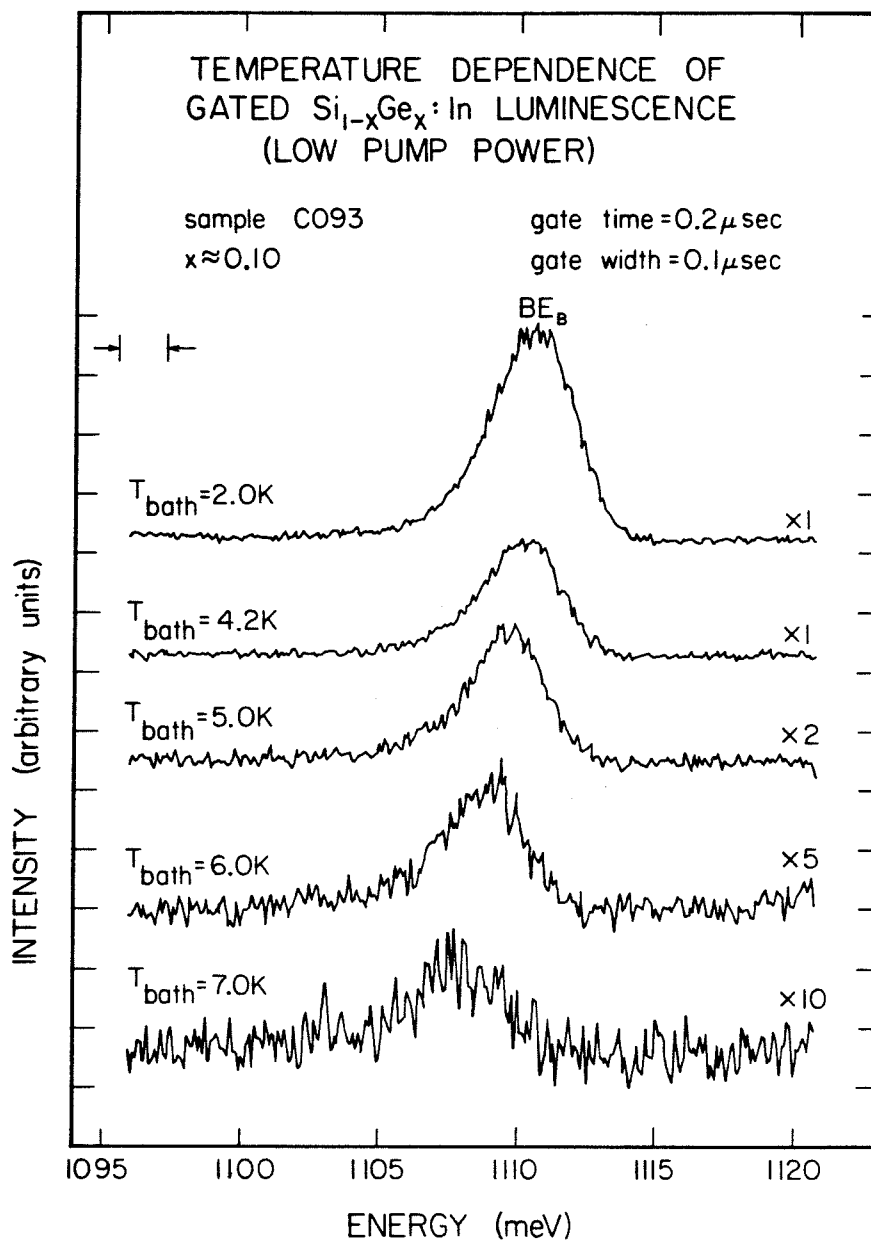


Figure 4.19. Gated, temperature-resolved spectra of $\text{Si}_{1-x}\text{Ge}_x:\text{In}$ sample C093 at low pump power. The scale factors (e.g., "X2") give the relative intensity magnification. Note that the BE_B peak position shifts to lower energy as the temperature is increased. This effect is discussed in the text.

dependence of the BE_B luminescence is measured at very low pump powers. Comparison of Fig. 4.19 with Fig. 4.2 shows that the behaviour of the BE_B component is almost identical to that of the BE_P luminescence from undoped $Si_{1-x}Ge_x$. We are tempted, therefore, to apply the reasoning used in the analysis of undoped $Si_{1-x}Ge_x$ luminescence, and propose that the high temperature BE_B luminescence is dominated by the $BE_B(0)$ component. Then the $BE_B(0)$ peak position obtained from the 7.0 K spectrum is 1107.80 meV. However, the FE threshold energy for sample C093 is 1115.8 meV, which implies that the $BE_B(0)$ binding energy is 8 meV, which is much too large.

This discrepancy is probably due to an incomplete separation of the L luminescence. At low temperatures, we observe primarily the BE_B luminescence. However, as the temperature increases the BE_B components thermalize faster than whatever BE_{In} components have not been eliminated by the time resolution. The presence of these BE_{In} components is clearly demonstrated by Fig. 4.18. At high temperatures, therefore, we again see the combined BE luminescence, which will effectively lower the energy measured for the $BE(0)$ peak.

In spite of these difficulties, a method can be developed for comparing the $Si_{1-x}Ge_x:In$ and $Si:In$ spectra. Since samples C077 and C093 differ in composition by only about 1%, we assume that the FE binding energies in the two samples are the same. This leads to the comparison schematically illustrated in Fig. 4.20. The gap energy for sample C093, 1129.14 meV, was determined by adding

SCHEMATIC COMPARISON OF
Si : In AND $\text{Si}_{1-x}\text{Ge}_x$: In
LUMINESCENCE ENERGIES

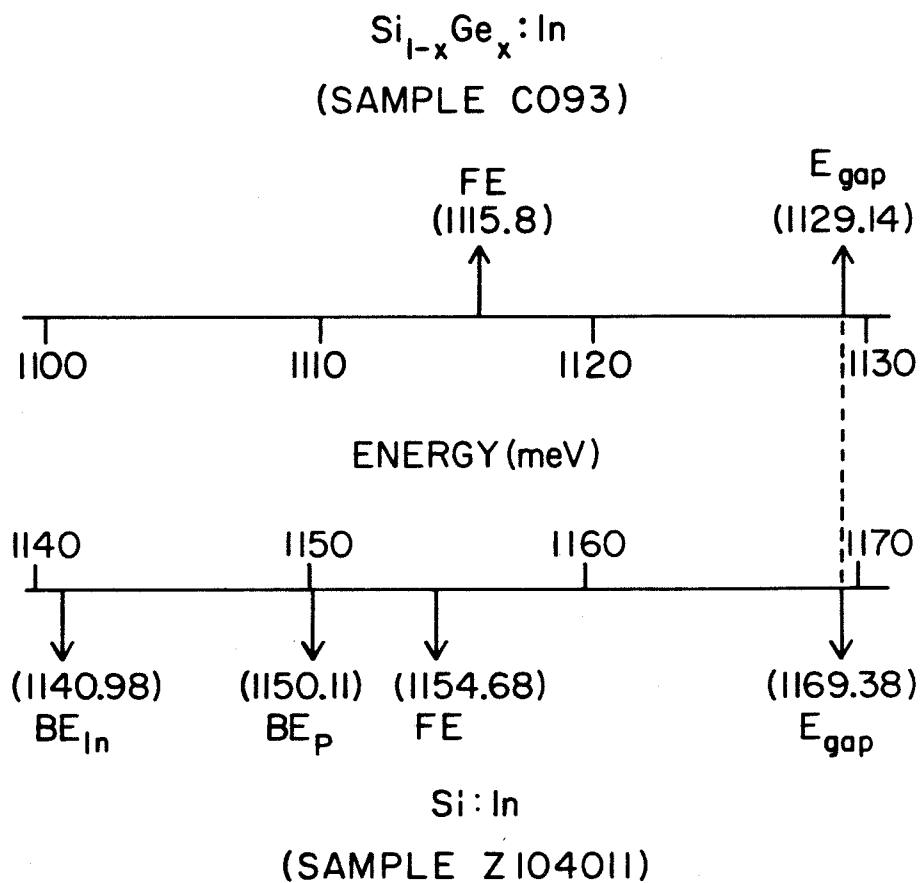


Figure 4.20. Schematic line position comparison between Si and $\text{Si}_{1-x}\text{Ge}_x$: In sample C093. This comparison is based on the assumption that the FE binding energy in sample C093 and sample C077 is identical. This fixes the alloy gap energy. The spectra are then compared by lining up the Si and $\text{Si}_{1-x}\text{Ge}_x$: In gap energies.

the assumed FE binding energy, 13.34 meV, to the FE threshold energy, 1115.8 meV. This results in a measured band gap shift of 40.2 meV for the $x = 0.104$ alloy. The band gap shifts and alloy composition measurements are reasonably consistent, assuming a linear relationship between the alloy composition and change in band gap. The composition ratio between samples C077 and C093 is .920 while the ratio of measured band gap shifts is .971. Samples C021-3 and C093 agree exactly - the composition ratio and the ratio of measured band gap shifts are both 0.644.

4.5 SUMMARY AND CONCLUSION

In this chapter, the photoluminescence spectra of undoped Si-rich $\text{Si}_{1-x}\text{Ge}_x$ were extensively studied for the first time. Samples for which $x = 0.11$ and $x = 0.067$ were considered. The following results were obtained:

- (i) Free exciton (FE) luminescence was observed and identified. The FE luminescence is described very accurately by the Si NP FE lineshape, Eq. (4.1). As a result, a NP FE threshold energy was obtained.
- (ii) Bound exciton (BE) luminescence was also observed. The BE luminescence is predominantly a result of recombination of excitons bound to P impurities (BE_p). A model has been proposed to explain the observed behaviour of the BE_p luminescence line, which is consistent with previous studies of hopping conduction ⁽¹²⁾ and Hall effect ⁽¹³⁾ in these alloys. According to this model BE_p luminescence

is a result of several overlapping components labelled $BE_p(k)$, where $0 \leq k \leq 4$ is the number of nearest-neighbour Ge atoms. At high temperatures, only $BE_p(0)$ luminescence is observed. The $BE_p(0)$ luminescence is observed. The $BE_p(0)$ peak position was measured.

(iii) Measurement of the line positions described above resulted in a determination of the decrease in band gap for the $x = 0.067$ and $x = 0.11$ alloys. In addition, a determination of the decrease in FE binding energy for the $x = 0.11$ alloy was possible. These results are summarized in Table 4.2.

(iv) At low temperatures, a feature ascribed to the recombination of excitons bound to fluctuations in alloy composition is observed.

The photoluminescence spectra of $Si_{1-x}Ge_x:In$ were also extensively investigated. One sample for which $x = 0.10$ was available. The following results were obtained;

(i) Free exciton (FE) luminescence was observed. The FE luminescence is described very accurately by Eq. (4.1), and a FE threshold energy was obtained. However, the sample temperatures determined on the basis of the above fits are systematically high. This effect was ascribed to laser induced sample heating.

(ii) Bound exciton (BE) luminescence was also observed. The BE luminescence is composed of overlapping components due to recombination of excitons bound to B and In impurities (BE_B and BE_{In} , respectively). These components were systematically isolated using

Table 4.2. Results of the investigation of photoluminescence properties of undoped $\text{Si}_{1-x}\text{Ge}_x$ and $\text{Si}_{1-x}\text{Ge}_x:\text{In}$.

SAMPLE	x	LINE POSITIONS (Å)		BAND GAP SHIFT (meV)	FE BINDING ENERGY (meV)
		FE	$\text{BE}_p(0)$		
C077	0.11	1114.64	1108.69	41.4	13.34
C021-3	0.067		1124.19	25.9	
C093	0.10	1115.8		40.2	

a combination of time and temperature resolution. While the BE_B component behaves as expected, the BE_{In} peak position moves to lower energy than anticipated as the temperature is increased. We were not able to explain this effect.

(iii) Measurement of the FE threshold energy resulted in a determination of the decrease in band gap for the $x = 0.10$ alloy. This result is consistent with those previously obtained for the undoped $Si_{1-x}Ge_x$ material, and is summarized in Table 4.2.

REFERENCES

1. A. Onton, J. Lumin. 7, 95 (1973) and references therein.
2. D. J. Wolford, R. E. Anderson and B. G. Streetman, J. Appl. Phys. 48, 2442 (1977) and references therein.
3. Zh. I. Alferov, V. I. Amosov, D. Z. Garbuzov, Yu. V. Zhilyaev, S. G. Konnikov, P. S. Kop'ev and V. G. Trofim, Fiz. Tekh. Poluprov. 6, 1879 (1972) [Sov. Phys.-Semicond. 6, 1620 (1973)] and references therein.
4. A. T. Hunter, D. L. Smith, and T. C. McGill, Appl. Phys. Lett. 37, 200 (1980) and references therein.
5. E. F. Gross, N. S. Sokolov, and A. N. Titkov, Fiz. Tverd. Tela 14, 2004 (1972) [Sov. Phys.-Solid State 14, 1732 (1973)].
6. R. Rentzsch and I. S. Shlimak, Fiz. Tekh. Poluprov. 12, 713 (1978) [Sov. Phys.-Semicond. 12, 416 (1978)].
7. C. Benoit à la Guillaume and M. Voos, Phys. Rev. B10, 4995 (1974).
8. R. B. Hammond, D. L. Smith, and T. C. McGill, Phys. Rev. Lett. 35, 1535 (1975).
9. S. A. Lyon, D. L. Smith, and T. C. McGill, Phys. Rev. Lett. 41, 56 (1978).
10. Zh. I. Alferov, E. L. Portnoi and A. A. Rogachev, Fiz. Tekh. Poluprov. 2, 1194 (1968) [Sov. Phys.-Semicond. 2, 1001 (1969)].
11. J. P. Dismukes, L. Ekstrom, and R. J. Paff, J. Phys. Chem. 68, 3021 (1964).

12. R. Braunstein, A. R. Moore, and F. Herman, Phys. Rev. 109, 695 (1958).
13. B. L. Gel'Mont, A. R. Gadzhiev, B. I. Shklovskii, I. S. Shlimak, and A. L. Efros, Fiz. Tekh. Poluprov. 8, 2377 (1974) [Sov. Phys.-Semicond. 8, 1549 (1975)].
14. R. Baron, M. H. Young, H. Winston, H. Kimura, G. S. Mitchard, and T. C. McGill, Proceedings of the Eleventh International Conference on Defects and Radiation Effects in Semiconductors, Japan, 1980.
15. R. B. Hammond and R. N. Silver, Appl. Phys. Lett. 36, 68 (1980).
16. R. M. Feenstra and T. C. McGill, Solid State Commun. 36, 1039 (1980).
17. K. R. Elliott, D. L. Smith, and T. C. McGill, Solid State Commun. 24, 461 (1977).
18. G. C. Osbourn, S. A. Lyon, K. R. Elliott, D. L. Smith, and T. C. McGill, Solid-State Electron. 21, 1339 (1978).
19. W. Schmid, Phys. Stat. Sol. (b) 84, 529 (1977).
20. S. D. Baranovskii and A. L. Efros, Fiz. Tekh. Poluprov. 12, 2233 (1978) Sov. Phys.-Semicond. 12, 1328 (1978).
21. S. Lai and M. V. Klein, Phys. Rev. Lett. 44, 1087 (1980).
22. S. A. Lyon, D. L. Smith, and T. C. McGill, Phys. Rev. B17, 2620 (1978).